

University of Texas at Arlington

**MavMatrix**

---

Mathematics Dissertations

Department of Mathematics

---

2023

## Mechanism of Hairpin Vortex Formation by Liutex

Yifei Yu

Follow this and additional works at: [https://mavmatrix.uta.edu/math\\_dissertations](https://mavmatrix.uta.edu/math_dissertations)



Part of the [Mathematics Commons](#)

---

### Recommended Citation

Yu, Yifei, "Mechanism of Hairpin Vortex Formation by Liutex" (2023). *Mathematics Dissertations*. 247.  
[https://mavmatrix.uta.edu/math\\_dissertations/247](https://mavmatrix.uta.edu/math_dissertations/247)

This Dissertation is brought to you for free and open access by the Department of Mathematics at MavMatrix. It has been accepted for inclusion in Mathematics Dissertations by an authorized administrator of MavMatrix. For more information, please contact [leah.mccurdy@uta.edu](mailto:leah.mccurdy@uta.edu), [erica.rousseau@uta.edu](mailto:erica.rousseau@uta.edu), [vanessa.garrett@uta.edu](mailto:vanessa.garrett@uta.edu).

Mechanism of Hairpin Vortex Formation by Liutex

Yifei Yu

Presented to the Faculty of the Graduate School of  
The University of Texas at Arlington in Partial Fulfillment  
of the Requirements  
for the Degree of

DOCTOR OF PHILOSOPHY

THE UNIVERSITY OF TEXAS AT ARLINGTON

May 2023

Copyright © by Yifei Yu 2023

All Rights Reserved



## Acknowledgements

Firstly, I am very grateful to my supervisor Dr. Chaoqun Liu, who is a kind, patient, and professional supervisor. He guided me how to do research with great responsibility during my five-year Ph.D. life. I could not achieve my Ph.D. degree without his help. I would like to express my gratefulness to Yisheng Gao, Yiqian Wang, Xiangrui Dong, Oscar Alvarez, Vishwa Patel and my other colleagues.

Also, I would like to thank my committee members, Dr. Yue Liu, Dr. Jianzhong Su, Dr. Benito Chen, and Dr. Habib Ahmari for their understanding, support and professional academic suggestions.

I would like to appreciate the Department of Mathematics for providing financial support through Graduate Teaching Assistantships and College of Science for awarding me Maverick Research Fellowship so that I can focus on my research.

Finally, I would like to express my deep gratitude to family members, Qinghua Hou, Xiaofeng Yu, Yue Yang and others for their unconditional sacrifice, support, love, encouragement and understanding.

May 10, 2023

## Abstract

### Mechanism of Hairpin Vortex Formation by Liutex

Yifei Yu, Ph.D.

The University of Texas at Arlington, 2023

Supervising Professor: Chaoqun Liu

Turbulence is still a mystery for human after more than one century's development of fluid dynamics. Hairpin vortex formation is regarded as an essential process for a laminar flow transition to the turbulent flow. A new correct third generation vortex identification method, Liutex, was proposed in 2018, which can represent local rotation direction and reveal the local angular speed correctly. Using this powerful tool, the mechanism of hairpin vortex formation is re-examined. This dissertation (1) explains the mechanism of hairpin vortex formation by solving Orr-Sommerfeld equation using Chebyshev spectrum method (2) observes the DNS result of flat plate boundary layer transition (3) develops objective Liutex (4) finds correlations between Liutex and other popular vortex identification methods (5) defines principal coordinate and principal decomposition (6) defines Liutex core line. Formation of hairpin vortex usually goes through three stages: (1) spanwise vortex (2)  $\Lambda$ -vortex (3) hairpin vortex. Spanwise vortex is formed because the Blasius solution has unstable 2D mode which is called Tollmien–Schlichting wave and this mode leads to the spanwise vortex. 3D mode enforced in DNS case is originally stable for Blasius solution profile, however, with the development of the flow, the base flow velocity profile is changed. Use the new

velocity profile as the base flow, we will find the 3D mode becomes unstable.  $\Lambda$ -vortex appears with the growth of the 3D perturbation. The “eject” and “sweep” motion of  $\Lambda$ -vortex generate strong shear region. This region is unstable and results in the hairpin vortex. The  $\Lambda$ -and hairpin vortex roll up since z-component of  $\text{Liutex}$  is positive. Principal decomposition decomposes velocity gradient tensor into parts with clear physical meanings. Objective  $\text{Liutex}$  can obtain  $\text{Liutex}$  structure in an inertial frame from the data collected in the non-inertial frames.  $\text{Liutex}$  core line method is threshold-free and provides a unique vortex structure. Correlation analysis between  $\text{Liutex}$  and other methods show other methods are contaminated by shear or stretching.

## Table of Contents

Acknowledgements .....	iii
Abstract.....	iv
List of Illustrations.....	ix
List of Tables .....	xiii
Chapter1 Introduction .....	1
Chapter2 Direct Numerical Simulation .....	9
2.1 Governing equations.....	10
2.2 Numerical Methods.....	12
2.3 DNS case set up.....	13
2.4 Code validation.....	15
2.5 Chapter Summary .....	16
Chapter 3 Three Generations of Vortex definitions and Identification methods .....	17
3.1 First- and second-generation methods.....	17
3.2 Common problems of the second-generation methods.....	21
3.3 Liutex—third generation method .....	21
3.4 Validation of Liutex.....	24
3.5 Liutex core lines .....	24
3.6 Principal coordinate and principal decomposition .....	26

3.7 Correlation between Liutex and some popular previous vortex identification methods ...	28
3.8 Chapter summary .....	29
Chapter 4 Objective Vortex.....	31
4.1 Galilean invariance .....	32
4.2 Objective Liutex.....	34
4.3 Numerical Examples.....	37
4.4 Chapter summary .....	41
Chapter 5 Stability theory .....	43
5.1 Orr-Sommerfeld equation .....	43
5.2 Solve Orr-Sommerfeld equation.....	46
5.3 Chapter summary .....	49
Chapter 6 Mechanism of Hairpin Vortex formation by Liutex .....	50
6.1 DNS result observation .....	50
6.2 Spanwise vortex formation.....	77
6.3 $\Lambda$ -vortex formation .....	81
6.4 Hairpin Vortex formation .....	84
6.5 Chapter summary .....	90
Chapter 7 Summary .....	91
Appendix Algorithm to find principal coordinate .....	93
Reference: .....	97

BIOGRAPHICAL INFORMATION ..... 103

## List of Illustrations

Figure 1-1 vortex region and vorticity lines.....	3
Figure 1-2 A side view of the Liutex core line for early transition stage .....	5
Figure 2-1 Physical domain of boundary layer flow transition.....	14
Figure 2-2 Schematics of coordinate transformation .....	15
Figure 2-3 Log-linear plots of the time-and spanwise-averaged velocity profile in wall unit .....	16
Figure 3-1 Couette flow .....	18
Figure 3-2 Coordinate transformation. ....	22
Figure 3-3 Liutex core lines of the plat plate boundary transition without iso-surface .....	25
Figure 3-4 Liutex core lines of the plat plate boundary transition with iso-surface .....	26
Figure 3-5 Correlations between Liutex and vorticity, $Q$ , $\lambda_{ci}$ , $\lambda_2$ and $\Delta$ .....	29
Figure 4-1 Streamline in the original coordinate system.....	31
Figure 4-2 Streamline in the moving coordinate system at the same velocity of the selected point .....	32
Figure 4-3 Relation between the velocity in the inertial and non-inertial frames .....	34
Figure 4-4 Vortex structure in the inertial original coordinate with Liutex=0.07 iso-surface (a) overall (b) from the top.....	38
Figure 4-5 Vortex structure in the observer's coordinate with Liutex=0.07 iso-surface (a) overall (b) from the top.....	39
Figure 4-6 Objective Vortex with Liutex=0.07 iso-surface (a) overall (b) from the top .....	40

Figure 4-7 Inertial, objective and non-inertial Liutex values at different x positions with $y=10$ and $z=0.5$ .....	41
Figure 6-1 spanwise vortices and Liutex magnitude distribution .....	50
Figure 6-2 distribution of $du/dz$ .....	51
Figure 6-3 distribution of $dw/dx$ .....	51
Figure 6-4 distribution of $w$ .....	52
Figure 6-5 Spanwise vortices and Liutex magnitude .....	52
Figure 6-6 Spanwise vortices with Liutex core lines .....	53
Figure 6-7 Contour of velocity at two spanwise slices ( $Sy_1$ and $Sy_2$ ) and seven streamwise slices ( $Sx_1\sim Sx_7$ ): (a) $u$ in slice $Sy_1$ and $Sy_2$ ; (b) $v$ in slice $Sy_1$ and $Sy_2$ ; (c) $w$ in slice $Sy_1$ and $Sy_2$ ; (d) $u$ in slice $Sx_1\sim Sy_2$ ; (e) $v$ in slice $Sx_1\sim Sy_2$ ; (f) $w$ slice in $Sx_1\sim Sy_2$ ; .....	56
Figure 6-8 Contour of velocity derivatives at two spanwise slices ( $Sy_1$ and $Sy_2$ ) and seven streamwise slices ( $Sx_1\sim Sx_7$ ): (a) derivatives of streamwise velocity in slice $Sy_1$ and $Sy_2$ ; (b) derivatives of spanwise velocity in slice $Sy_1$ and $Sy_2$ ; (c) derivatives of normal velocity in slice $Sy_1$ and $Sy_2$ ; (d) derivatives of streamwise velocity in slice $Sx_1\sim Sy_2$ ; (e) derivatives of spanwise velocity in slice $Sx_1\sim Sy_2$ ; (f) derivatives of normal velocity in slice $Sx_1\sim Sy_2$ ; .....	61
Figure 6-9 Typical shape of Ring like hairpin-vortex .....	62
Figure 6-10 Typical shape of Ring like hairpin-vortex packet .....	62
Figure 6-11 The distributions of flow parameters near the top of the $\Lambda$ -vortex head: (a) positions of slices; (b) streamtraces in the slices; (c) the distribution of streamwise velocity; (d) the distribution	

of normal velocity; (e) the derivative of streamwise velocity in the two slices; (f) the derivative of normal velocity in the two slices.....	68
Figure 6-12 The iso-surface of vortices and profiles of the three velocity components in plane across the first ring-like vortex at (a) $t=6.1T$ ; (b) $t=6.25T$ ; (c) $t=6.50$ . The black close curves are the cut section of iso-surface of ring-like vortex plotted by $\Omega=0.52$ .....	72
Figure 6-13 roll up of $\Lambda$ -vortex and hairpin vortex.....	73
Figure 6-14 roll up angle of $\Lambda$ -vortex and hairpin vortex .....	74
Figure 6-15 The growth of disturbance velocity along streamwise direction.....	75
Figure 6-16 The development of the maximum and minimum velocity in spanwise direction along streamwise.....	76
Figure 6-17 The development of the maximum and minimum velocity in normal direction along streamwise.....	76
Figure 6-18 Eigenvalues of 2D modes .....	77
Figure 6-19 Eigenfunction of the unstable 2D modes( $v=0$ ).....	78
Figure 6-20 Spanwise vortex direction.....	79
Figure 6-21 Eigenvalues of 3D modes at inlet.....	80
Figure 6-22 Eigenvalues of 3D modes at $x=400$ .....	81
Figure 6-23 Eigenfunctions of 3D modes at $x=400$ .....	81
Figure 6-24 Angle between $\Lambda$ -vortex and spanwise direction without iso-surface.....	83
Figure 6-25 Angle between $\Lambda$ -vortex and spanwise direction with iso-surface.....	84

Figure 6-26 shear region between two $\Lambda$ -vortices .....	85
Figure 6-27 Shear region between two $\Lambda$ -vortices (top view).....	86
Figure 6-28 Shear region between two $\Lambda$ -vortices (side view) .....	87
Figure 6-29 Modes at the shear region .....	88
Figure 6-30 Eigenfunctions of the unstable mode at shear region .....	88
Figure 6-31 $R_z$ distribution at the slice .....	89
Figure 8-1 Rotation around the z-axis.....	93
Figure 8-2 Rotation around the $y'$ -axis .....	94

List of Tables

Table 1 Geometry parameters .....	15
Table 2 Inflow parameters.....	15

## Chapter1

### Introduction

Vortex is a widely existing phenomenon in the world such as tornado, turbulence and star vortex in Galaxy. People usually intuitively recognize vortex as rotational motion of fluids, however, not until recently there is a rigorous vortex mathematical definition. Vortex was first defined by Helmholtz[1] as the vortex tubes and vortex filaments which are essentially vorticity tubes. We call the vorticity and vorticity related vortex identification methods as the first generation (G1). Vorticity method comes from the fact that vorticity does represent rotation for ideal rigid body. However, Gao et al.[2] found that vorticity actually is made up of rigid body rotation and shear deformation. There is no shear deformation for ideal rigid body, thus vorticity can reveal the rotation very well. However, when it comes to fluid for which shear deformation can exist, vorticity is no longer accurate especially in the region where there is strong shear. Yu et al.[3] did research on the correlation between Liutex[4, 5] (third generation method and will be introduced later) and some popular vortex identification methods including vorticity. It is found that in the boundary layer region where shear is strong, the correlation between Liutex and vorticity is weak but, in the region far away from the boundary where shear is small, the correlation is strong. G1 methods have been adopted by almost all textbooks for more than one century. It is pointed out by Nitsche[6] in the Encyclopedia of that “A vortex is commonly associated with the rotational motion of fluid around a common centerline. It is defined by the vorticity in the fluid which measures the rate of local fluid rotation”. Wu et al.[7] stated in their textbook that “vortex is a connected fluid region with high concentration of vorticity

compared with its surrounding”. In Ref [8], he gave a clearer definition that “a vortex is a vorticity tube surrounded by irrotational fluid”. However, many evidences showing vortex is not vorticity arouse scientists’ attention. In 1989, Robinson et al.[9] pointed out that “the association between regions of strong vorticity and actual vortices can be rather weak in the turbulent boundary layer, especially in the near wall region” Wang et al.[10] found that the vorticity lines are not align vortex regions and vorticity is even small inside vortex region but big outside as shown in Fig.1-1. Some counter examples can also be immediately provided. For the laminar channel flow whose analytical velocity profile is  $u(y) = 4y(1 - y)$ , it is easily to calculated out that vorticity is non-zero, but the streamlines are all parallel straight lines, and no vortex can be found. Around 1990s, researchers gradually recognized the problems of vorticity and started to find better vortex identification methods. In the trend of finding better vortex identification methods, some popular methods have been proposed including Q criterion[11],  $\Delta$  criterion[12],  $\lambda_2$  criterion[13],  $\lambda_{ci}$  criterion[14] and etc. These methods are classified as the second generation[4]. The appearance of the second-generation methods itself is a strong evidence that vortex is not vorticity as there is no need for human to develop new methods if vorticity works well. Although, these methods perform better than vorticity, they share some common problems. Firstly, they are all scalar methods which lose the important information about rotation axis. Secondly, the relation between the values provided by these methods and the real angular velocity is unclear, i.e., these methods reflect relative rotation strength. It is very common that for the same case, different second-generation methods can give vortex strengths with orders difference. Thirdly, to visualize the vortex, a threshold needs to be

chosen to draw the iso-surface. However, the choice of threshold is empirical and different threshold choice will lead to different conclusions on vortex for the same case. For example, if the threshold is big the vortex breaks down, but if the threshold is small, the vortex is continuous. Then, here comes the problem, the vortex indeed breaks down or not. Fourthly, the second-generation methods are not accurate and are more or less contaminated by shear or stretching/compression. A good vortex identification method should satisfy the following criteria simultaneously[15]:(1) absolute strength (2) relative strength (3) local rotational axis (4) vortex rotation (5) vortex core size and (6) vortex boundary. To overcome previously-mentioned drawbacks, Liutex[5], which is classified as the third generation method, was proposed by Liu et al. Liutex is a vector whose magnitude is twice angular speed and whose direction reveals the local rotation axis direction. Liutex represents pure rigid body rotation which is not contaminated by shear or stretching/compression.

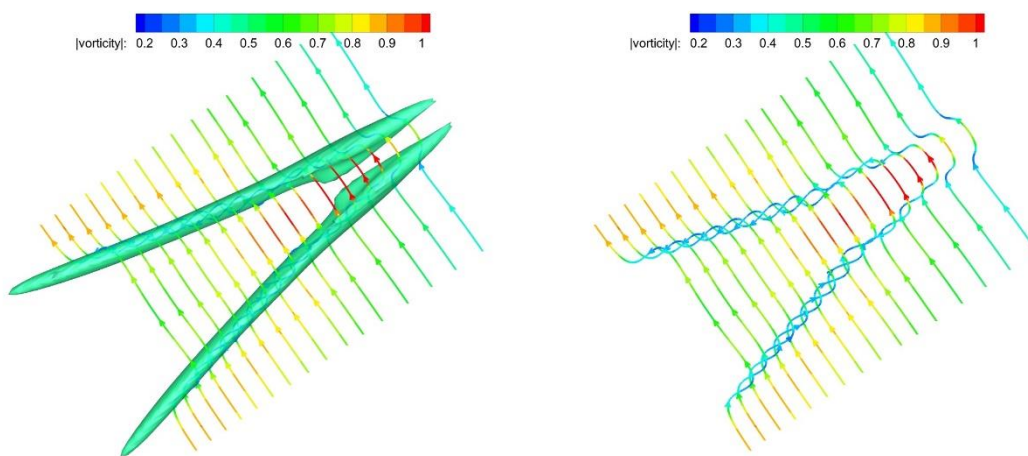


Figure 1-1 vortex region and vorticity lines[16]

The definition of Liutex direction (local rotation axis) comes from the basic idea that the local

rotation axis can only be stretched or compressed along its direction, i.e.,  $d\vec{v} = \text{grad}\vec{v} \cdot \vec{r} = \lambda\vec{r}$

where  $d\vec{v}$  is the velocity increment and  $\vec{r}$  is the local rotation axis. The definition of Liutex magnitude

comes from extracting rigid rotation part from the velocity gradient tensor and can be evaluated by

the following formula[17]:

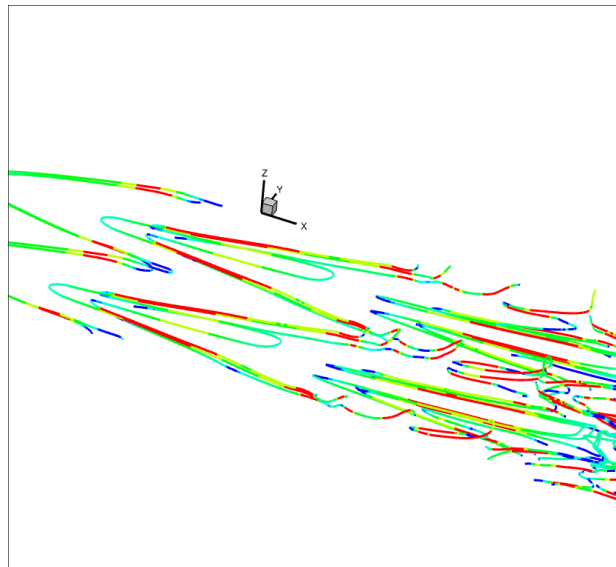
$$R = \vec{\omega} \cdot \vec{r} - \sqrt{(\vec{\omega} \cdot \vec{r})^2 - 4\lambda_{ci}^2}$$

Detailed explanation can be found in section 3. Apart from Liutex, some other progress has

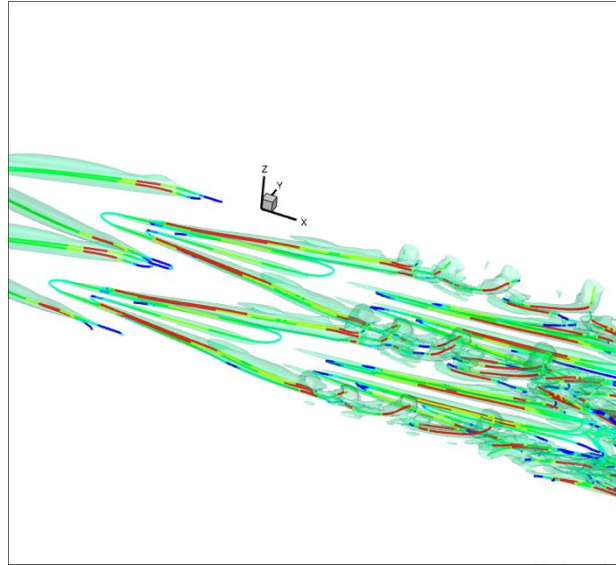
been made on vortex identification. Liutex core line method[18] can provide a unique vortex

structure which avoid choosing threshold. It shows the strength of vortex by different colors

meanwhile.



(a) without iso-surface



(b) with iso-surface

Figure 1-2 A side view of the Liutex core line for early transition stage

Although the Liutex core line method is currently best method to exhibit the vortex structure, people have not developed an ideal program to automatically draw Liutex core lines. Xu et al[19, 20] attempted to solve the problem by selecting seed points and achieved good success, but for different cases, parameters need to be adjusted. Right now, the most convenient vortex visualization is still by iso-surface. To avoid adjusting the threshold, modified Liutex-Omega method[21] which develops from Omega[22] method is proposed. Omega method is a scalar vortex identification method whose advantage is that the proper threshold for drawing iso-surface is always around 0.52. Considering the range of Omega method is  $[0.5,1]$ , it is much easier to find the proper threshold method compared to the second-generation methods. Liutex-Omega[21] method uses Liutex to remove the shear contamination from Omega method and yields a more accurate method at the same time keeps the original advantages.

Since the appearance of Liutex, many researchers have tested and analyzed Liutex method, and the correctness of Liutex definition has been repeatedly verified. Guo et al.[23] compared vortex predicted by Liutex and other methods based on the observation of a vortex evolution experiment result, and found that Liutex matches the experiment best. Cuissa[24] tested Liutex based on the Lamb-Oseen vortex which has analytical solution. He found that Liutex is the only one that correctly indicated the vortex region and the only one that coincides with the analytical rotational period. In the paper published in Space Science Reviews[25], it states that "*it (Liutex) is the only reliable quantity for the extraction of physical information about a vortex, such as the rotational period and the curvature radius*". Borisov et al.[26] from Russian Academy of Sciences used Liutex to analyze vortex structures in the supersonic flow around a tandem of wings.

After having the powerful tool for detecting vortex, we will revisit a classical topic in fluid dynamics, the mechanism of hairpin vortex formation which is an essential step for the laminar flow transition to turbulence. Turbulence is a natural phenomenon that can be widely observed, and most practical flows are turbulent. However, the mechanism of turbulence generation and development and the turbulence structure are still mysterious. Usually, people believe that flow transition from laminar to turbulent flow in a boundary layer includes four main stages: (i) receptivity, (ii) linear instability, (iii) non-linear growth, and (iv) vortex breakdown to turbulence. Many direct numerical simulation (DNS) results and experiments show that straight spanwise vortices appear first and then they are gradually distorted followed by the formation of  $\Lambda$ -vortex. After that, hairpin vortex will be formed and then the flow will become turbulence.

The most famous early study of laminar flow transition was conducted by Reynolds[27]. Reynolds did research on the transition of pipe flow and found the transition is highly related to  $\frac{\rho UL}{\mu}$  which is named as Reynolds number in memory of his extraordinary contribution. At that time, people commonly thought that inviscid dynamics governs the phenomena at high Reynolds number. In 1880, Lord Rayleigh[28] proposed the linear stability theorem for inviscid parallel flow which successfully explained the “roll-up” instability of inflectional shear flows but not yet solved the problem of wall-bounded flow, e.g., Blasius boundary-layer solution and Poiseuille flow. It is because viscosity which plays a necessary role in the instability was not taken into consideration. Taylor[29] perhaps first noticed this reason and Prandtl[30] emphasized it later. According to Rayleigh’s inviscid stability theory, existence of an inflection point is the necessary condition for plane-parallel shear flow to have unstable modes. However, experiments together with the observations from people’s daily life show that Poiseuille flow, pipe flow, which do not contain any inflection points, are unstable if their Reynolds number are sufficiently high. To find a more accurate instability theory, Orr[31] and Sommerfeld[32] developed the incompressible viscous stability theory which is called Orr-Sommerfeld equation by today’s scientists. Orr-Sommerfeld equation is not easy to solve. Even for the simplest flows, researchers faced huge difficulty to analyze Orr-Sommerfeld equation for the large Reynolds numbers at which transition occurs. To solve the Orr-Sommerfeld equation, Heisenberg[33], Schlichting[34], Lin[35] and others proposed complicated asymptotic techniques. With the development of computer technique and numerical methods, it is not difficult to get numerical solution of the Orr-Sommerfeld equation. Malik[36] proposed a fourth order compact scheme and successfully achieved high accuracy. Orszag[37] suggested using Chebyshev polynomial expansion and achieved good results as well.

In this dissertation, the author reviews the three generations of vortex identification methods and compares Liutex with other widely used methods, finding those methods are contaminated by shear or stretching/compression; the author develops principal coordinate and principal decomposition which can decomposes velocity gradient tensor into parts with clear physical meanings; the author participates in defining, as the auxiliary contributor, Liutex core line which is threshold free and can provide unique vortex structure; the author proposes the steps to obtain objective Liutex which can get Liutex structure in the inertial frame from non-inertial kinematic data; the author explains the mechanism of hairpin vortex formation.

This dissertation is organized as follows. In chapter 2, the direct numerical simulation (DNS) of flat plate boundary layer transition set up is introduced, including governing equations, numerical methods, and parameters. This DNS was done by Chen et al.[38] and Wang et al.[10], and its result will be used in the following chapters as the numerical example. Chapter 3 introduces three generations of vortex identification methods and exhibits the advantages of Liutex. In chapter 4, the method to obtain objective Liutex based on a zero-vorticity reference point is provided. Chapter 5 introduces stability theory and the way to solve the equation. The mechanism of hairpin vortex formation is explained in chapter 7. This dissertation content is summarized in chapter 7.

## Chapter2

### Direct Numerical Simulation

This chapter introduces the direct numerical simulation (DNS) of the flat plat boundary layer transition including the governing equations, numerical methods and code validation. This simulation was done by Chen[38] and Wang[10], and the author uses the result to do analysis in the following chapters. DNS is a computational technique used in fluid dynamics to numerically solve the Navier-Stokes equations, which describe the motion of viscous fluids such as water and air. In DNS, all small vortices are resolved by extremely small mesh sizes and small time steps and high order numerical schemes. For a simple problem, tens of millions grid points and millions of time steps are required. The equations are solved without any approximations or simplifications, making it a highly accurate and detailed method for studying fluid flows.

DNS involves discretizing the Navier-Stokes equations in space and time and solving them numerically on a computer. This requires high-performance computing resources and efficient algorithms to handle the large amount of data generated in the simulation.

DNS can provide detailed information on the flow field, including the velocity and pressure distributions, turbulence statistics, and the interaction between different fluid structures. This level of detail is particularly useful for understanding complex fluid phenomena such as turbulent flows, which are notoriously difficult to model and analyze using other techniques.

## 2.1 Governing equations

Navier-Stokes equations (N-S equation), which are a set of partial differential equations are the governing equations of fluid dynamics. These equations were first derived by Claude-Louis Navier and George Gabriel Stokes in the early 19<sup>th</sup> century, and therefore these equations are named after them. The 3D compressible N-S equations in curvilinear coordinates can be written in the following conservation form.

$$\frac{1}{J} \frac{\partial \mathbf{Q}}{\partial t} + \frac{\partial(\mathbf{E}-\mathbf{E}_v)}{\partial \xi} + \frac{\partial(\mathbf{F}-\mathbf{F}_v)}{\partial \eta} + \frac{\partial(\mathbf{H}-\mathbf{H}_v)}{\partial \zeta} = 0 \quad (2.1)$$

The vector of conserved quantities  $\mathbf{Q}$ , inviscid flux vector  $(\mathbf{E}, \mathbf{F}, \mathbf{H})$ , and viscous flux vector  $(\mathbf{E}_v, \mathbf{F}_v, \mathbf{H}_v)$  are defined as

$$\mathbf{Q} = \begin{pmatrix} \rho \\ \rho u \\ \rho v \\ \rho w \\ e \end{pmatrix} \quad (2.2)$$

$$\mathbf{E} = \frac{1}{J} \begin{pmatrix} \rho U \\ \rho u U + p \xi_x \\ \rho v U + p \xi_y \\ \rho w U + p \xi_z \\ (e + p)U \end{pmatrix} \quad (2.3)$$

$$\mathbf{F} = \frac{1}{J} \begin{pmatrix} \rho V \\ \rho u V + p \eta_x \\ \rho v V + p \eta_y \\ \rho w V + p \eta_z \\ (e + p)V \end{pmatrix} \quad (2.4)$$

$$\mathbf{H} = \frac{1}{J} \begin{pmatrix} \rho W \\ \rho u W + p \zeta_x \\ \rho v W + p \zeta_y \\ \rho w W + p \zeta_z \\ (e + p)W \end{pmatrix} \quad (2.5)$$

$$\mathbf{E}_v = \frac{1}{J} \begin{pmatrix} 0 \\ \tau_{xx} \xi_x + \tau_{yx} \xi_y + \tau_{zx} \xi_z \\ \tau_{xy} \xi_x + \tau_{yy} \xi_y + \tau_{zy} \xi_z \\ \tau_{xz} \xi_x + \tau_{yz} \xi_y + \tau_{zz} \xi_z \\ q_x \xi_x + q_y \xi_y + q_z \xi_z \end{pmatrix} \quad (2.6)$$

$$\mathbf{F}_v = \frac{1}{J} \begin{pmatrix} 0 \\ \tau_{xx}\eta_x + \tau_{yx}\eta_y + \tau_{zx}\eta_z \\ \tau_{xy}\eta_x + \tau_{yy}\eta_y + \tau_{zy}\eta_z \\ \tau_{xz}\eta_x + \tau_{yz}\eta_y + \tau_{zz}\eta_z \\ q_x\eta_x + q_y\eta_y + q_z\eta_z \end{pmatrix} \quad (2.7)$$

$$\mathbf{E}_v = \frac{1}{J} \begin{pmatrix} 0 \\ \tau_{xx}\zeta_x + \tau_{yx}\zeta_y + \tau_{zx}\zeta_z \\ \tau_{xy}\zeta_x + \tau_{yy}\zeta_y + \tau_{zy}\zeta_z \\ \tau_{xz}\zeta_x + \tau_{yz}\zeta_y + \tau_{zz}\zeta_z \\ q_x\zeta_x + q_y\zeta_y + q_z\zeta_z \end{pmatrix} \quad (2.8)$$

where  $J$  is the Jacobian of the coordinate transformation between the curvilinear  $(\xi, \eta, \zeta)$  and Cartesian frames  $(x, y, z)$ , and  $\xi_x, \xi_y, \xi_z, \eta_x, \eta_y, \eta_z, \zeta_x, \zeta_y, \zeta_z$  are coordinate transformation metrics. The contravariant velocity components  $(U, V, W)$  are defined as  $U = u\xi_x + v\xi_y + w\xi_z$ ,  $V = u\eta_x + v\eta_y + w\eta_z$ ,  $U = u\zeta_x + v\zeta_y + w\zeta_z$ .  $e$  is the total energy and defined as

$$e = \frac{p}{\gamma-1} + \frac{1}{2}(u^2 + v^2 + w^2) \quad (2.9)$$

The components of viscous stress and heat flux are denoted by  $\tau_{xx}, \tau_{yx}, \tau_{zx}, \tau_{xy}, \tau_{yy}, \tau_{zy}, \tau_{xz}, \tau_{yz}, \tau_{zz}$  and  $q_x, q_y, q_z$ , respectively. Their expressions are

$$q_x = u\tau_{xx} + v\tau_{xy} + w\tau_{xz} - \frac{1}{(\gamma-1)PrM_\infty^2} \frac{\mu(T)}{Re} \frac{\partial T}{\partial x} \quad (2.10)$$

$$q_y = u\tau_{xy} + v\tau_{yy} + w\tau_{yz} - \frac{1}{(\gamma-1)PrM_\infty^2} \frac{\mu(T)}{Re} \frac{\partial T}{\partial y} \quad (2.11)$$

$$q_z = u\tau_{xz} + v\tau_{yz} + w\tau_{zz} - \frac{1}{(\gamma-1)PrM_\infty^2} \frac{\mu(T)}{Re} \frac{\partial T}{\partial z} \quad (2.12)$$

$$\begin{aligned} \tau_{xx} = \frac{\mu(T)}{Re} [2 \left( \xi_x \frac{\partial u}{\partial \xi} + \eta_x \frac{\partial u}{\partial \eta} + \zeta_x \frac{\partial u}{\partial \zeta} \right) - \frac{2}{3} \left( \xi_x \frac{\partial u}{\partial \xi} + \xi_y \frac{\partial v}{\partial \xi} + \xi_z \frac{\partial w}{\partial \xi} + \eta_x \frac{\partial u}{\partial \eta} + \right. \\ \left. \eta_y \frac{\partial v}{\partial \eta} + \eta_z \frac{\partial w}{\partial \eta} + \zeta_x \frac{\partial u}{\partial \zeta} + \zeta_y \frac{\partial v}{\partial \zeta} + \zeta_z \frac{\partial w}{\partial \zeta} \right)] \end{aligned} \quad (2.13)$$

$$\begin{aligned} \tau_{yy} = \frac{\mu(T)}{Re} [2 \left( \xi_y \frac{\partial v}{\partial \xi} + \eta_y \frac{\partial v}{\partial \eta} + \zeta_y \frac{\partial v}{\partial \zeta} \right) - \frac{2}{3} \left( \xi_x \frac{\partial u}{\partial \xi} + \xi_y \frac{\partial v}{\partial \xi} + \xi_z \frac{\partial w}{\partial \xi} + \eta_x \frac{\partial u}{\partial \eta} + \right. \\ \left. \eta_y \frac{\partial v}{\partial \eta} + \eta_z \frac{\partial w}{\partial \eta} + \zeta_x \frac{\partial u}{\partial \zeta} + \zeta_y \frac{\partial v}{\partial \zeta} + \zeta_z \frac{\partial w}{\partial \zeta} \right)] \end{aligned} \quad (2.14)$$

$$\tau_{zz} = \frac{\mu(T)}{Re} [2 \left( \xi_z \frac{\partial w}{\partial \xi} + \eta_z \frac{\partial w}{\partial \eta} + \zeta_z \frac{\partial w}{\partial \zeta} \right) - \frac{2}{3} \left( \xi_x \frac{\partial u}{\partial \xi} + \xi_y \frac{\partial v}{\partial \xi} + \xi_z \frac{\partial w}{\partial \xi} + \eta_x \frac{\partial u}{\partial \eta} + \right.$$

$$\eta_y \frac{\partial v}{\partial \eta} + \eta_z \frac{\partial w}{\partial \eta} + \zeta_x \frac{\partial u}{\partial \zeta} + \zeta_y \frac{\partial v}{\partial \zeta} + \zeta_z \frac{\partial w}{\partial \zeta} \quad (2.15)$$

$$\tau_{xy} = \frac{\mu(T)}{Re} \left[ \xi_x \frac{\partial v}{\partial \xi} + \xi_y \frac{\partial u}{\partial \xi} + \eta_x \frac{\partial v}{\partial \eta} + \eta_y \frac{\partial u}{\partial \eta} + \zeta_x \frac{\partial v}{\partial \zeta} + \zeta_y \frac{\partial u}{\partial \zeta} \right] \quad (2.16)$$

$$\tau_{xz} = \frac{\mu(T)}{Re} \left[ \xi_x \frac{\partial w}{\partial \xi} + \xi_z \frac{\partial u}{\partial \xi} + \eta_x \frac{\partial w}{\partial \eta} + \eta_z \frac{\partial u}{\partial \eta} + \zeta_x \frac{\partial w}{\partial \zeta} + \zeta_z \frac{\partial u}{\partial \zeta} \right] \quad (2.17)$$

$$\tau_{yz} = \frac{\mu(T)}{Re} \left[ \xi_y \frac{\partial w}{\partial \xi} + \xi_z \frac{\partial v}{\partial \xi} + \eta_y \frac{\partial w}{\partial \eta} + \eta_z \frac{\partial v}{\partial \eta} + \zeta_y \frac{\partial w}{\partial \zeta} + \zeta_z \frac{\partial v}{\partial \zeta} \right] \quad (2.18)$$

For the purpose of dimensionless,  $\delta_{in}$ ,  $\rho_\infty$ ,  $U_\infty$ ,  $T_\infty$  and  $\rho_\infty U_\infty^2$  are reference values for length, density, velocity, temperature and pressure, where  $\delta_{in}$  is the inflow displacement thickness. Mach number  $M_\infty$ , Reynolds number  $Re$ , Prandtl number  $Pr$  and specific heat ratio  $\gamma$  are

$$M_\infty = \frac{U_\infty}{\sqrt{\gamma R T_\infty}} \quad (2.19)$$

$$Re = \frac{\rho_\infty U_\infty \delta_{in}}{\mu_\infty} \quad (2.20)$$

$$Pr = \frac{C_p \mu_\infty}{k_\infty} \quad (2.21)$$

$$\gamma = \frac{C_p}{C_v} \quad (2.22)$$

where  $R$  represents ideal gas constant,  $C_p$  and  $C_v$  represent Specific Heat at Constant Pressure and Specific Heat Capacity respectively. Viscosity coefficient is evaluated by Sutherland formula,

$$\mu = \frac{T^{\frac{3}{2}}(1+S)}{T+S} \quad (2.23)$$

where

$$S = \frac{110.3K}{T_\infty} \quad (2.24)$$

## 2.2 Numerical Methods

Compact schemes are able to achieve high order of accuracy with fewer grid points compared

to non-compact schemes. A sixth order compact scheme is used for the space discretization in the streamwise and wall normal directions. Lele[39] proposed a series of compact schemes which have the following general expressions,

$$\beta_- f'_{j-2} + \alpha_- f'_{j-1} + f'_j + \alpha_+ f'_{j+1} + \beta_+ f'_{j+2} = \frac{1}{h}(b_- f_{j-2} + a_- f_{j-1} + c f_j + a_+ f_{j+1} + b_+ f_{j+2}) \quad (2.25)$$

where  $f'_j$  are the derivative at point j. For the sixth order scheme used in this simulation,

$$\beta_- = 0, \alpha_- = \frac{1}{3}, \beta_+ = 0, \alpha_+ = \frac{1}{3}, b_- = -\frac{1}{36}, a_- = -\frac{7}{9}, a_+ = \frac{7}{9}, b_+ = \frac{1}{36} \quad (2.26)$$

In spanwise direction, the pseudo-spectral method is used because it has periodic boundary conditions in the spanwise direction and pseudo-spectral itself satisfies periodic conditions and can achieve higher accuracy.

For time discretization, a total variation diminishing (TVD) third order Runge-Kutta method is applied.

$$Q^{(0)} = Q^{(n)} \quad (2.27)$$

$$Q^{(1)} = Q^{(0)} + \Delta t R^{(0)} \quad (2.28)$$

$$Q^{(2)} = \frac{3}{4} Q^{(0)} + \frac{1}{4} Q^{(1)} + \frac{1}{4} \Delta t R^{(1)} \quad (2.29)$$

$$Q^{(n+1)} = \frac{1}{3} Q^{(0)} + \frac{2}{3} Q^{(2)} + \frac{2}{3} \Delta t R^2 \quad (2.30)$$

### 2.3 DNS case set up

The Direct Numerical Simulation method is used to study the process of the boundary layer flow transition on the plate plane. The physical domain and coordination system are illustrated in Fig. 2-1, where  $x_{in}$  represents the distance between leading edge of plate and inlet of physical simulation domain,  $L_x$  and  $L_y$  are the lengths of the computational domain in streamwise and spanwise directions

respectively, and  $L_{zin}$  is the height of the inlet. The details are listed in table 1. The dimension of grid is  $1920 \times 128 \times 241$  which is the number of grid points in streamwise, spanwise, and wall normal directions. The grid is stretched in the normal direction and uniform in the streamwise and spanwise directions. The length of the first layer of grid in the normal direction at the entrance is found to be 0.43 in wall units ( $z^+ = 0.43$ ). The Jacobian coordinate transformation is employed from the physical domain to the computational domain, as shown in Fig.2-2. The inflow parameters, including Mach number, Reynolds number, etc. are listed in table 2. At the wall boundary on the flat plate, adiabatic and non-slipping conditions are used. The non-reflecting boundary conditions are applied at the far field and the outflow boundaries. The inflow is given in the form of

$$q = q_{lam} + A_{t2d}q'_{2d} + A_{t3d}q'_{3d} \quad (2.31)$$

where  $q$  represents  $u, v, w, p$ ,  $u, v, w, p$ , and  $T$ , while  $q_{lam}$  is the Blasius solution for a two-dimensional laminar flat plate boundary layer.  $q'_{2d}$  and  $q'_{3d}$  are the 2-D and 3-D Tollmien-Schlichting (T-S) waves which are added into inflow as enforced perturbations.

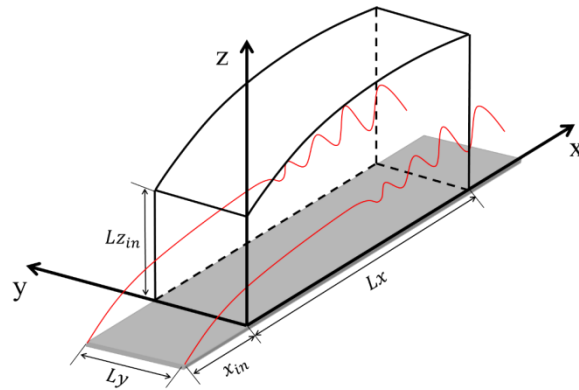


Figure 2-1 Physical domain of boundary layer flow transition simulation

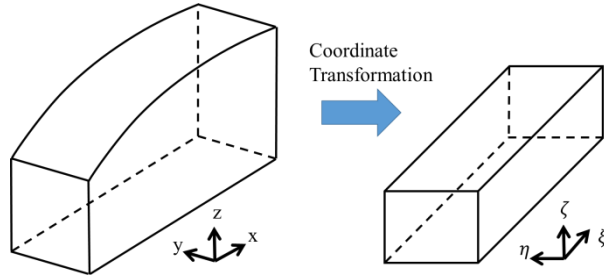


Figure 2-2 Schematics of coordinate transformation

$x_{in}$	$Lx$	$Ly$	$Lz_{in}$
$300.79\delta_{in}$	$798.03\delta_{in}$	$22\delta_{in}$	$40\delta_{in}$

Table 1 Geometry parameters

$M_{\infty}$	$Re$	$T_w$	$T_{\infty}$
0.5	1000	273.15K	273.15K

Table 2 Inflow parameters

## 2.4 Code validation

The DNS code, “DNSUTA”, has been validated by UTA researchers[38, 40, 41] and NASA Langley. And the detailed code validation has been reported by Liu et al.[42]. We only provide a brief code validation here. Fig. 2-3 shows the time and spanwise-averaged streamwise velocity distribution in two different grid levels with the log law result. This comparison shows the DNS result matches the log law and the grid convergence has been achieved.

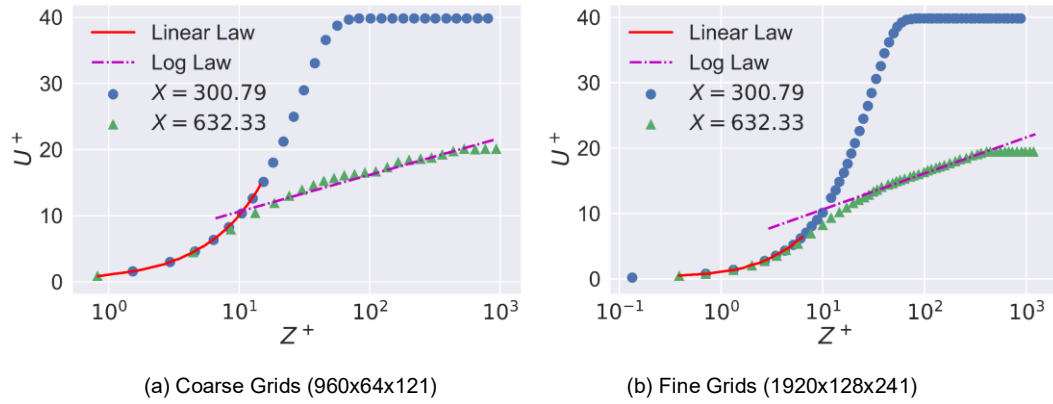


Figure 2-3 Log-linear plots of the time- and spanwise-averaged velocity profile in wall unit

## 2.5 Chapter Summary

This chapter is on the case set up of the DNS, including the governing equations, numerical methods and validation. Governing equations are the compressible N-S equations. Sixth order compact scheme and Runge-Kunnta method are used as the numerical methods for spatial discretization and time discretization respectively. Code validation shows the DNS result is reliable.

## Chapter 3

### Three Generations of Vortex definitions and Identification methods

This chapter is on vortex detection. It first introduces some existing popular vortex identification methods and the third-generation method—Liutex. After that, the correlations between these methods are exhibited which shows the first- and second-generation methods are contaminated by shear or stretching/compression. Principal coordinate and principal decomposition are proposed to find a decomposition of velocity gradient tensor that have clear physical meanings.

#### 3.1 First- and second-generation methods

Vorticity method is the first-generation vortex identification method.

**Definition 1:** The Vorticity vector  $rot\vec{v}$  is defined as:

$$rot\vec{v} = \nabla \times \vec{v} = \begin{bmatrix} \frac{\partial w}{\partial y} - \frac{\partial v}{\partial z} \\ \frac{\partial u}{\partial z} - \frac{\partial w}{\partial x} \\ \frac{\partial v}{\partial x} - \frac{\partial u}{\partial y} \end{bmatrix} \quad (3.1)$$

where  $\nabla$  represents Hamilton operator. Initially, people believe the direction of vorticity represents rotation direction and the magnitude of vorticity represents twice angular speed. Helmholtz first introduced the vorticity tube/filament concepts in 1858 and used them as measurements of vortices. He also gave the definitions of vortex lines and vortex filaments based on the vorticity vector. Vortex lines are the lines whose tangential direction at each point coincides with the direction of the rotation axis. Vortex filament is really an infinitesimal vorticity tube-like structure formed by vortex lines through all points of a closed circumference. Lamb[43] said, “If

through every point of a small, closed curve we draw the corresponding vortex-line, we mark out a tube known as vortex-tube.”

In practical applications, scientists and researchers found that vortices detected by vorticity do not match the actual situations very well. Robinson[44] reported that strong vorticity regions and actual vortices have weak correlations. Wang[10] observed a similar result that vorticity is small inside the  $\Lambda$ -vortex but big outside. Epps[45] found that vorticity may be unable to distinguish between a vortex region and a strong shear region. Some counterexamples that vorticity does not match the actual vortex can be immediately provided, e.g. the Couette flow. In a typical Couette flow, the flows are all straight lines without any curves. Apparently, there does not exist vortices, but vorticity is large if  $u$  is large. .

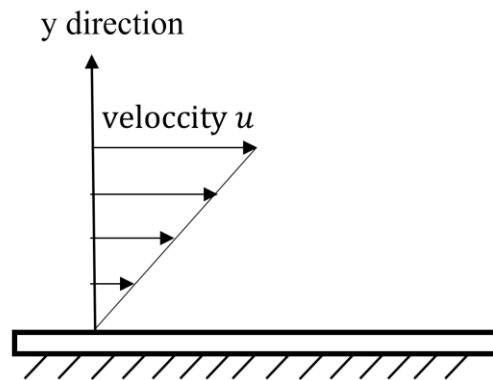


Figure 3-1 Couette flow

To find out more appropriate vortex identification methods, scientists developed the second-generation methods around 1990s.  $\Delta$  criterion[12], Q criterion[11] and  $\lambda_{ci}$  criterion[14] will be introduced in this section.

**Definition 1**( $\Delta$  criterion[12]): Let the characteristic equation of the velocity gradient tensor

$grad\vec{v}$  is in the following format.

$$\lambda^3 + I_1\lambda^2 + I_2\lambda + I_3 = 0 \quad (3.2)$$

where  $I_1$ ,  $I_2$ , and  $I_3$  represent the first, second, and third principal invariants of the characteristic equation respectively and have the following expressions.

$$I_1 = (\lambda_1 + \lambda_2 + \lambda_3) = tr(grad\vec{v}) \quad (3.3)$$

$$I_2 = \lambda_1\lambda_2 + \lambda_2\lambda_3 + \lambda_3\lambda_1 = -\frac{1}{2}[\text{tr}(grad\vec{v}^2) - \text{tr}(grad\vec{v})^2] \quad (3.4)$$

$$I_3 = \lambda_1\lambda_2\lambda_3 = \det(\nabla\vec{v}) \quad (3.5)$$

where  $\lambda_1, \lambda_2$  and  $\lambda_3$  are the eigenvalues of the Eq. (3.2).  $\Delta$  criterion is defined by

$$\Delta = \left(\frac{\tilde{Q}}{3}\right)^3 + \left(\frac{\tilde{R}}{2}\right)^2 \quad (3.6)$$

where

$$\tilde{Q} = I_2 - \frac{1}{3}I_1^2 \quad (3.7)$$

$$\tilde{R} = -I_3 - \frac{2}{27}I_1^3 + \frac{1}{3}I_1I_2 \quad (3.8)$$

If the  $\Delta > 0$ , it means the point is inside a vortex region.

**Definition 2**(Q criterion[11]): Q criterion is defined by

$$Q = \frac{1}{2}(\|B\|_F^2 - \|A\|_F^2) \quad (3.9)$$

where  $A$  and  $B$  refer to symmetric and anti-symmetric part of the velocity gradient tensor respectively.  $\|\cdot\|_F$  represents Frobenius norm.

$$A = \frac{1}{2}(grad\vec{v} + grad\vec{v}^T) = \begin{bmatrix} \frac{\partial u}{\partial x} & \frac{1}{2}\left(\frac{\partial u}{\partial y} + \frac{\partial v}{\partial x}\right) & \frac{1}{2}\left(\frac{\partial u}{\partial z} + \frac{\partial w}{\partial x}\right) \\ \frac{1}{2}\left(\frac{\partial v}{\partial x} + \frac{\partial u}{\partial y}\right) & \frac{\partial v}{\partial y} & \frac{1}{2}\left(\frac{\partial v}{\partial z} + \frac{\partial w}{\partial y}\right) \\ \frac{1}{2}\left(\frac{\partial w}{\partial x} + \frac{\partial u}{\partial z}\right) & \frac{1}{2}\left(\frac{\partial w}{\partial y} + \frac{\partial v}{\partial z}\right) & \frac{\partial w}{\partial z} \end{bmatrix} \quad (3.10)$$

$$B = \frac{1}{2}(\mathit{grad}\vec{v} - \mathit{grad}\vec{v}^T) = \begin{bmatrix} 0 & \frac{1}{2}\left(\frac{\partial u}{\partial y} - \frac{\partial v}{\partial x}\right) & \frac{1}{2}\left(\frac{\partial u}{\partial z} - \frac{\partial w}{\partial x}\right) \\ \frac{1}{2}\left(\frac{\partial v}{\partial x} - \frac{\partial u}{\partial y}\right) & 0 & \frac{1}{2}\left(\frac{\partial v}{\partial z} - \frac{\partial w}{\partial y}\right) \\ \frac{1}{2}\left(\frac{\partial w}{\partial x} - \frac{\partial u}{\partial z}\right) & \frac{1}{2}\left(\frac{\partial w}{\partial y} - \frac{\partial v}{\partial z}\right) & 0 \end{bmatrix} \quad (3.11)$$

For Q criterion,  $Q > 0$  implies the existence of vortices and the bigger Q is, the stronger vortex is. Q criterion realizes that vorticity is contaminated, and the contamination should be removed from vorticity. However,  $\|A\|_F^2$  used by Q criterion to estimate the contamination is not accurate. More detailed discussion can be found in section 3.7.

**Definition 3**( $\lambda_{ci}$  criterion[14]):  $\lambda_{ci}$  criterion defines the vortex strength by the imaginary part  $\lambda_{ci}$  of the complex eigenvalue of the velocity gradient tensor  $\mathit{grad}\vec{v}$ .

The definition of  $\lambda_{ci}$  criterion comes from the idea that time-frozen streamlines exhibit the flow structure if the velocity gradient tensor  $\mathit{grad}\vec{v}$  has a pair of conjugate complex eigenvalues and a real eigenvalue. Under such a situation,

$$\mathit{grad}\vec{v} = [\vec{v}_r \ \vec{v}_{cr} \ \vec{v}_{ci}] \begin{bmatrix} \lambda_r & 0 & 0 \\ 0 & \lambda_{cr} & \lambda_{ci} \\ 0 & -\lambda_{ci} & \lambda_{cr} \end{bmatrix} [\vec{v}_r \ \vec{v}_{cr} \ \vec{v}_{ci}]^{-1} \quad (3.12)$$

where  $\lambda_r, \vec{v}_r$  represent the real eigenvalue and corresponding real eigenvector,  $\lambda_{cr} \pm i\lambda_{ci}$  and  $\vec{v}_{cr} \pm i\vec{v}_{ci}$  are the pair of complex conjugate eigenvalues and corresponding eigenvectors. In the curvilinear coordinate system  $\{c_1, c_2, c_3\}$  spanned by  $\{\vec{v}_r, \vec{v}_{cr}, \vec{v}_{ci}\}$ , the streamlines' equations are

$$c_1(t) = c_1(0)e^{\lambda_r t} \quad (3.13)$$

$$c_2(t) = [c_2(0) \cos(\lambda_{ci}t) + c_3(0) \sin(\lambda_{ci}t)]e^{\lambda_{cr}t} \quad (3.14)$$

$$c_3(t) = [c_3(0) \cos(\lambda_{ci}t) + c_2(0) \sin(\lambda_{ci}t)]e^{\lambda_{cr}t} \quad (3.15)$$

Eq. (3.13)-(3.15) implies  $\lambda_{ci}$  indicates rotation strength.

$\lambda_{ci}$  criterion may not correctly reveal the strength of rotation because the translation made by Eq. (3.12) is a similar translation but not an orthogonal translation (eigenvectors are linearly independent but not orthogonal) which means the new space is distorted compared with the original one. And this distortion leads to the inaccuracy.

### 3.2 Common problems of the second-generation methods

Some problems of specific second-generation methods have been stated in section 3.1, and this section is on some common problems of these methods.

1. Although second-generation methods have their own theoretical foundation, the angular speed in the original coordinate system is still unclear. For the same case, the values of second-generation methods can vary greatly.
2. Second-generation methods are all scalars which do not included the information of rotation axis. Rotation axis is a vector and cannot be revealed from a scalar. Therefore, the only way to display the vortex structure is by iso-surface. Since the values of second-generation methods are scalars, visualization requires a threshold, and the thresholds chosen by different second-generation methods can be greatly different.
3. The values of second-generation methods are not pure rigid-rotation. They are more or less contaminated by shear or stretching/compression. Detailed can be found in section 3.7.

### 3.3 Liutex—third generation method

**Definition 4** (Liutex[5]): Liutex  $\vec{R} = R\vec{r}$  is a vector whose direction indicates the local rotation axis and whose magnitude is the twice angular speed. Its direction  $\vec{r}$  is the real eigenvector of the velocity gradient tensor  $grad\vec{v}$  that satisfies  $\vec{\omega} \cdot \vec{r} > 0$  where  $\vec{\omega}$  represents vorticity vector. Its magnitude[17] can be evaluated by

$$R = \vec{\omega} \cdot \vec{r} - \sqrt{(\vec{\omega} \cdot \vec{r})^2 - 4\lambda_{ci}^2} \quad (3.16)$$

where  $\lambda_{ci}$  is the imaginary part of the complex conjugate eigenvalues of  $grad\vec{v}$ .

Liutex direction comes from the basic idea that the velocity increment in the local rotation axis direction should be only stretching or compression, i.e.  $d\vec{v} = grad\vec{v} \cdot \vec{r} = \lambda\vec{r}$  which implies local rotation axis is the eigenvector of  $grad\vec{v}$ . One eigenvector can have positive or negative two direction, so to further constrain the local axis direction, the condition  $\vec{\omega} \cdot \vec{r} > 0$  is applied. As for the magnitude, it originally comes from finding the minimal rotation matrix among all possible coordinates systems. Since Liutex direction (local rotation axis) can be determined by finding the real eigenvector, a 3D rotation can be simplified to a 2D rotation by choosing a new coordinate system whose z-axis is parallel to the Liutex direction as shown in Fig. 3-2. Therefore, we discuss the Liutex strength in the 2D situation.

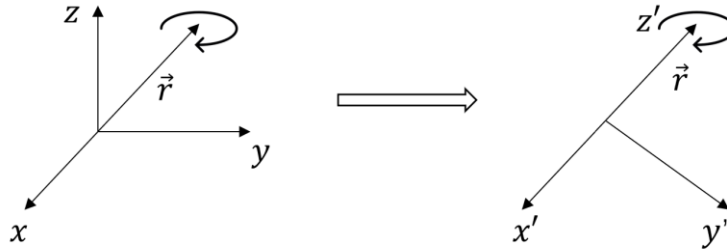


Figure 3-2 Coordinate transformation.

If a rigid body is doing rotation, its velocity distribution can be described as

$$\vec{v}(x, y) = \overline{AV} \times \vec{r} = \begin{bmatrix} (AV)_y z - (AV)_z y \\ (AV)_z x - (AV)_x z \end{bmatrix} \quad (3.17)$$

Here,  $\overline{AV}$  represents angular velocity vector. The reason not using the commonly used symbol  $\vec{\omega}$  for angular velocity is  $\vec{\omega}$  has been used for vorticity. Since the rotation is two dimensional, i.e.,  $(AV)_y = 0$ , the velocity distribution can be simplified to

$$\vec{v}(x, y) = \begin{bmatrix} -(AV)_z y \\ (AV)_z x \end{bmatrix} \quad (3.18)$$

Hence, the rigid rotation matrix is

$$\begin{bmatrix} \frac{\partial u}{\partial x} & \frac{\partial u}{\partial y} \\ \frac{\partial v}{\partial x} & \frac{\partial v}{\partial y} \end{bmatrix} = \begin{bmatrix} 0 & -(AV)_z \\ (AV)_z & 0 \end{bmatrix} \quad (3.19)$$

So, the typical feature for rotation matrix is diagonal entries being zeros and the other two entries are opposite numbers to each other. If the motion is pure rotation, then it is easy to figure out the angular speed directly from its velocity gradient tensor. The problem is that in practical, the motion is not pure rigid body rotation, and it can also have deformations for fluids. In this situation, people need to decompose the rigid rotation matrix from the velocity gradient tensor. Consider the following velocity distribution case.

$$\begin{cases} u = 2y \\ v = 0 \end{cases} \quad (3.20)$$

Its velocity gradient is

$$grad \vec{v} = \begin{bmatrix} 0 & 2 \\ 0 & 0 \end{bmatrix} \quad (3.21)$$

Apparently, it does not satisfy the feature of rigid body rotation matrix. One way to decompose the rigid body rotation matrix is what vorticity does.

$$grad \vec{v} = A + B \quad (3.22)$$

where A and B are defined by Eq. (3.10) and (3.11). In this case,

$$B = \begin{bmatrix} 0 & 1 \\ -1 & 0 \end{bmatrix} \quad (3.23)$$

which indicates the rotation strength by vorticity is 1. However, the flows are all straight without any curves and there should not be any vortex in it.

Liutex, on the other hand, decomposes  $grad\vec{v}$  by choosing the minimal of absolute values of the anti-diagonal elements, i.e.

$$grad\vec{v} = \begin{bmatrix} 0 & 0 \\ 0 & 0 \end{bmatrix} + \begin{bmatrix} 0 & 2 \\ 0 & 0 \end{bmatrix} \quad (3.24)$$

where  $\begin{bmatrix} 0 & 0 \\ 0 & 0 \end{bmatrix}$  is the rotation matrix. It indicates the rotation strength is zero which coincides with the physics. The expression of the velocity gradient matrix relies on the choice of coordinate systems. So, in reality, the minimal of the anti-diagonal entries can be different under different coordinate systems. In this situation, Liutex chooses the smallest one as the rotation strength and Liutex magnitude is set as the twice rotation strength. An explicit expression to evaluate Liutex magnitude was first proposed by Wang as shown in Eq. (3.16).

### 3.4 Validation of Liutex

After Liutex appears, it has been used and tested by various scientists and researchers. Guo et al.[23] compared Liutex and other vortex identification methods with an experimental result and found Liutex matches the vortex regions best. In Ref [46], Liutex is said as “the most reliable criterion for the extraction of physical information from vortical flows”. Cuissa et al.[24] tested Liutex by Lamb-Oseen vortex which has analytical solution. It shows Liutex exactly matches analytical solution. Borisov et al.[26] used Liutex to investigate vortex structure in the supersonic flow around a tandem of wings. A lot of applications have proven the correctness of Liutex.

### 3.5 Liutex core lines

Although, Liutex is a vector definition on rotation, it still needs iso-surface to display the vortex

structure. In this section, Liutex core line method[18] is developed which can provides the vortex core lines.

**Definition 5** (Liutex core line[18]): The Liutex core lines are defined as lines formed by points that satisfy the condition

$$\nabla R \times \vec{r} = 0, \quad R > 0 \quad (3.25)$$

where  $R$  and  $\vec{r}$  are Liutex magnitude and direction respectively.

The assumption of Liutex core lines is the rotation strength at the vortex core should be the largest in the plane perpendicular to the rotation axis. The necessary condition for a point being maximum in the plane is that the projection of its gradient to the plane has to be zero, or, in another word, its magnitude gradient direction can only be perpendicular to the plane. And we know the plane is perpendicular to the  $\vec{r}$ . Therefore, the gradient  $\nabla R$  has to be parallel to the  $\vec{r}$  as described by Eq. (3.25). Fig. 3-3 and 3-4 show the Liutex lines in a flat plate boundary layer DNS simulation.

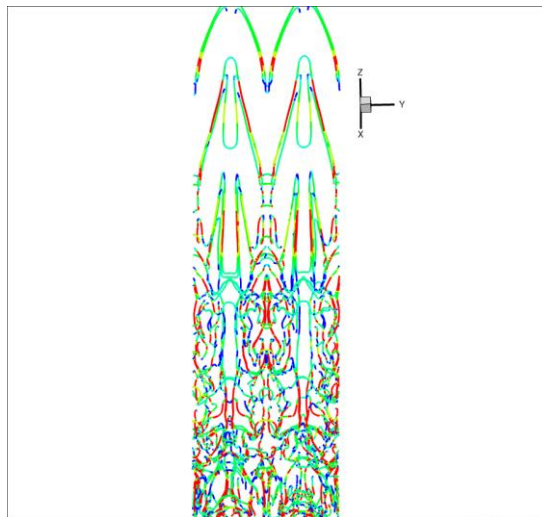


Figure 3-3 Liutex core lines of the plat plate boundary transition without iso-surface

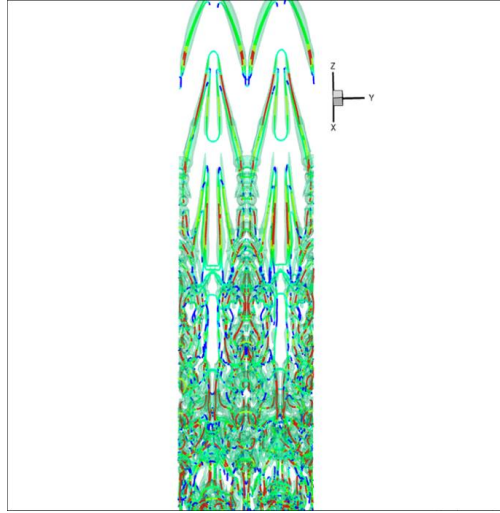


Figure 3-4 Liutex core lines of the plate boundary transition with iso-surface

### 3.6 Principal coordinate and principal decomposition

The traditional decomposition of the velocity gradient tensor is Cauchy-Stokes decomposition which decomposes velocity gradient tensor into symmetric part and anti-symmetric part. As shown in section 3.4, the physical meaning of Cauchy-Stokes decomposition actually is not as what people used to consider. To find a decomposition that can correctly represent rotation, shear and stretching/compression parts, principal coordinate and principal decomposition[47] are proposed.

**Definition 6**(principal coordinate[47]): Principal coordinate is the coordinate under which the minimal anti-diagonal entry described in section 3.4 can be achieved. It satisfies the following conditions.

1. Its Z-axis is parallel to the  $\vec{r}$  (direction of Liutex) and  $\vec{\omega} \cdot \vec{Z} > 0$
2. The velocity gradient tensor under this coordinate is in the form of:

$$grad\vec{v} = \begin{bmatrix} \lambda_{cr} & -\frac{R}{2} & 0 \\ \frac{\partial v}{\partial x} & \lambda_{cr} & 0 \\ \frac{\partial w}{\partial x} & \frac{\partial w}{\partial y} & \lambda_r \end{bmatrix} \quad (3.26)$$

where  $\lambda_{cr}$ ,  $\lambda_r$  and  $R$  are the real eigenvalue and real part of the conjugate complex eigenvalue pair of the velocity gradient tensor and Liutex magnitude, respectively, for rotation points.

$$3. \quad \frac{\partial u}{\partial y} < 0 \text{ and } \left| \frac{\partial u}{\partial y} \right| \leq \left| \frac{\partial v}{\partial x} \right|.$$

4. The rotational angle of the X-Y coordinates around the Z-axis must be smaller than  $90^\circ$  or  $-90^\circ < \theta \leq 90^\circ$

The algorithm to find principal coordinate can be found in appendix. The purpose to give principal matrix is to define a unique matrix for the velocity gradient tensor. A tensor is unique but its corresponding matrix is uncertain, depending on the coordinate systems.

Rewrite Eq.(3.26) in the following form.

$$grad\vec{v} = \begin{bmatrix} \lambda_{cr} & -\frac{1}{2}R & 0 \\ \frac{1}{2}R + \varepsilon & \lambda_{cr} & 0 \\ \xi & \eta & \lambda_r \end{bmatrix} \quad (3.27)$$

**Definition 7**(principal decomposition[47]): Principal decomposition is the decomposition in the principal decomposition s.t.

$$grad\vec{v} = \begin{bmatrix} \lambda_{cr} & -\frac{R}{2} & 0 \\ \frac{R}{2} + \varepsilon & \lambda_{cr} & 0 \\ \xi & \eta & \lambda_r \end{bmatrix} = \begin{bmatrix} 0 & -\frac{R}{2} & 0 \\ \frac{R}{2} & 0 & 0 \\ 0 & 0 & 0 \end{bmatrix} + \begin{bmatrix} 0 & 0 & 0 \\ \varepsilon & 0 & 0 \\ \xi & \eta & 0 \end{bmatrix} + \begin{bmatrix} \lambda_{cr} & 0 & 0 \\ 0 & \lambda_{cr} & 0 \\ 0 & 0 & \lambda_r \end{bmatrix} = R + S + C \quad (3.28)$$

Here  $R$ ,  $S$ ,  $C$  are matrices of rotation, shear and stretching/compression respectively.

### 3.7 Correlation between Liutex and some popular previous vortex identification methods

In the solid mechanics, people believe that the direction of vorticity is the rotation axis, and one half of the vorticity magnitude represents the rotation strength. According to the solid mechanics knowledge, the velocity  $\vec{v}$  of a fixed axis rotation can be expressed as

$$\vec{v} = \overline{AV} \times \vec{r} = \begin{bmatrix} (AV)_y z - (AV)_z y \\ (AV)_z x - (AV)_x z \\ (AV)_x y - (AV)_y x \end{bmatrix} \quad (3.29)$$

where  $\overline{AV}$  represents angular velocity vector. Vorticity  $\vec{\omega}$  can be written as

$$\vec{\omega} = \nabla \times \vec{v} = \begin{bmatrix} 2(AV)_x \\ 2(AV)_y \\ 2(AV)_z \end{bmatrix} = 2\overline{AV} \quad (3.30)$$

From the above derivation, people strongly believe that  $\vec{\omega}$  is the twice angular velocity vector and it has solid mathematical foundation. The problem is that in the above derivation the prerequisite is the velocity gradient tensors are the same at all the points which fluid do not satisfy. The case provided in section 3.4 shows vorticity can be contaminated by shear. Liutex magnitude formula can be understood as removing the shear contamination part  $\sqrt{(\vec{\omega} \cdot \vec{r})^2 - 4\lambda_{ci}^2}$  from the vorticity  $\vec{\omega} \cdot \vec{r}$ .

The expressions of vorticity,  $\Delta$  criterion, Q criterion and  $\lambda_{ci}$  criterion in the principal coordinate system can be written as

$$\Delta = \frac{1}{243} \left[ 9 \left( \frac{R}{2} \right)^3 \left( \frac{R}{2} + \varepsilon \right)^3 - 6 \left( \frac{R}{2} \right)^2 \left( \frac{R}{2} + \varepsilon \right)^2 (\lambda_{cr} - \lambda_r)^2 + \frac{5R}{2} \left( \frac{R}{2} + \varepsilon \right) (\lambda_{cr} - \lambda_r)^4 \right] \quad (3.31)$$

$$\vec{\omega} = \begin{bmatrix} \eta \\ -\xi \\ R + \varepsilon \end{bmatrix} \quad (3.32)$$

$$\|\vec{\omega}\| = \sqrt{\eta^2 + \xi^2 + (R + \varepsilon)^2} \quad (3.33)$$

$$Q = \frac{1}{2} (\|B\|_F^2 - \|A\|_F^2)$$

$$\begin{aligned}
&= \frac{1}{2} \left[ 2 \left( \frac{R}{2} + \frac{\varepsilon}{2} \right) + 2 \left( \frac{\xi}{2} \right)^2 + 2 \left( \frac{\eta}{2} \right)^2 \right] - \frac{1}{2} \left[ 2 \lambda_{cr}^2 + \lambda_r^2 + 2 \left( \frac{\varepsilon}{2} \right)^2 + 2 \left( \frac{\xi}{2} \right)^2 + 2 \left( \frac{\eta}{2} \right)^2 \right] \\
&= \left( \frac{R}{2} \right)^2 + \frac{1}{2} R \cdot \varepsilon - \lambda_{cr}^2 - \frac{1}{2} \lambda_r^2 \tag{3.34}
\end{aligned}$$

$$\lambda_{ci} = \sqrt{\frac{R}{2} \left( \frac{R}{2} + \varepsilon \right)} \tag{3.35}$$

Eq. (3.31)-(3.35) show that vorticity,  $\Delta$  criterion, Q criterion and  $\lambda_{ci}$  criterion contains elements in the shear, or stretching/compression matrices.

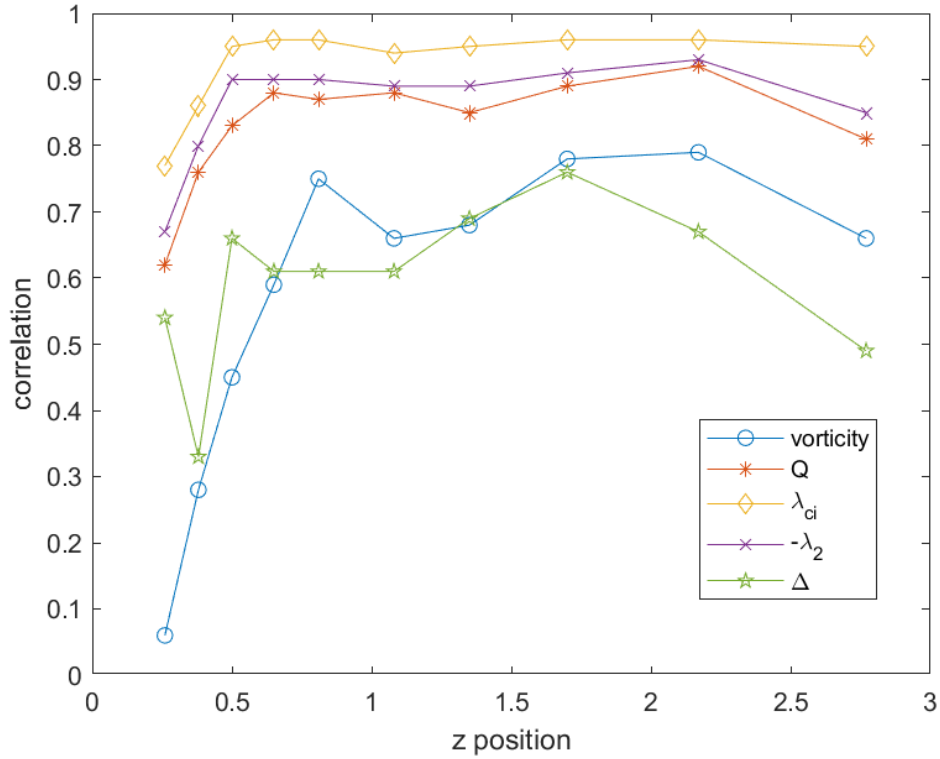


Figure 3-5 Correlations between Liutex and vorticity, Q,  $\lambda_{ci}$ ,  $\lambda_2$  and  $\Delta$  [3]

### 3.8 Chapter summary

In this chapter, first, second and third generation vortex identification methods are reviewed.

Why Liutex is reasonable is explained in section 3.4. Principal coordinate and principal decomposition are defined to decompose rotation, shear and stretching/compressing part from

velocity gradient tensor. It also exhibits the relations between Liutex and some other methods. The result shows first- and second-generation methods are contaminated by shear or stretching/compression.

## Chapter 4

### Objective Vortex

This chapter derives the steps to get Liutex in inertial frames from non-inertial data. This process is fully based on kinematics aspect and there is nothing related to dynamics involved. Objectivity refers to the ability to keep invariant under different coordinate systems. Most of the popular vortex identification methods are not objective. This may cause the confusion about the vortex structure which should be unique. For example, people intuitively reckon that curved streamlines reflect vortices. However, the shape of streamlines depends on the choice of the coordinates. Streamlines can look like a straight line in one coordinate system and have obvious spiral shape in the other. As shown in Fig.4-1 and 4-2, the two coordinates are the same except the one in Fig. 4-2 is doing translation motion at the velocity of the selected point.

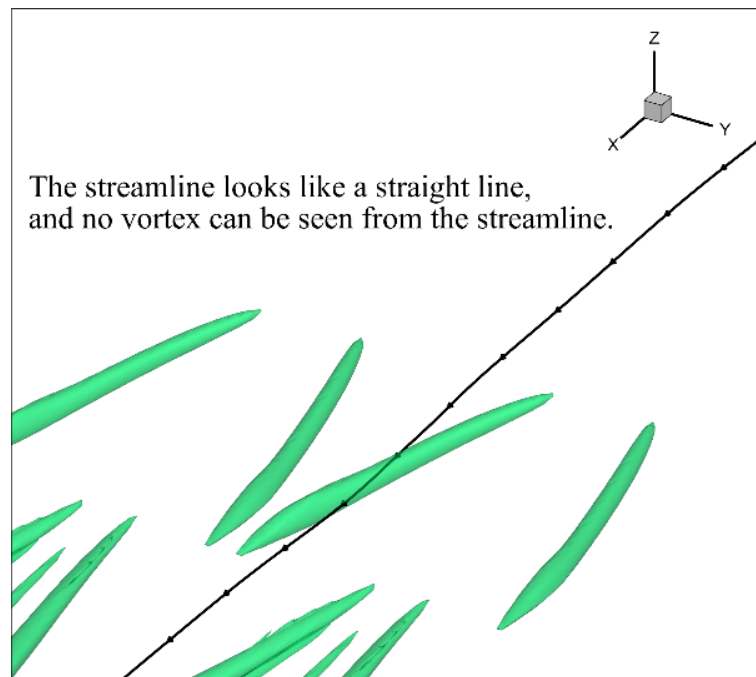


Figure 4-1 Streamline in the original coordinate system

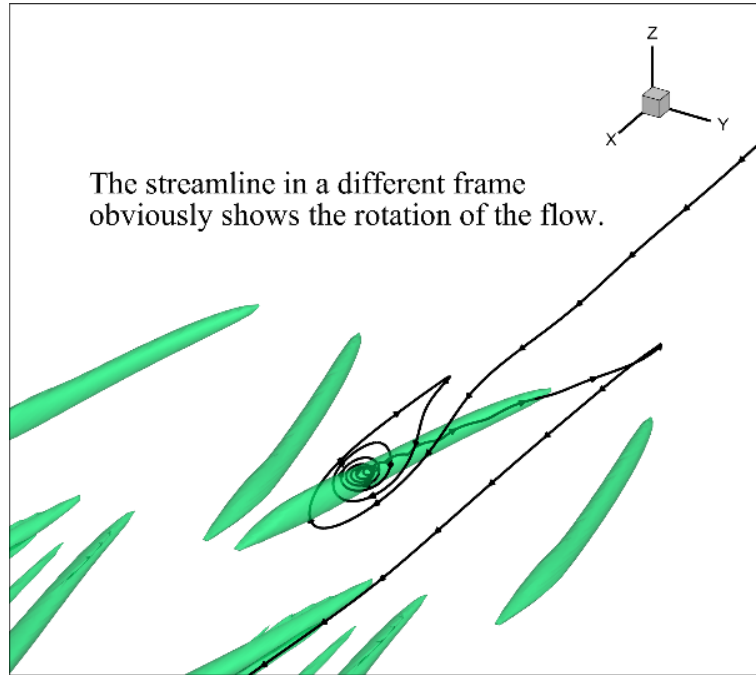


Figure 4-2 Streamline in the moving coordinate system at the same velocity of the selected point

Similar situation happens to other vortex identification methods. Unfortunately, Liutex is not objective as well although it is Galilean invariant which means it is invariant under initial coordinate systems. To eliminate the influence of coordinate systems, this chapter introduces a method to obtain objective Liutex. In section 4.1, it first shows that Liutex is Galilean invariant. Next the question can be simplified to how to find Liutex in any one inertial coordinate system from the data collected in the non-inertial coordinate system.

#### 4.1 Galilean invariance

Wang proves the Galilean invariance of Liutex[48] in 2018. The Galilean transformation between two inertial frames is

$$\begin{bmatrix} x' \\ y' \\ z' \end{bmatrix} = Q_c \begin{bmatrix} x \\ y \\ z \end{bmatrix} + \vec{c}_1 t + \vec{c}_2 \quad (4.1)$$

where  $Q_c$  is an orthogonal  $3 \times 3$  matrix,  $x, y, z$  are the coordinates in one inertial frame and  $x', y', z'$  are the coordinates in another inertial frame. For simplicity, we assume the time variable is identical for these two frames. So, the velocities in these two frames have the following relation.

$$\begin{bmatrix} u' \\ v' \\ w' \end{bmatrix} = Q_c \begin{bmatrix} u \\ v \\ w \end{bmatrix} + \vec{c}_1 \quad (4.2)$$

where  $u, v, w$  and  $u', v', w'$  are the velocity components in the two frames. Eq. (4.2) implies

$$grad\vec{v}' = Q_c(grad\vec{v})Q_c^{-1} \quad (4.3)$$

where  $grad\vec{v}$  and  $grad\vec{v}'$  are the velocity gradient tensor in the two frames.

Let  $\vec{r}$  be the Liutex direction vector, so

$$grad\vec{v} \cdot \vec{r} = \lambda_r \vec{r} \quad (4.4)$$

$$Q_c(grad\vec{v}) \cdot \vec{r} = Q_c(grad\vec{v})(Q_c^{-1}Q_c) \cdot \vec{r} = [Q_c(grad\vec{v})Q_c^{-1}] \cdot (Q_c\vec{r}) = grad\vec{v}' \cdot (Q_c\vec{r}) \quad (4.5)$$

Substitute Eq. (4.4) into Eq. (4.5)

$$grad\vec{v}' \cdot (Q_c\vec{r}) = \lambda_r(Q_c\vec{r}) \quad (4.6)$$

which indicates  $Q_c\vec{r}$  is the Liutex direction in the other inertial frame.

Suppose

$$\vec{r} = \begin{bmatrix} x_1 \\ y_1 \\ z_1 \end{bmatrix} - \begin{bmatrix} x_0 \\ y_0 \\ z_0 \end{bmatrix} \quad (4.7)$$

And the corresponding vector  $\vec{r}'$  after Galilean invariant is

$$\vec{r}' = \left( Q_c \begin{bmatrix} x_1 \\ y_1 \\ z_1 \end{bmatrix} + \vec{c}_1 t + \vec{c}_2 \right) - \left( Q_c \begin{bmatrix} x_0 \\ y_0 \\ z_0 \end{bmatrix} + \vec{c}_1 t + \vec{c}_2 \right) \quad (4.9)$$

$$\vec{r}' = Q_c \left( \begin{bmatrix} x_1 \\ y_1 \\ z_1 \end{bmatrix} - \begin{bmatrix} x_0 \\ y_0 \\ z_0 \end{bmatrix} \right) \quad (4.10)$$

$$\vec{r}' = Q_c \vec{r} \quad (4.11)$$

So,  $Q_c \vec{r}$  is the corresponding vector after Galilean transformation and Liutex direction is Galilean invariant. As for the Liutex magnitude, it is Galilean invariant as well since all elements in Eq. (3.16) are Galilean invariant.

Therefore, both direction and magnitude of Liutex are Galilean invariant.

#### 4.2 Objective Liutex

Let upper-case letters denote the variables in the inertial frame and lower-case letters denote the variables in the non-inertial frame. Based on the knowledge of kinetics,  $\vec{V}$  and  $\vec{v}$  have the following relation (see Fig.4-3),

$$\vec{V}(\vec{P}) = \vec{v}(\vec{p}) + \vec{V}_t(t) + \vec{V}_a(t) \times \vec{p} \quad (4.12)$$

where  $\vec{V}, \vec{P}, \vec{V}_t, \vec{V}_a$  are the velocity vector, position vector, translation velocity of the non-inertial frame and the angular velocity of the non-inertial frame in the inertial frame, respectively.  $\vec{v}, \vec{p}$  are the velocity vector and position vector in the non-inertial frame.

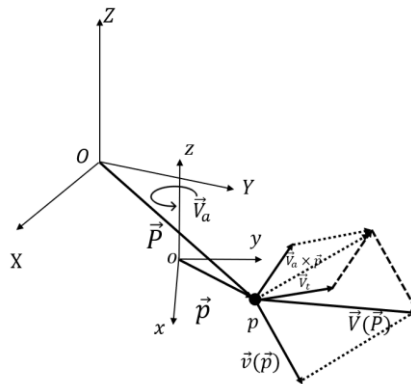


Figure 4-3 Relation between the velocity in the inertial and non-inertial frames

Since our purpose is to find the Liutex in any one inertial frame, a special inertial frame can be

chosen to simplify the calculation. Let the origin point and the X, Y, Z axes of the special coordinate system be the same as the non-inertial coordinate system, and the special coordinate system is doing the same translation motion as the non-inertial coordinate system. In short, the only difference between these two frames is the non-inertial frame can do rotation but the inertial one cannot. In this case,  $\vec{V}_t = 0$  and  $\vec{P} = \vec{p}$ . The Eq. (4.12) can be simplified to

$$\vec{V}(\vec{P}) = \vec{v}(\vec{P}) + \vec{V}_a(t) \times \vec{P} \quad (4.13)$$

which can be rewritten as

$$\begin{bmatrix} U \\ V \\ W \end{bmatrix} = \begin{bmatrix} u \\ v \\ w \end{bmatrix} + \begin{bmatrix} V_{ay}Z - V_{az}Y \\ V_{az}X - V_{ax}Z \\ V_{ax}Y - V_{ay}X \end{bmatrix} \quad (4.14)$$

Take partial derivatives with respect to  $\vec{X}(\vec{x})$

$$\begin{bmatrix} \frac{\partial U}{\partial X} \\ \frac{\partial V}{\partial X} \\ \frac{\partial W}{\partial X} \end{bmatrix} = \begin{bmatrix} \frac{\partial u}{\partial x} \\ \frac{\partial v}{\partial x} \\ \frac{\partial w}{\partial x} \end{bmatrix} + \begin{bmatrix} 0 \\ V_{az} \\ -V_{ay} \end{bmatrix} \quad (4.15)$$

Similarly,

$$\begin{bmatrix} \frac{\partial U}{\partial Y} \\ \frac{\partial V}{\partial Y} \\ \frac{\partial W}{\partial Y} \end{bmatrix} = \begin{bmatrix} \frac{\partial u}{\partial y} \\ \frac{\partial v}{\partial y} \\ \frac{\partial w}{\partial y} \end{bmatrix} + \begin{bmatrix} -V_{az} \\ 0 \\ V_{ax} \end{bmatrix} \quad (4.16)$$

$$\begin{bmatrix} \frac{\partial U}{\partial Z} \\ \frac{\partial V}{\partial Z} \\ \frac{\partial W}{\partial Z} \end{bmatrix} = \begin{bmatrix} \frac{\partial u}{\partial z} \\ \frac{\partial v}{\partial z} \\ \frac{\partial w}{\partial z} \end{bmatrix} + \begin{bmatrix} V_{ay} \\ -V_{ax} \\ 0 \end{bmatrix} \quad (4.17)$$

Therefore, the velocity gradient tensors in the inertial and non-inertial frames have the following relation.

$$\begin{bmatrix} \frac{\partial U}{\partial X} & \frac{\partial U}{\partial Y} & \frac{\partial U}{\partial Z} \\ \frac{\partial V}{\partial X} & \frac{\partial V}{\partial Y} & \frac{\partial V}{\partial Z} \\ \frac{\partial W}{\partial X} & \frac{\partial W}{\partial Y} & \frac{\partial W}{\partial Z} \end{bmatrix} = \begin{bmatrix} \frac{\partial u}{\partial x} & \frac{\partial u}{\partial y} & \frac{\partial u}{\partial z} \\ \frac{\partial v}{\partial x} & \frac{\partial v}{\partial y} & \frac{\partial v}{\partial z} \\ \frac{\partial w}{\partial x} & \frac{\partial w}{\partial y} & \frac{\partial w}{\partial z} \end{bmatrix} + \begin{bmatrix} 0 & -V_{az} & V_{ay} \\ V_{az} & 0 & -V_{ax} \\ -V_{ay} & V_{ax} & 0 \end{bmatrix} \quad (4.18)$$

where  $\vec{V}_a = V_{ax}\vec{X} + V_{ay}\vec{Y} + V_{az}\vec{Z}$  is the angular velocity of the non-inertial frame measured in the inertial coordinate.

It is noted that  $V_{ax}, V_{ay}$  and  $V_{az}$  do not rely on  $X, Y, Z$  since one non-inertial frame can only have one angular velocity. So, if  $V_{ax}, V_{ay}$  and  $V_{az}$  can be found from one single point, their values can be used for the whole space. The method to obtain objective Liutex comes from this idea. A zero-vorticity reference point will be selected to find out  $V_{ax}, V_{ay}$  and  $V_{az}$ .

Theorem 1: If  $\vec{P}$ , in the special inertial frame described above, is the point corresponding to  $\vec{p}$  s.t. vorticity of  $\vec{P}$  measured in the inertial frame is zero, then  $[V_{ax}, V_{ay}, V_{az}]^T = -\frac{1}{2} [\omega_x, \omega_y, \omega_z]^T$  where  $\omega_x, \omega_y, \omega_z$  are the vorticity components of  $\vec{p}$ , which is measured in the observer's frame..

Proof: Decompose  $grad\vec{V}$  into symmetric  $A$  and antisymmetric part  $B$ ,

$$grad\vec{V} = A + B \quad (4.19)$$

where

$$A = \frac{1}{2} [grad\vec{V} + (grad\vec{V})^T] \quad (4.20)$$

$$B = \frac{1}{2} [grad\vec{V} - (grad\vec{V})^T] \quad (4.21)$$

$B$  is a zero matrix because the vorticity is zero at the point.

Substitute Eq. (4.19) into Eq. (4.18)

$$A = grad\vec{v} + \begin{bmatrix} 0 & -V_{az} & V_{ay} \\ V_{az} & 0 & -V_{ax} \\ -V_{ay} & V_{ax} & 0 \end{bmatrix} \quad (4.22)$$

$$\text{grad}\vec{v} = A - \begin{bmatrix} 0 & -V_{az} & V_{ay} \\ V_{az} & 0 & -V_{ax} \\ -V_{ay} & V_{ax} & 0 \end{bmatrix} = A + \begin{bmatrix} 0 & V_{az} & -V_{ay} \\ -V_{az} & 0 & V_{ax} \\ V_{ay} & -V_{ax} & 0 \end{bmatrix} \quad (4.23)$$

Obviously,  $\begin{bmatrix} 0 & V_{az} & -V_{ay} \\ -V_{az} & 0 & V_{ax} \\ V_{ay} & -V_{ax} & 0 \end{bmatrix}$  is the vorticity matrix measured in the observer's coordinate

since  $A$  is a symmetric matrix. Thus,

$$\begin{bmatrix} V_{ax} \\ V_{ay} \\ V_{az} \end{bmatrix} = -\frac{1}{2} \begin{bmatrix} \omega_x \\ \omega_y \\ \omega_z \end{bmatrix} \quad (4.24)$$

where  $\omega_x, \omega_y, \omega_z$  are the vorticity components of  $\vec{p}$ . The theorem is proved.

Steps to obtain objective Liutex:

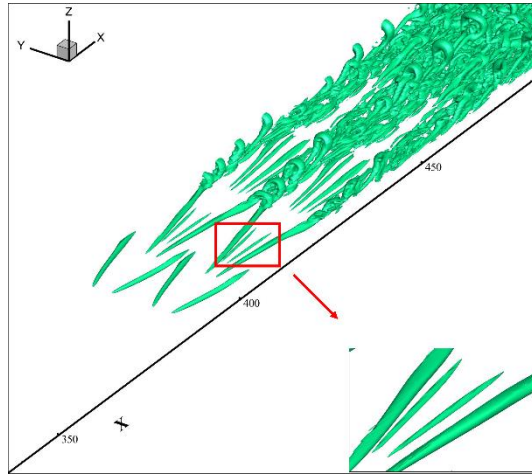
1. Pick a point with zero vorticity measured in the inertial frame. The point can be selected based on physical properties of the flow e.g., points in the inviscid region.
2. Calculate vorticity at the selected reference point. Then  $[V_{ax}, V_{ay}, V_{az}]^T = -\frac{1}{2} [\omega_x, \omega_y, \omega_z]^T$ .
3. The velocity gradient tensor of all points in an inertial coordinate can be obtained from

$$\text{grad}\vec{V} = \text{grad}\vec{v} + \begin{bmatrix} 0 & -V_{az} & V_{ay} \\ V_{az} & 0 & -V_{ax} \\ -V_{ay} & V_{ax} & 0 \end{bmatrix} \quad (4.25)$$

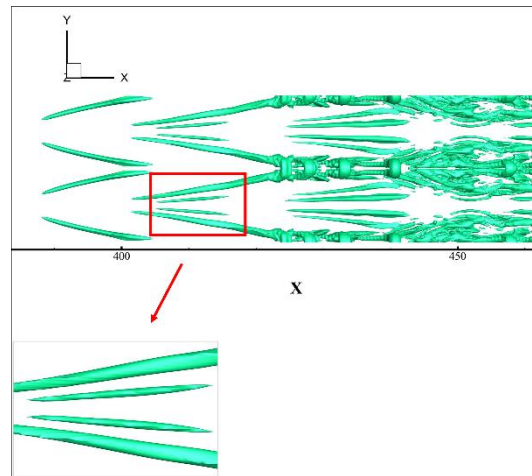
4. Calculate Liutex from  $\text{grad}\vec{V}$ , which is objective or coordinate-independent, no matter the observer's frame is inertial or non-inertial, which is particularly important for aerial survey or satellite measurement.

### 4.3 Numerical Examples

The DNS result in Chapter 2 is used to test provided objective Liutex method. The vortex structure in the original inertial frame shown by Liutex iso-surface is shown in Fig. 4-4.



(a)

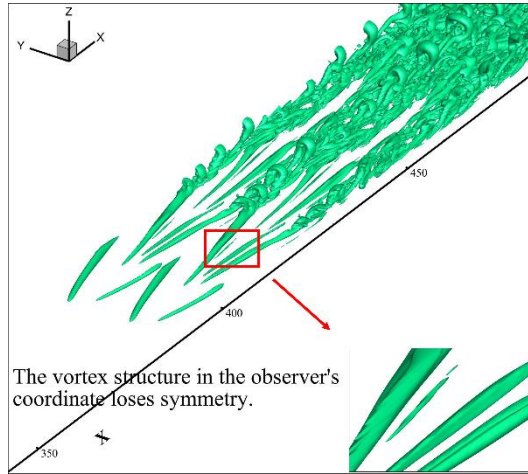


(b)

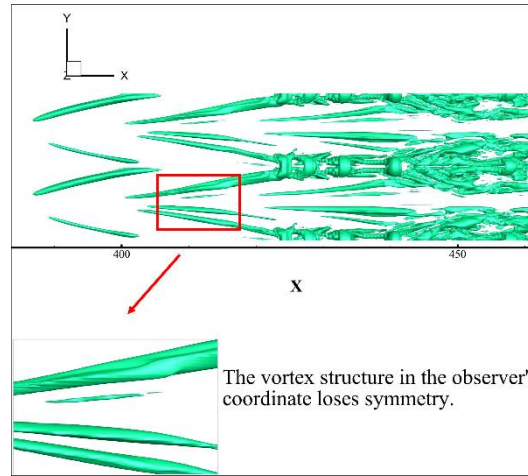
Figure 4-4 Vortex structure in the inertial original coordinate with Liutex=0.07 iso-surface (a) overall (b) from the top

We artificially apply an angular velocity  $\vec{V}_a = [0.009 \quad 0.008 \quad 0.007]^T$  and generate a new non-

inertial data. The Liutex iso-surface in the non-inertial frame is shown in Fig. 4-5. The vortex



(a)



(b)

Figure 4-5 Vortex structure in the observer's coordinate with  $Liutex=0.07$  iso-surface (a) overall (b) from the top structure loses symmetry in the non-inertial frame while in the inertial frame, it has symmetry.

The vorticity of the reference point  $(456.38, 20.62, 13.36)$  is

$[-0.0179999905974 \quad -0.0159999989568 \quad -0.0140000715749]^T$ . Based on Eq. (4.24), the

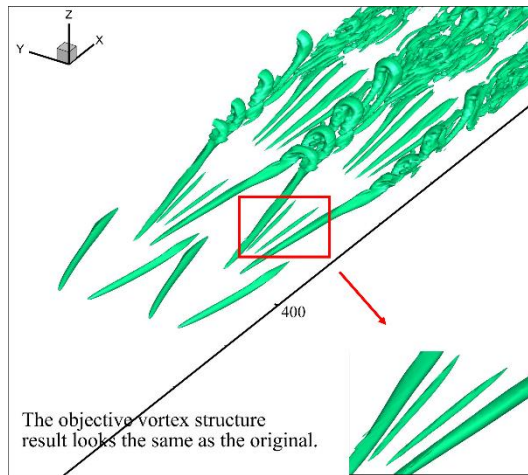
angular velocity of the non-inertial frame is

$$\begin{bmatrix} V_{ax} \\ V_{ay} \\ V_{az} \end{bmatrix} = -\frac{1}{2} \begin{bmatrix} -0.0179999905974 \\ -0.0159999989568 \\ -0.0140000715749 \end{bmatrix} = \begin{bmatrix} 0.0089999952986874916 \\ 0.0079999994783875872 \\ 0.0070000357874608187 \end{bmatrix} \quad (4.26)$$

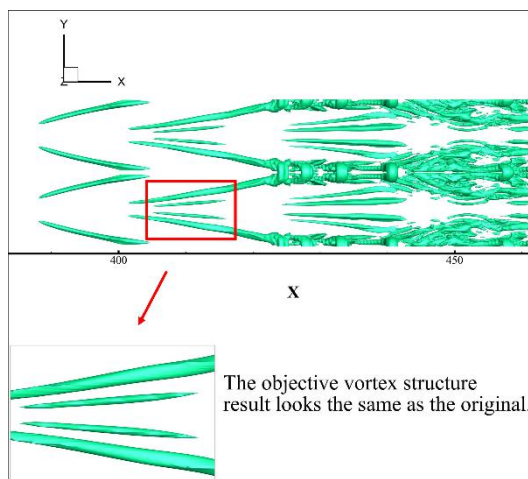
which is very close to the actual angular velocity.

The apply step 3 and step 4 in section 4.4 and get the objective Liutex iso-surface shown in

Fig. 4-6.



(a)



(b)

Figure 4-6 Objective Vortex with Liutex=0.07 iso-surface (a) overall (b) from the top

Compared with the original inertial Liutex iso-surface in Fig.4-4, the objective Liutex looks the same. Objective Liutex gets back the symmetry which is lost in the non-inertial frame. To further

analyze this method quantitatively, ten points are selected to compare their Liutex magnitudes. These points are located at  $y=10$  and  $z=0.5$  from 400 to 500 with step 10. The result is shown in Fig. 4-7.

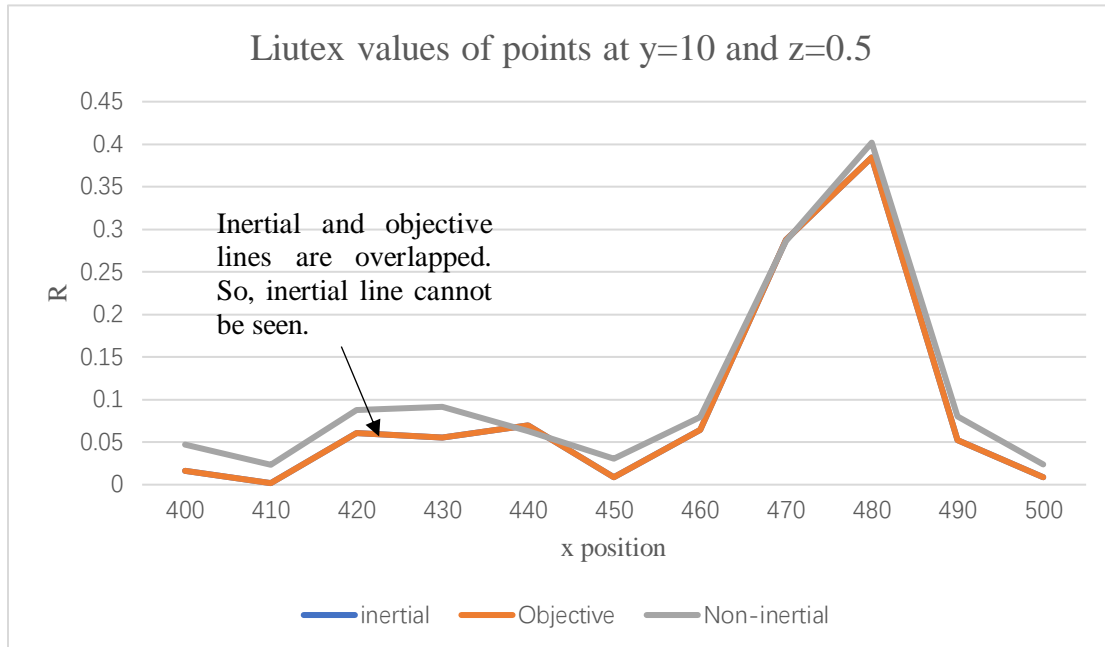


Figure 4-7 Inertial, objective and non-inertial Liutex values at different x positions with  $y=10$  and  $z=0.5$

The inertial line and the objective Liutex line are overlapped which exhibits the accuracy of the proposed objective Liutex method.

#### 4.4 Chapter summary

This chapter derives steps to obtain objective Liutex from kinematic aspect. The basic idea is Liutex itself is a Galilean invariant variable which means it is invariant in all inertial frames. Then the problem is simplified to how to find Liutex in any one inertial frame from the data in the non-inertial frame. For simplicity, a special inertial frame is chosen s.t. the only difference between it and the non-inertial frame is the special inertial frame does not do rotation. Then the angular

velocity of the non-inertial frame can be evaluated through  $[V_{ax}, V_{ay}, V_{az}]^T = -\frac{1}{2} [\omega_x, \omega_y, \omega_z]^T$  based on a zero-vorticity reference point. After that, the velocity gradient tensor in the special inertial frame can be calculated and thus objective Liutex can be obtained.

## Chapter 5

### Stability theory

This chapter introduces linear stability theory and how to solve the Orr-Sommerfeld equation by Chebyshev polynomial expansions.

#### 5.1 Orr-Sommerfeld equation

The Orr-Sommerfeld equation is a fundamental equation in fluid mechanics that describes the linear stability of parallel, incompressible flows. It was first introduced by Vincenzo Orr and Arnold Sommerfeld in the early 20th century. The equation is derived from the Navier-Stokes equations, which can be written as

$$\begin{cases} \frac{\partial \vec{u}}{\partial t} + (\vec{u} \cdot \nabla) \vec{u} + \nabla p = \frac{1}{Re} \nabla^2 \vec{u} \\ \nabla \cdot \vec{u} = 0 \end{cases} \quad (5.1)$$

where  $\vec{u}$  represents velocity vector,  $p$  represents pressure,  $Re$  represents Reynolds number,  $\nabla$  is Hamilton operator and  $\nabla^2$  is the Laplace operator.

The flow stability refers to whether disturbances can decay after the base flow is perturbed at a certain moment. If the disturbance can decay, it is stable, otherwise it is unstable. So, to analyze instability, we suppose the base flow has perturbations.

$$\begin{cases} \vec{u} = \vec{u}_0 + \vec{u}' \\ p = p_0 + p' \end{cases} \quad (5.2)$$

where  $\vec{u}_0$  and  $p_0$  are the solution of the base flow and  $\vec{u}'$  and  $p'$  are the velocity disturbance and pressure disturbance respectively.

$\vec{u}, p$  and  $\vec{u}_0, p_0$  all satisfy the governing equation Eq. (5.1), so we have

$$\begin{cases} \frac{\partial \vec{u}_0}{\partial t} + (\vec{u}_0 \cdot \nabla) \vec{u}_0 + \nabla p_0 = \frac{1}{Re} \nabla^2 \vec{u}_0 \\ \nabla \cdot \vec{u}_0 = 0 \end{cases} \quad (5.3)$$

$$\begin{cases} \frac{\partial (\vec{u}_0 + \vec{u}')}{\partial t} + [(\vec{u}_0 + \vec{u}') \cdot \nabla] (\vec{u}_0 + \vec{u}') + \nabla (p_0 + p') = \frac{1}{Re} \nabla^2 (\vec{u}_0 + \vec{u}') \\ \nabla \cdot (\vec{u}_0 + \vec{u}') = 0 \end{cases} \quad (5.4)$$

Use Eq. (5.3) to simplify Eq.(5.4), we get

$$\frac{\partial \vec{u}'}{\partial t} + (\vec{u}_0 \cdot \nabla) \vec{u}' + (\vec{u}' \cdot \nabla) \vec{u}_0 + \nabla p' = \frac{1}{Re} \nabla^2 \vec{u}' - (\vec{u}' \cdot \nabla) \vec{u}' \quad (5.5)$$

$$\nabla \cdot \vec{u}' = 0 \quad (5.6)$$

Eliminating the second order terms of  $\vec{u}'$ , Eq. (5.5) becomes

$$\frac{\partial \vec{u}'}{\partial t} + (\vec{u}_0 \cdot \nabla) \vec{u}' + (\vec{u}' \cdot \nabla) \vec{u}_0 + \nabla p' = \frac{1}{Re} \nabla^2 \vec{u}' \quad (5.7)$$

$$\nabla \cdot \vec{u}' = 0 \quad (5.8)$$

Since Orr-Sommerfeld equation analyzes parallel flow,  $\vec{u}'$  and  $p'$  are waves with eigenfunctions which are only dependent on  $z$ , and independent on  $t, x, y$ .  $\vec{u}'$  and  $p'$  can be written in the following format.

$$\vec{u}' = \hat{u} e^{i(\alpha x + \beta y - \omega t)} + c.c. \quad (5.9)$$

$$p' = \hat{p} e^{i(\alpha x + \beta y - \omega t)} + c.c. \quad (5.10)$$

where  $c.c.$  represents conjugate complex. Substitute Eq. (5.9) and (5.10) into Eq. (5.7) and (5.8),

$$L \hat{u} = Re(Du_0) \hat{w} + i \alpha Re \hat{p} \quad (5.11)$$

$$L \hat{w} = Re(D \hat{p}) \quad (5.12)$$

$$L \hat{v} = i \beta Re \hat{p} \quad (5.13)$$

$$i(\alpha \hat{u} + \beta \hat{v}) + D \hat{w} = 0 \quad (5.14)$$

where  $L = [D^2 - (\alpha^2 + \beta^2) - i Re(\alpha u_0 - \omega)]$  and  $D$  represents  $\frac{\partial}{\partial z}$ .

If perturbation is two dimensional, i.e.  $\hat{v} = \beta = 0$ , then above equation system can be further simplified to

$$L_0 \hat{u} = Re(Du_0) \hat{w} + i\alpha Re \hat{p} \quad (5.15)$$

$$L_0 \hat{w} = Re(D\hat{p}) \quad (5.16)$$

$$i\alpha \hat{u} + D\hat{w} = 0 \quad (5.17)$$

where  $L_0 = [D^2 - \alpha^2 - iRe(\alpha u_0 - \omega)]$ .

If the perturbation is three-dimensional, Squire transformation can be used to make it in the format of two dimensional. Squire transformation is

$$\alpha_1 u_1 = \alpha \hat{u} + \beta \hat{w}, \quad v_1 = \hat{v}, \quad p_1 Re_1 = \hat{p} Re \quad (5.18)$$

$$\alpha_1 Re_1 = \alpha Re, \quad \frac{\omega_1}{\alpha_1} = \frac{\omega}{\alpha}, \quad \alpha_1^2 = \alpha^2 + \beta^2 \quad (5.19)$$

After removing  $\hat{p}$  term in Eq. (5.15) by using Eq. (5.16) and removing  $\hat{u}$  term by using Eq. (5.17), the Orr-Sommerfeld equation which is a fourth order ordinary differential equation is obtained.

$$\left\{ (D^2 - \alpha^2)^2 - i\alpha Re \left[ \left( u_0 - \frac{\omega}{\alpha} \right) (D^2 - \alpha^2) - D^2 u_0 \right] \right\} \hat{w} = 0 \quad (5.20)$$

Suppose the interval of the domain is  $[-1,1]$ , then the boundary conditions should be

$$\hat{w}(\pm 1) = \hat{w}'(\pm 1) = 0 \quad (5.21)$$

Generally, the  $\alpha, \beta$  and  $\omega$  in Eq. (5.18)-(5.20) can be all complex numbers. However, in practice, people classify the solution of O-S equation problems into temporal or spatial problems. For the temporal stability analysis,  $\alpha$  and  $\beta$  are supposed to be real-valued numbers and complex eigenvalue  $\omega = \omega_r + i\omega_i$  is calculated. In this case, real part  $\omega_r$  determines the disturbance

frequency while the imaginary part controls the temporal growth of the corresponding eigenmodes.

On the other hand, for the spatial stability problem,  $\omega$  and  $\beta$  are supposed to be real numbers and the complex eigenvalue  $\alpha = \alpha_r + i\alpha_i$ . The real part of  $\alpha$  describes the streamwise disturbance wavenumber and the imaginary part reflects the spatial wave-magnitude growth rate in the streamwise direction.

## 5.2 Solve Orr-Sommerfeld equation

Chebyshev polynomials are a set of orthogonal polynomials that are named after the Russian mathematician Pafnuty Chebyshev. We will solve the O-S equation through Chebyshev polynomial expansion.

**Definition 8**(Chebyshev polynomial): Chebyshev polynomials are defined on the interval  $[-1,1]$  and their expressions are

$$T_n(z) = \cos(n \cos^{-1}(z)) \quad (5.22)$$

where  $n$  is the order of polynomials.

For example,

$$T_0(z) = 1 \quad (5.23)$$

$$T_1(z) = z \quad (5.24)$$

$$T_2(z) = 2z^2 - 1 \quad (5.25)$$

$$T_3(z) = 4z^3 - 3z \quad (5.26)$$

We expand  $\hat{w}$  in Chebyshev series

$$\hat{w}(z) = \sum_{n=0}^{\infty} a_n T_n(z) \approx \sum_{n=0}^{N-1} a_n T_n(z) \quad (5.27)$$

where  $N$  is the number of Chebyshev polynomials. Then  $D^2 \hat{w}(z)$  can be expressed as

$$D^2 \hat{w}(z) \approx \sum_{n=0}^{N-1} a_n T_n''(z) \quad (5.28)$$

The Gauss-Lobatto collocation points are selected as the interpolation points. The Gauss-Lobatto collocation points are

$$z_k = \cos\left(\frac{2k+1}{2N}\pi\right), \quad k = 0, 1, \dots, N-1 \quad (5.29)$$

The discretized boundary conditions are

$$\sum_{n=0}^{N-1} a_n T_n(1) = 0 \quad \sum_{n=0}^{N-1} a_n T_n(-1) = 0 \quad (5.30)$$

$$\sum_{n=0}^{N-1} a_n T_n'(1) = 0 \quad \sum_{n=0}^{N-1} a_n T_n'(-1) = 0 \quad (5.31)$$

First, we solve the temporal stability problem. Substitute Chebyshev expansion of  $\hat{v}$  into Eq. (5.20) and move all terms involving  $\frac{\omega}{\alpha}$  to the right-hand side and move other terms to the left-hand side. We get

$$\sum_{n=0}^{N-1} \left[ \left( -u_0 \alpha^2 - D^2 u_0 - \frac{\alpha^4}{i\alpha Re} \right) T_n + \left( u_0 + \frac{2\alpha^2}{i\alpha Re} \right) T_n'' - \frac{1}{i\alpha Re} T_n'''' \right] a_n = \frac{\omega}{\alpha} \sum_{n=0}^{N-1} a_n (T_n'' - \alpha^2 T_n) \quad (5.32)$$

Denote

$$W_n = \left( -u_0 \alpha^2 - D^2 u_0 - \frac{\alpha^4}{i\alpha Re} \right) T_n + \left( u_0 + \frac{2\alpha^2}{i\alpha Re} \right) T_n'' - \frac{1}{i\alpha Re} T_n'''' \quad (5.33)$$

$$Q_n = (T_n'' - \alpha^2 T_n) \quad (5.34)$$

Then Eq. (5.32) can be written as

$$[W_0 \quad W_1 \quad \dots \quad W_{N-1}] \begin{bmatrix} a_0 \\ a_1 \\ \vdots \\ a_{N-1} \end{bmatrix} = [Q_0 \quad Q_1 \quad \dots \quad Q_{N-1}] \begin{bmatrix} a_0 \\ a_1 \\ \vdots \\ a_{N-1} \end{bmatrix} \quad (5.35)$$

At each interpolation point  $y_j$ , the Eq. (5.35). is satisfied, so we have

$$Aa = \frac{\omega}{\alpha}Ba \quad (5.36)$$

where

$$A = \begin{bmatrix} W_0(z_0) & W_1(z_0) & \cdots & W_{N-1}(z_0) \\ W_0(z_1) & W_1(z_1) & \cdots & W_{N-1}(z_1) \\ \vdots & \vdots & \ddots & \vdots \\ W_0(z_{N-1}) & W_1(z_{N-1}) & \cdots & W_{N-1}(z_{N-1}) \end{bmatrix} \quad (5.37)$$

$$B = \begin{bmatrix} Q_0(z_0) & Q_1(z_0) & \cdots & Q_{N-1}(z_0) \\ Q_0(z_1) & Q_1(z_1) & \cdots & Q_{N-1}(z_1) \\ \vdots & \vdots & \ddots & \vdots \\ Q_0(z_{N-1}) & Q_1(z_{N-1}) & \cdots & Q_{N-1}(z_{N-1}) \end{bmatrix} \quad (5.38)$$

$$a = \begin{bmatrix} a_0 \\ a_1 \\ \vdots \\ a_{N-1} \end{bmatrix} \quad (5.39)$$

Eq. (5.36) describes a generalized eigenvalue problem and temporal stability problem can be solved.

Temporal stability problem indeed solves a linear eigenvalue problem for  $\omega$  but it becomes to a non-linear eigenvalue problem when solving for  $\alpha$  because  $\alpha$  has second power in the O-S equation. A common technique to deal with this problem is to extend the eigenvectors to  $\Phi = [\hat{u} \ \hat{w} \ \hat{v} \ \hat{p} \ i\alpha\hat{u} \ i\alpha\hat{w} \ i\alpha\hat{v}]^T$  and we can get a generalised linear eigenvalue problem for  $\alpha$ .

$$i\alpha M\Phi = N\Phi \quad (5.40)$$

where

$$M = \begin{bmatrix} -1 & 0 & 0 & 0 & 0 & 0 & 0 \\ -u_0 & 0 & 0 & -1 & \frac{1}{Re} & 0 & 0 \\ 0 & -u_0 & 0 & 0 & 0 & \frac{1}{Re} & 0 \\ 0 & 0 & -u_0 & 0 & 0 & 0 & \frac{1}{Re} \\ 1 & 0 & 0 & 0 & 0 & 0 & 0 \\ 0 & 1 & 0 & 0 & 0 & 0 & 0 \\ 0 & 0 & 1 & 0 & 0 & 0 & 0 \end{bmatrix} \quad (5.41)$$

$$N = \begin{bmatrix} 0 & D & i\beta & 0 & 0 & 0 & 0 \\ \kappa & Du_0 & 0 & 0 & 0 & 0 & 0 \\ 0 & \kappa & 0 & D & 0 & 0 & 0 \\ 0 & Dv_0 & \kappa & i\beta & 0 & 0 & 0 \\ 0 & 0 & 0 & 0 & 1 & 0 & 0 \\ 0 & 0 & 0 & 0 & 0 & 1 & 0 \\ 0 & 0 & 0 & 0 & 0 & 0 & 1 \end{bmatrix} \quad (5.42)$$

where

$$\kappa = -i\omega + i\beta v_0 + \frac{1}{Re}(\beta^2 - D^2) \quad (5.43)$$

By a process similar to what we do to solve the temporal stability problem, we can solve for  $\alpha$  by Chebyshev expansion.

### 5.3 Chapter summary

This chapter introduces the governing equation of the perturbation and the method to solve it numerically. This method will be used in chapter 6 to explain the mechanism of Hairpin vortex together with Liutex criterion.

## Chapter 6

### Mechanism of Hairpin Vortex formation by Liutex

This chapter explains the mechanism of hairpin vortex formation. The DNS result observation is first provided in section 6.1, describing the development of the flow from laminar to turbulent. Then, O-S equation is used to explain the growth of perturbation. Although the DNS is compressible, its Mach number is small, and the effect of density is small. So, we can still use the incompressible O-S equation to analyze the perturbation growth.

#### 6.1 DNS result observation

In the DNS result of the flat plate boundary layer transition, spanwise vortices first occur. As shown in Fig.6-1, spanwise vortices are a series of straight vortices align the spanwise direction.

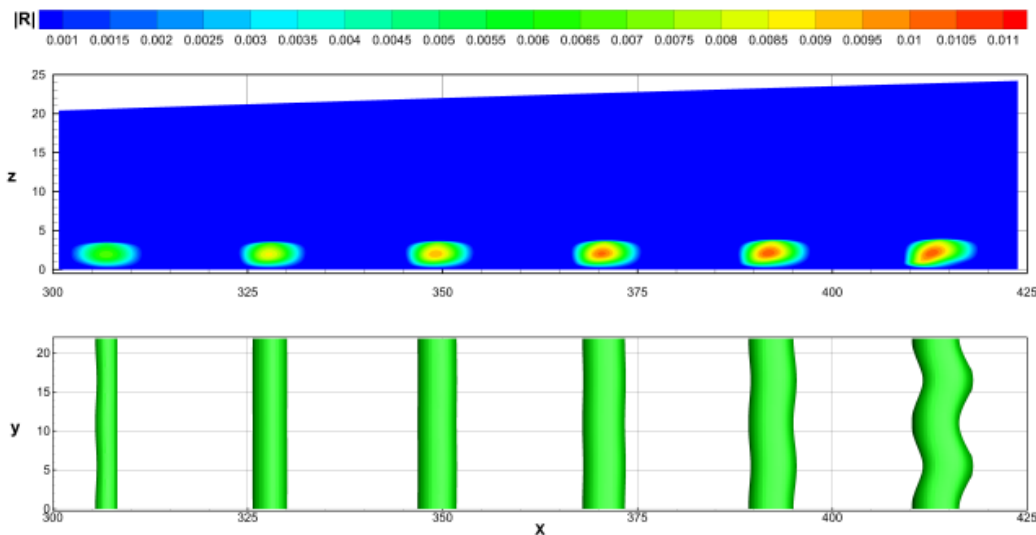


Figure 6-1 spanwise vortices and Liutex magnitude distribution

Based on our discussion in section 3.3, the vortex exists if we can decompose non-zero rotation matrix from the velocity gradient tensor. The distribution of  $\frac{du}{dz}$  and  $\frac{dw}{dx}$  are shown in Fig. 6-2

and 6-3 respectively.  $\frac{du}{dz}$  are all positive in the bottom layer. Recall that to form a rotation matrix,  $\frac{du}{dz}$

and  $\frac{dw}{dx}$  should have different signs, so vortex can exist only at the locations where  $\frac{dw}{dx}$  is negative.

In Fig. 6-3, we can see  $\frac{dw}{dx}$  have blue negative centers and yellow/red positive centers and the

vortices will only occur at the blue negative centers. The iso-surface of Liutex is shown in Fig. 6-5

which matches our prediction. If we observe the motion of fluid with the same velocity at the center

of the vortex, the vortex can be shown as the closed streamlines, see figure 6-4 in which the vortices

are shown by the black closed streamlines.

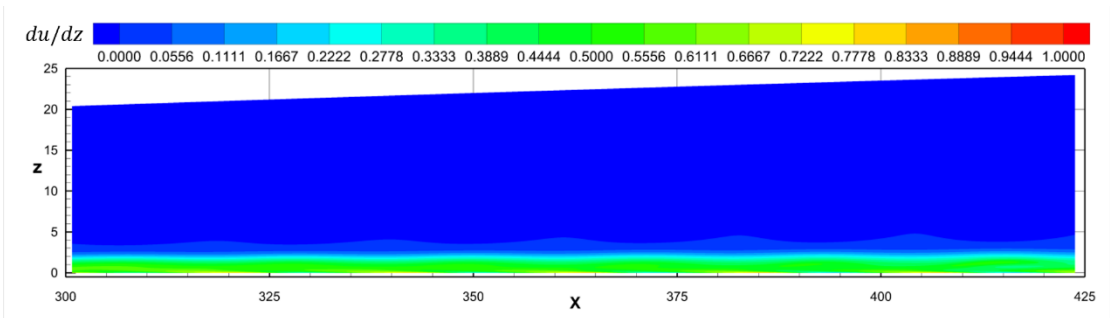


Figure 6-2 distribution of  $du/dz$

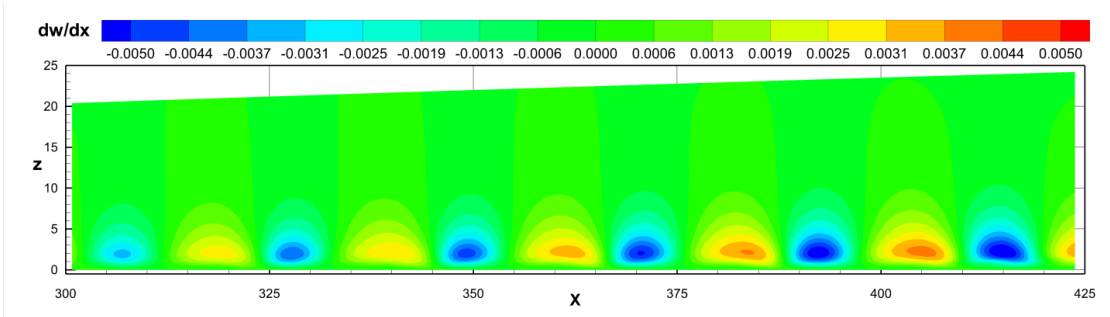


Figure 6-3 distribution of  $dw/dx$

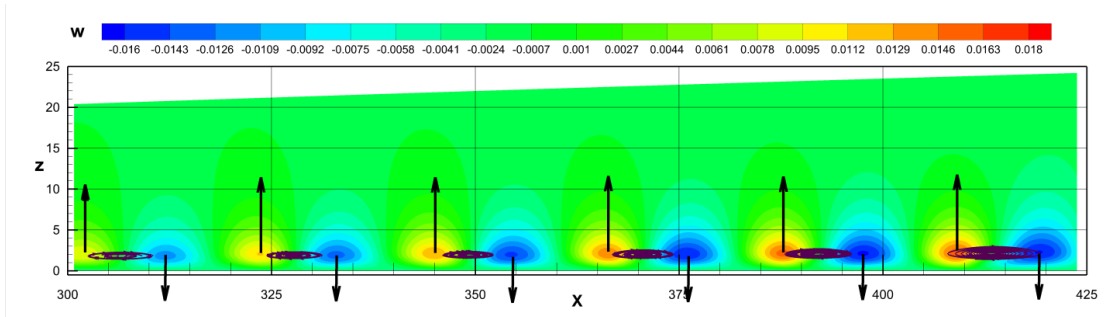


Figure 6-4 distribution of w

As for the rotation strength, it increases with x, as shown in Fig. 6-5. It can also be seen that the region covered by the iso-surface is gradually increasing with the strength at the vortices core increase simultaneously.

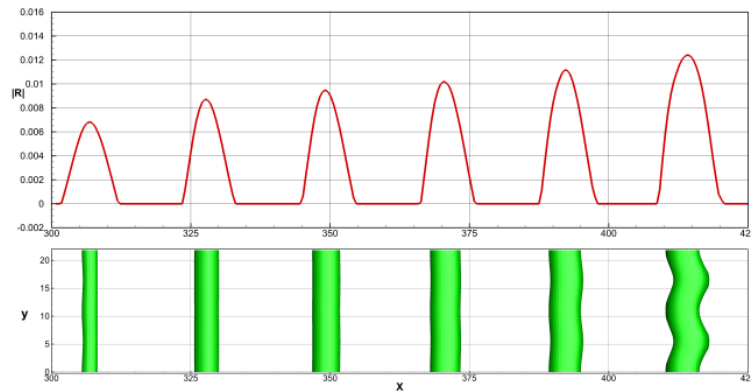


Figure 6-5 Spanwise vortices and Liutex magnitude

Use the Liutex core line method, people can get the vortex core structure which is shown in Fig.6-6. The vortex core lines are straight for the first two single vortices and from the third vortex, the vortex core lines start to become curved. And later on, these curved spanwise vortices are stretched and become  $\Lambda$ -vortices. To show the distributions in detail, two spanwise slices ( $Sy_1, Sy_2$ ) and seven streamwise slices ( $Sx_1-Sx_7$ ) are extracted and the iso-surface of  $|\vec{R}| = 0.005$  and contour line of  $|\vec{R}| = 0.075$  (black or white circles) are plotted in the figures to illustrate the positions of  $\Lambda$ -vortex and spanwise perturbation structures, as shown in Fig. 6-7. One major difference

between  $\Lambda$ -vortex and the spanwise vortex is  $\Lambda$ -vortex has strong spanwise speed compared with spanwise vortex. And from the distribution of  $v$  and  $w$ , we can find the curved spanwise vortex is stretched and the  $\Lambda$ -vortex is received a stronger stretching.

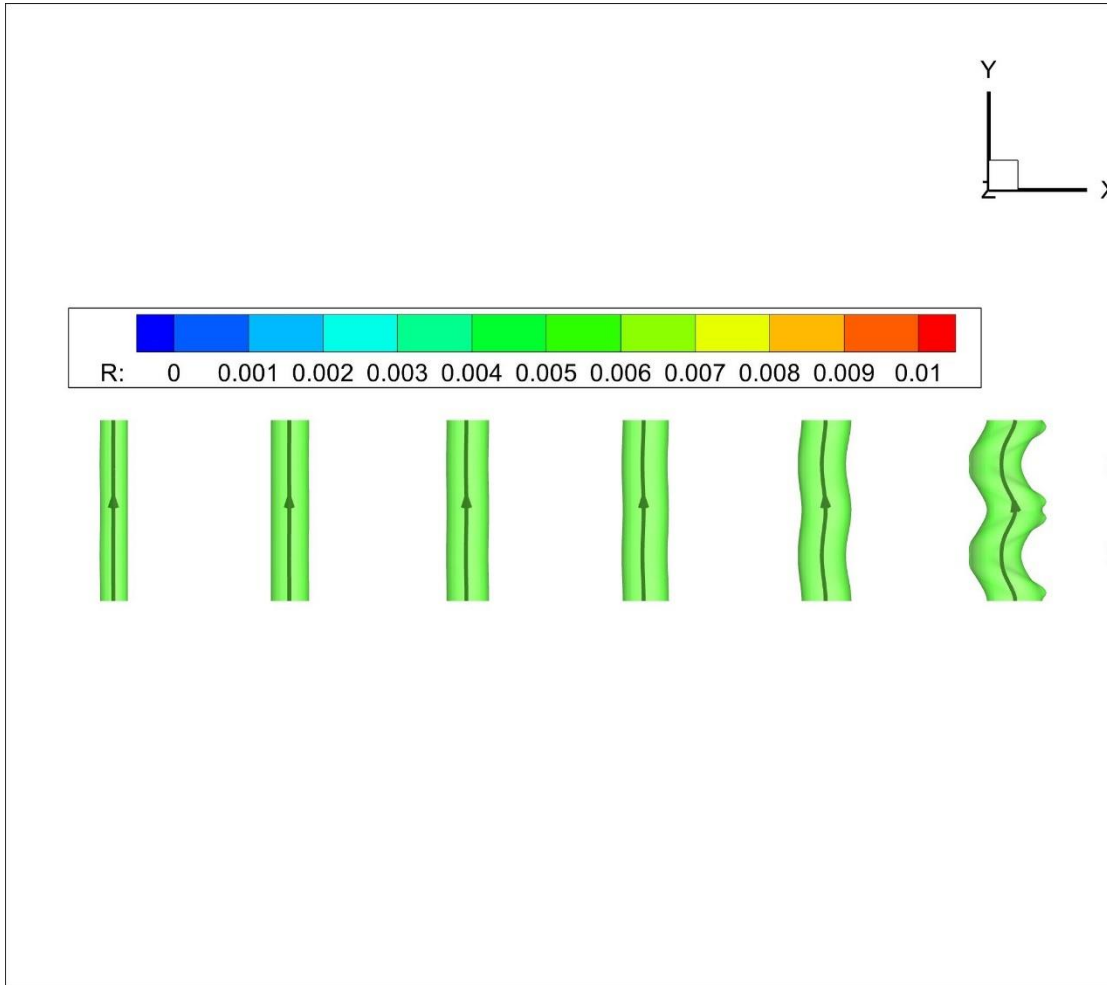
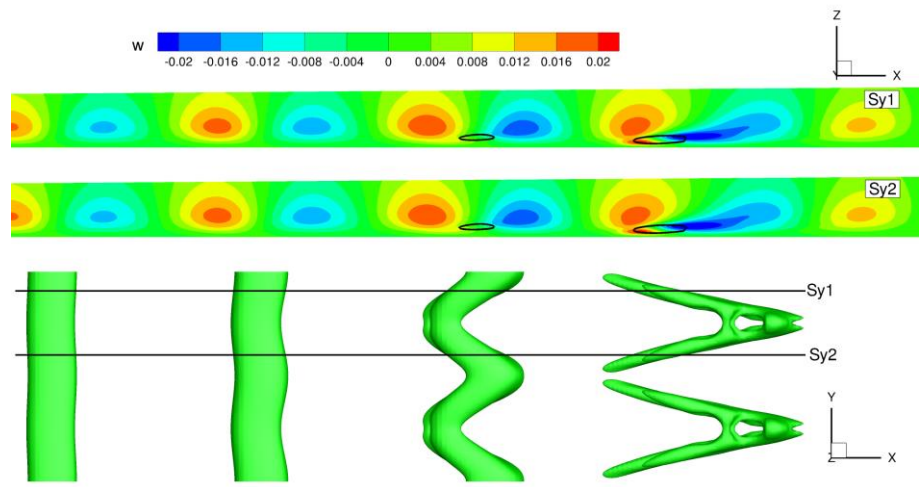
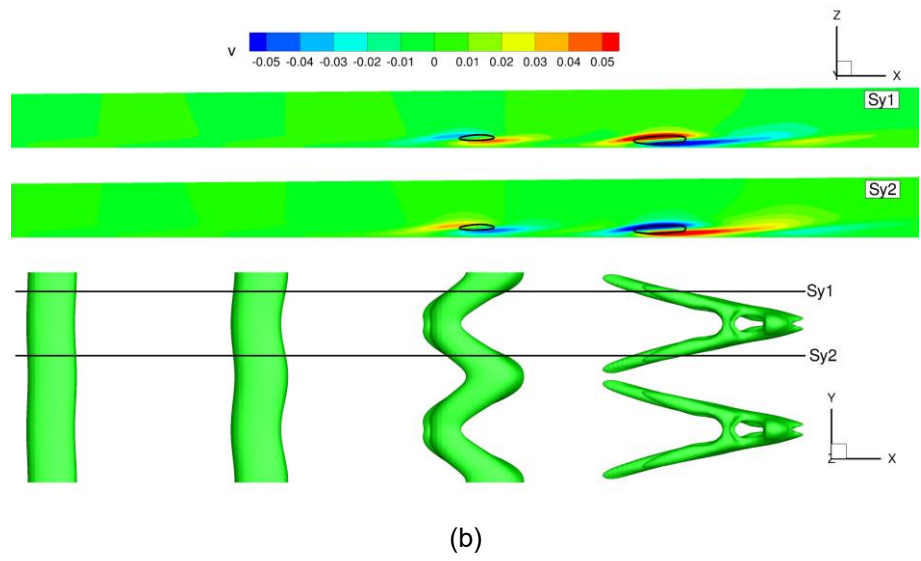
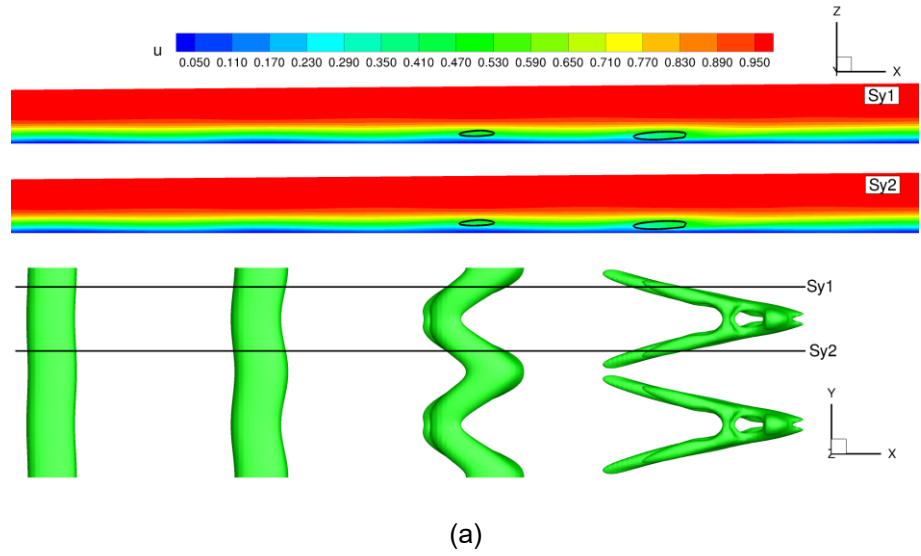
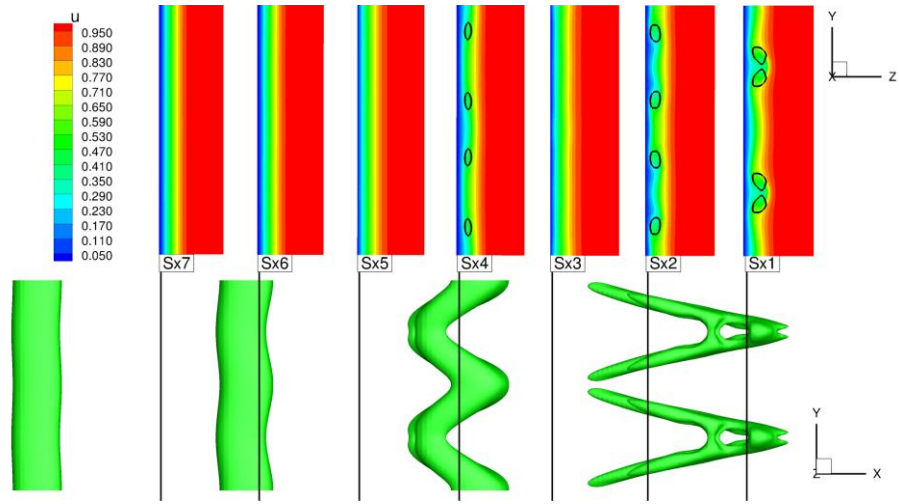


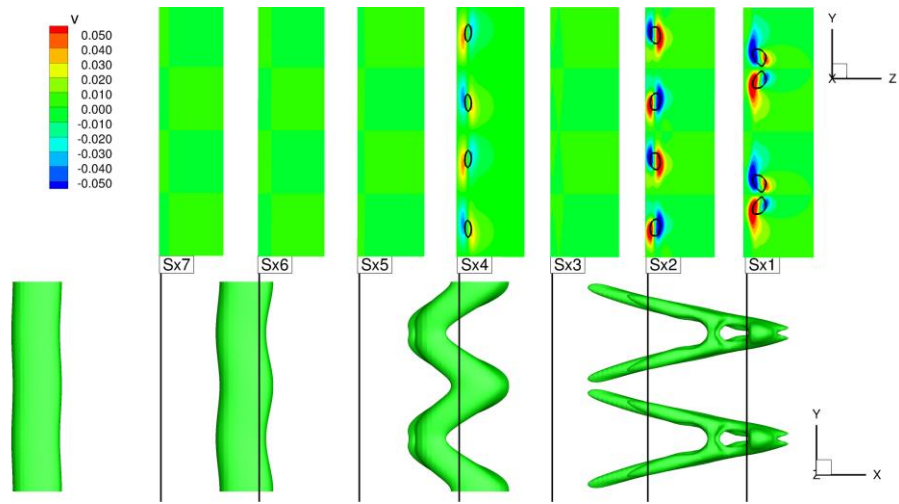
Figure 6-6 Spanwise vortices with Liutex core lines



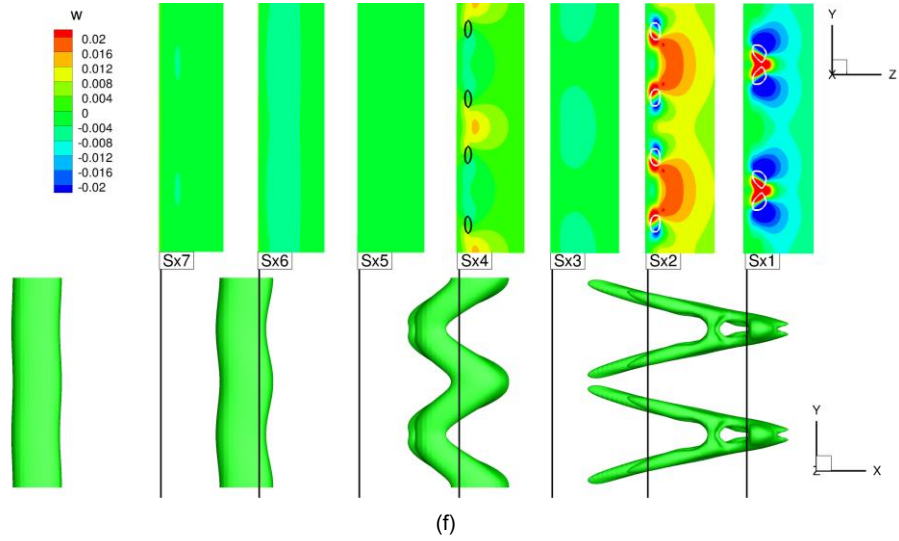
(c)



(d)

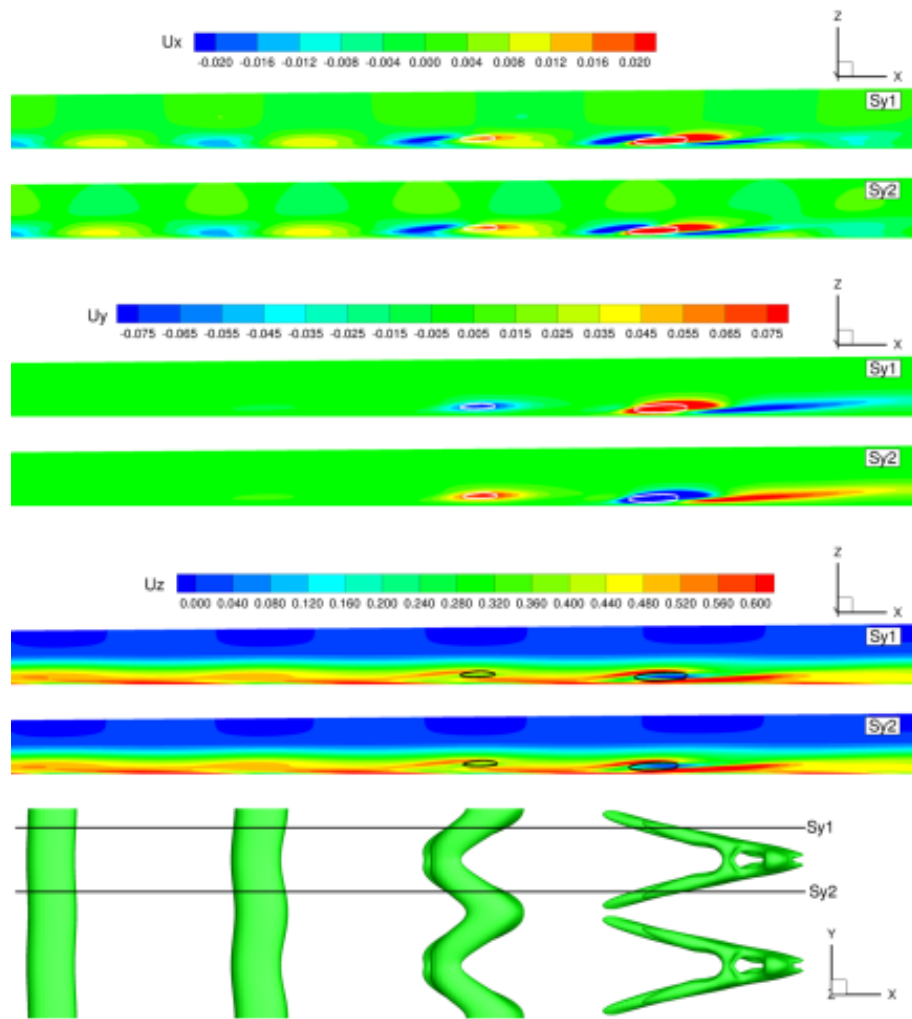


(e)

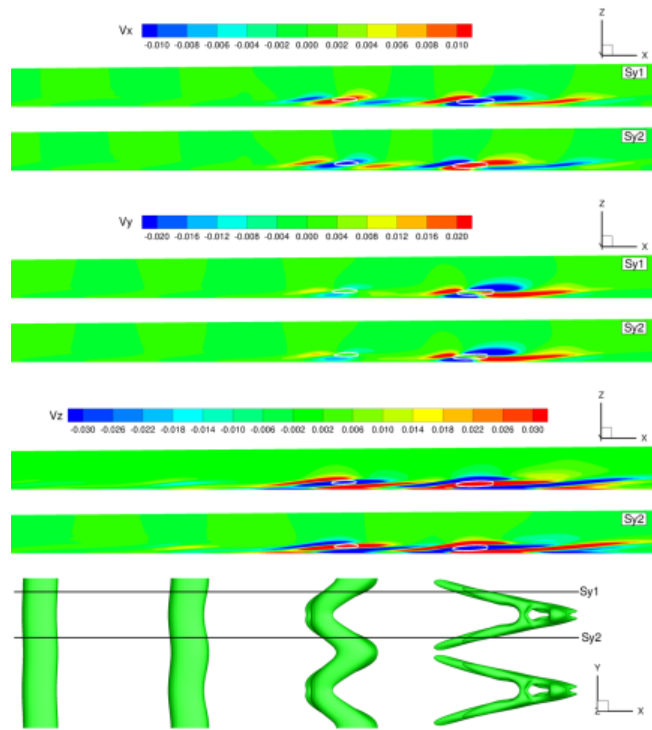


(f)

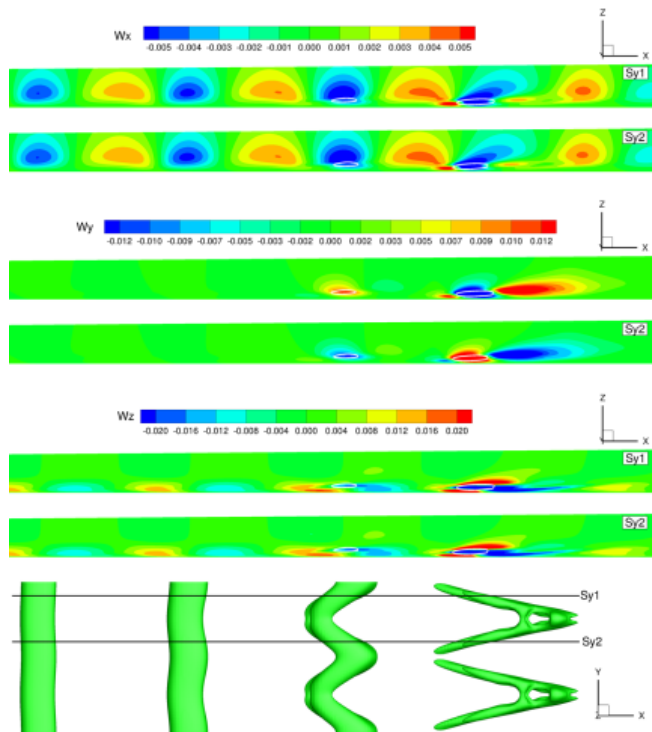
Figure 6-7 Contour of velocity at two spanwise slices ( $Sy_1$  and  $Sy_2$ ) and seven streamwise slices ( $Sx_1 \sim Sx_7$ ): (a)  $u$  in slice  $Sy_1$  and  $Sy_2$ ; (b)  $v$  in slice  $Sy_1$  and  $Sy_2$ ; (c)  $w$  in slice  $Sy_1$  and  $Sy_2$ ; (d)  $u$  in slice  $Sx_1 \sim Sx_7$ ; (e)  $v$  in slice  $Sx_1 \sim Sx_7$ ; (f)  $w$  slice in  $Sx_1 \sim Sx_7$ ;



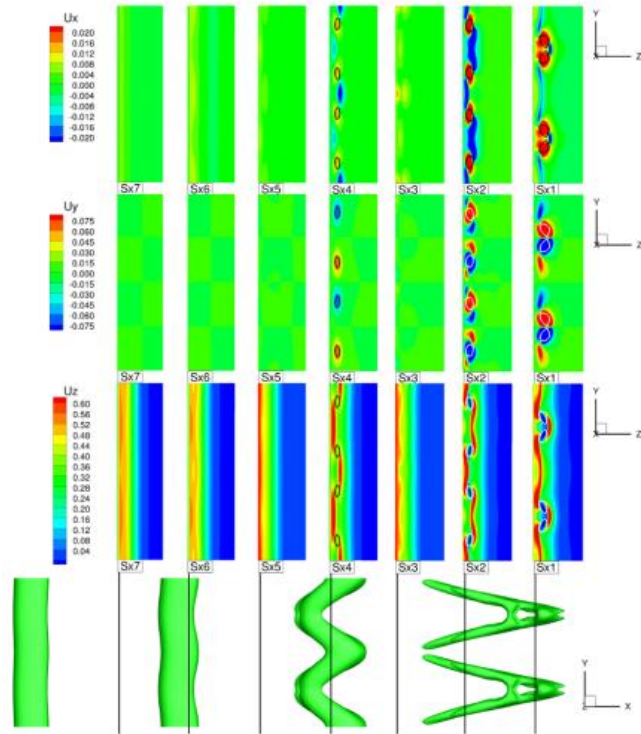
(a)



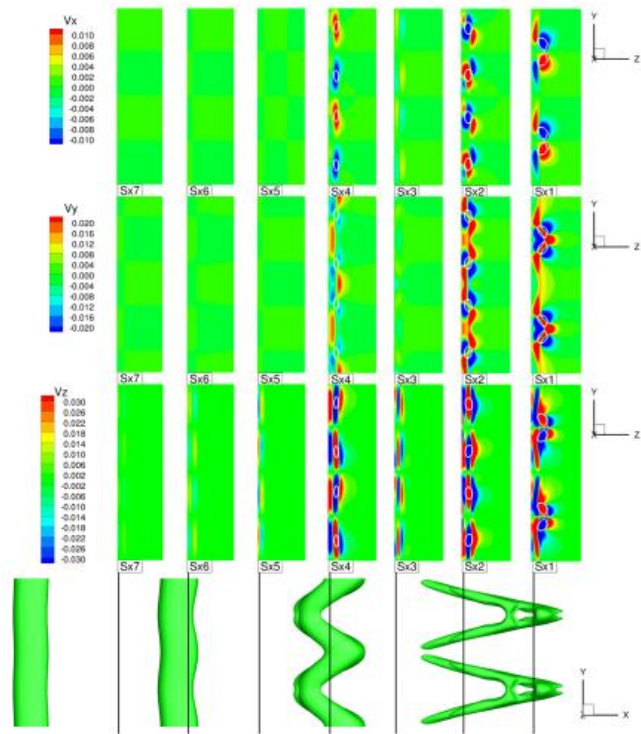
(b)



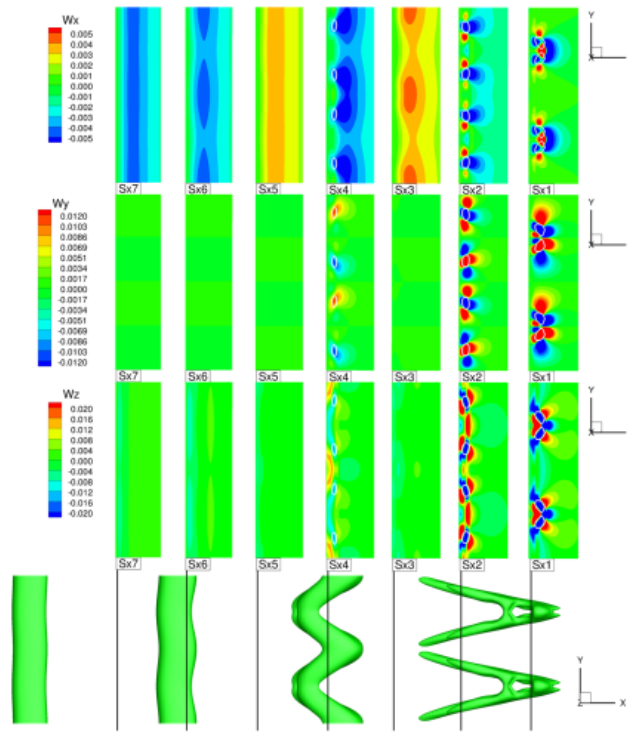
(c)



(d)



(e)



(f)

Figure 6-8 Contour of velocity derivatives at two spanwise slices (  $Sy_1$  and  $Sy_2$  ) and seven streamwise slices ( $Sx_1 \sim Sx_7$ ): (a) derivatives of streamwise velocity in slice  $Sy_1$  and  $Sy_2$ ; (b) derivatives of spanwise velocity in slice  $Sy_1$  and  $Sy_2$ ; (c) derivatives of normal velocity in slice  $Sy_1$  and  $Sy_2$ ; (d) derivatives of streamwise velocity in slice  $Sx_1 \sim Sx_7$ ; (e) derivatives of spanwise velocity in slice  $Sx_1 \sim Sx_2$ ; (f) derivatives of normal velocity in slice  $Sx_1 \sim Sx_2$ ;

Hairpin vortex is also a common vortex structure. The typical shape of hairpin vortex usually consists of three parts: (i) two counter-rotating quasi-streamwise vortices, which are close to but not attached to the wall surface, known as two legs; (ii) Ring-like vortex named as vortex head, where the spanwise vorticity is dominant; (iii) Necks connect the head and legs, as shown in Fig. 6-9. The head is always  $\Omega$ -shaped and the term “vortex ring” is often used alternatively to describe the combination of head and necks. In the orderly flow transition, the hairpin vortices always appear in packets, as shown in Fig. 6-10, which is a typical hairpin-vortex packet.

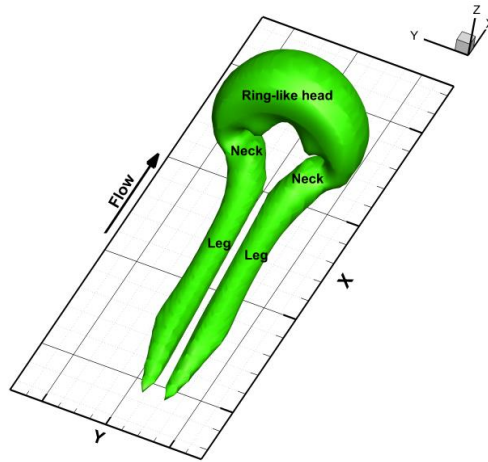


Figure 6-9 Typical shape of Ring like hairpin-vortex

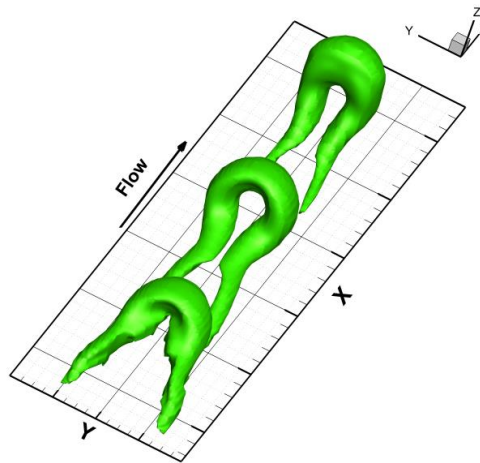
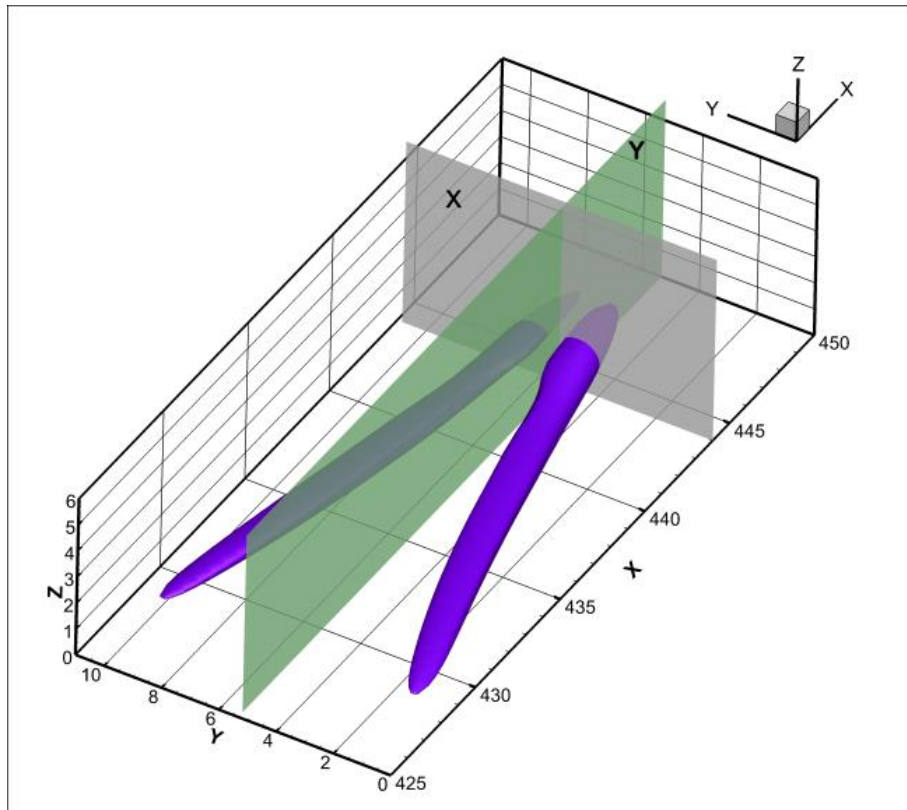


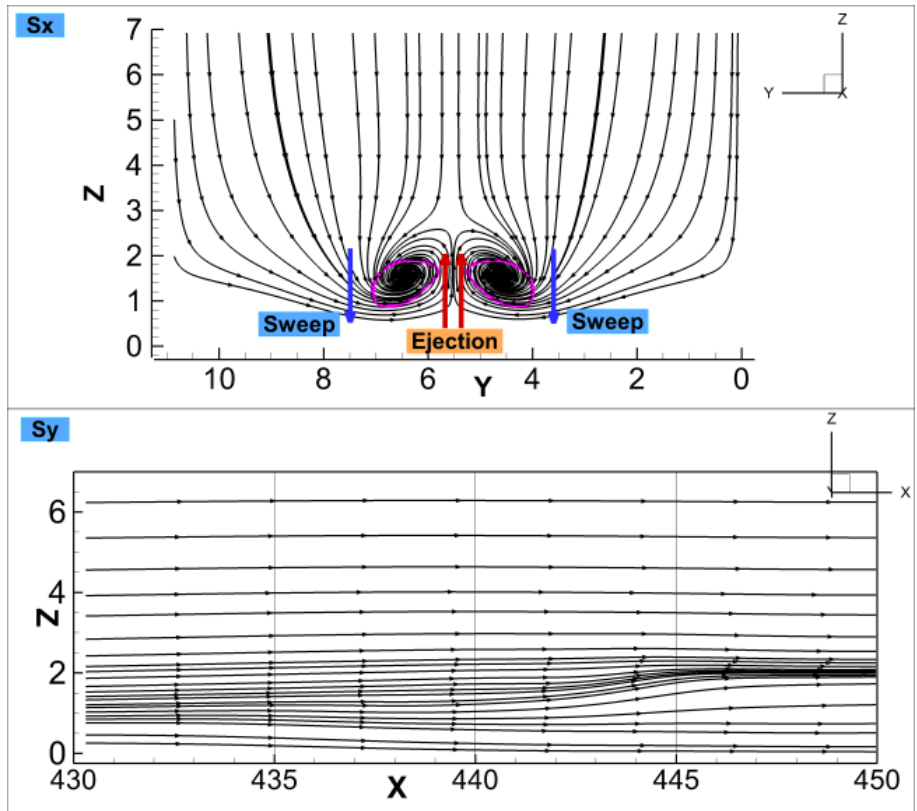
Figure 6-10 Typical shape of Ring like hairpin-vortex packet

After the  $\Lambda$ -vortex is well developed, its typical shape is shown as Fig. 6-9. At  $t=6.0T$ , a pair of  $\Lambda$ -vortices is located from  $x=428.3$  to  $x=446.2$  and two slices are created at  $x=444$  and  $y=5.5$ , see Fig. 6-11(a). The legs of  $\Lambda$ -vortex are two counter rotational cores and they can bring the low speed fluid near the bottom wall to the higher position between the legs and sweep the high speed fluid at the higher place to the wall, as shown in the Fig. 6-11 (b), (c) and (d) which give the stream

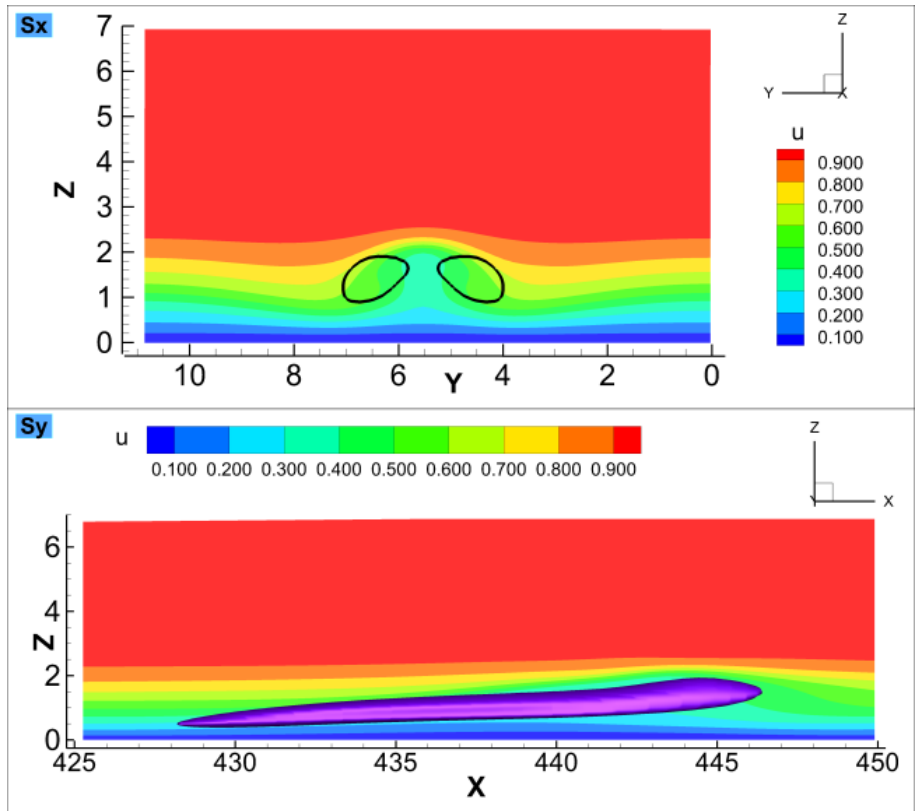
traces and the distribution of streamwise and normal velocity near the top of the  $\Lambda$ -vortex. After the low fluid ejects from the bottom wall and meets the high-speed fluid, high strain rate region will be formed at the top of  $\Lambda$ -vortex head (see Fig. 6-11 (e) and (f)). It can be seen from distributions of the velocity derivatives that, at the top of  $\Lambda$ -vortex head,  $\frac{\partial u}{\partial z}$  is larger than zero and  $\frac{\partial w}{\partial x}$  is less than zero. From the DNS results, it can be seen that the hairpin vortex appears firstly at the top of  $\Lambda$ -vortex head at time  $t=6.05T$  and it is separate from the head of  $\Lambda$ -vortex at the initial stage (see Fig. 6-12 (a)). The head of original  $\Lambda$ -vortex keeps moving up



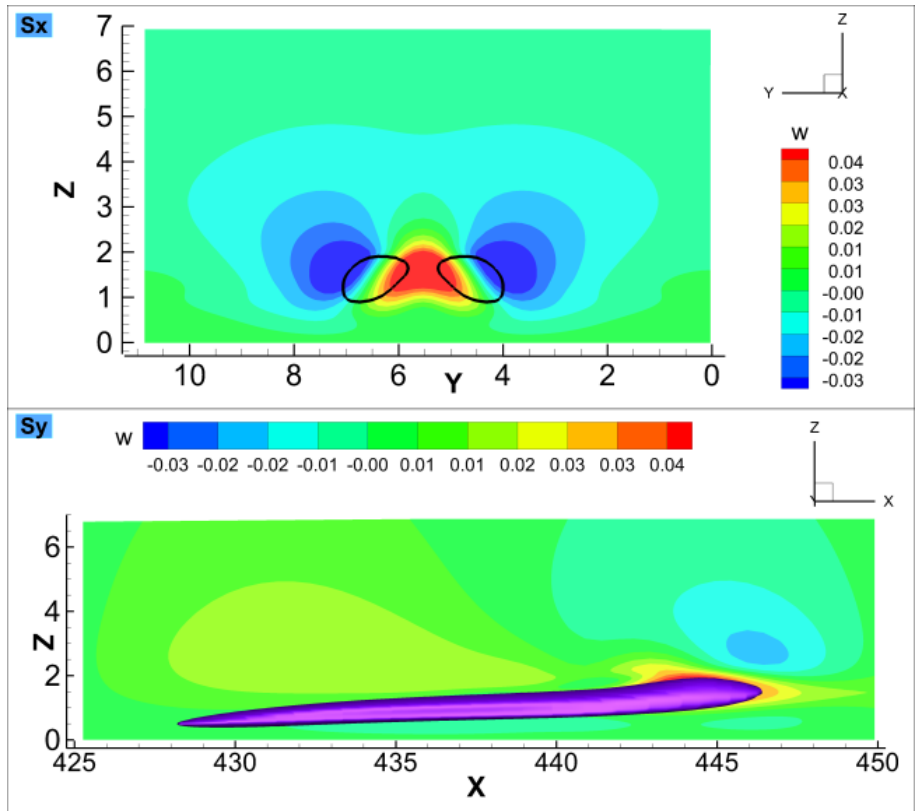
(a)



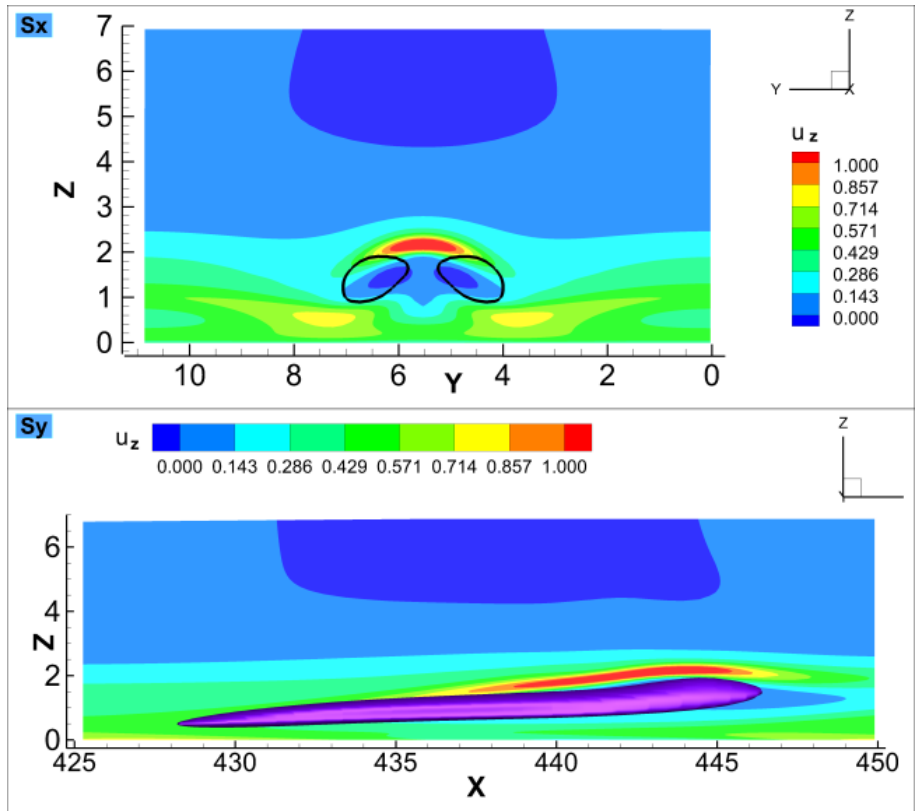
(b)



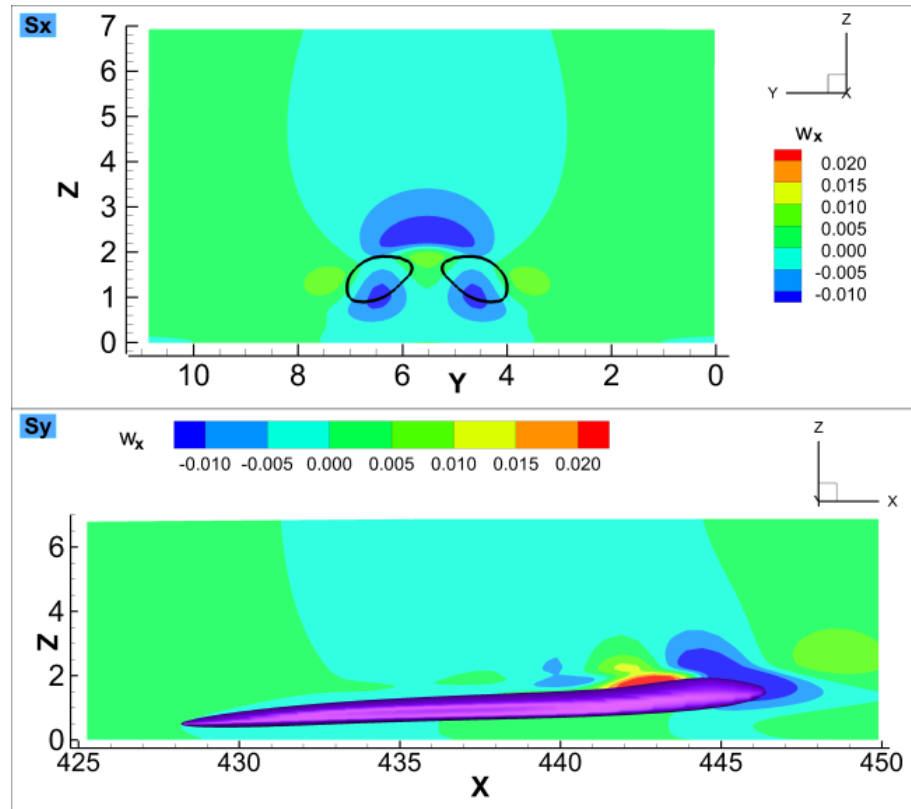
(c)



(d)



(e)

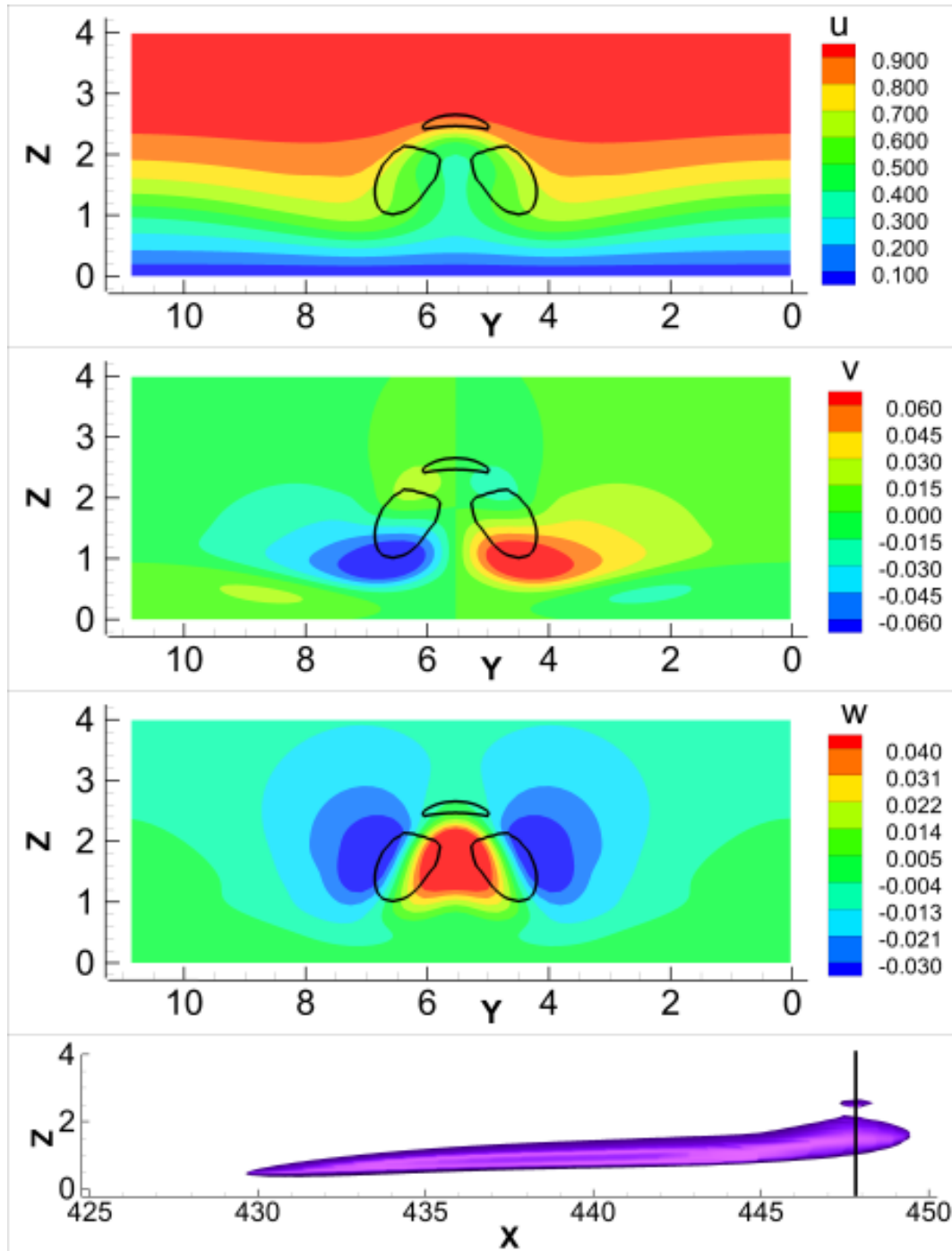


(f)

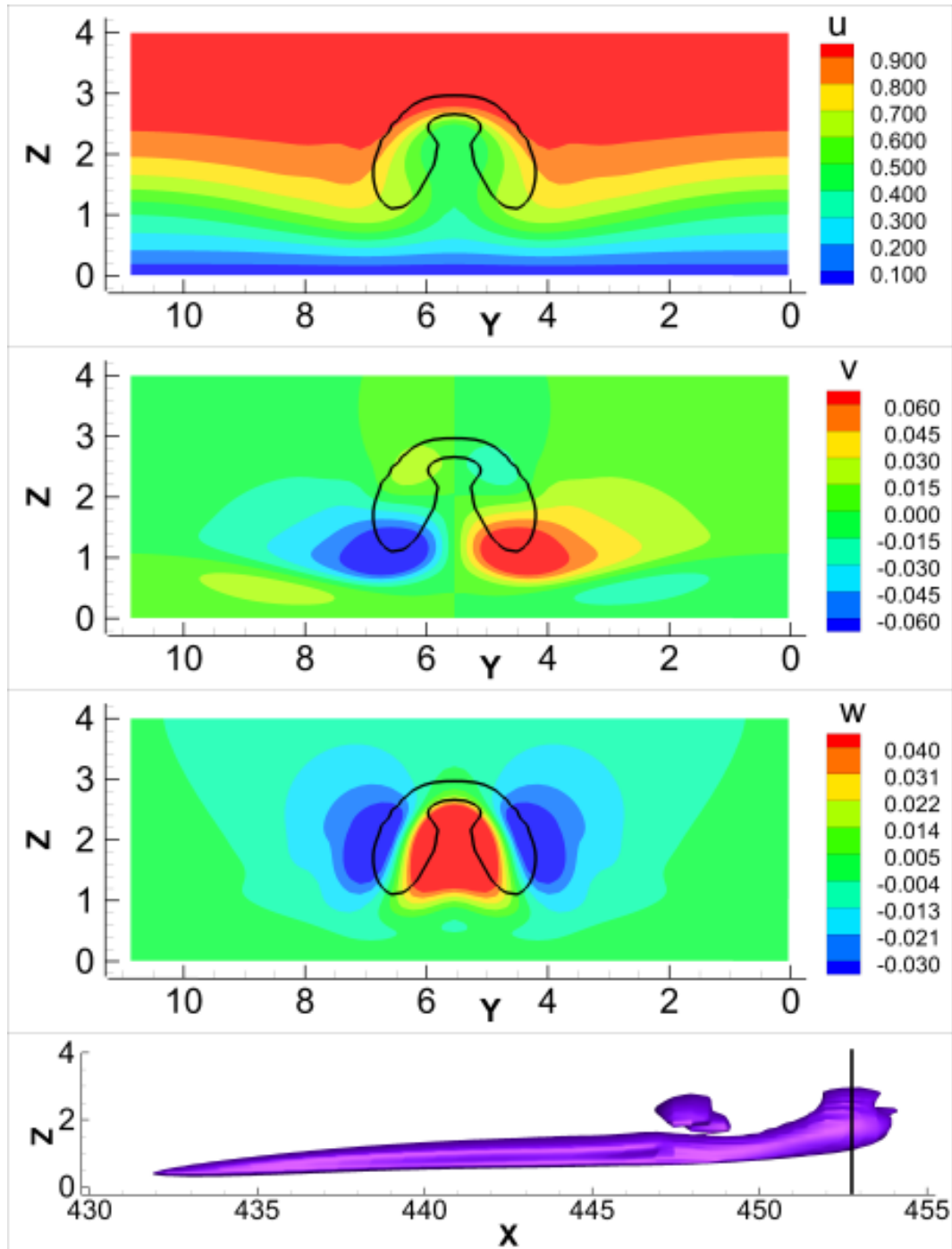
Figure 6-11 The distributions of flow parameters near the top of the  $\Lambda$ -vortex head: (a) positions of slices; (b) streamtraces in the slices; (c) the distribution of streamwise velocity; (d) the distribution of normal velocity; (e) the derivative of streamwise velocity in the two slices; (f) the derivative of normal velocity in the two slices.

and this will make the shear layer stronger, strengthen the new formed vortex and make its scale larger. With the increase of size of the new formed vortex, it will meet the head of  $\Lambda$ -vortex and they will combine together and form a  $\Omega$ -shape or ring-like vortex, see Fig. 6-12 (b), which shows the iso-surface of new generated ring-like vortex and velocity profiles of three components. Since the ring-like vortex rolls up, it will get a larger streamwise velocity than that of the original  $\Lambda$ -vortex's heads and legs which will develop to the necks and legs of the new formed hairpin vortex. The speed difference between the ring-like vortex and the heads and legs of  $\Lambda$ -vortex will make the heads and the legs be stretched and form the first ring-like hairpin vortex, as shown in Fig. 6-12 (c).

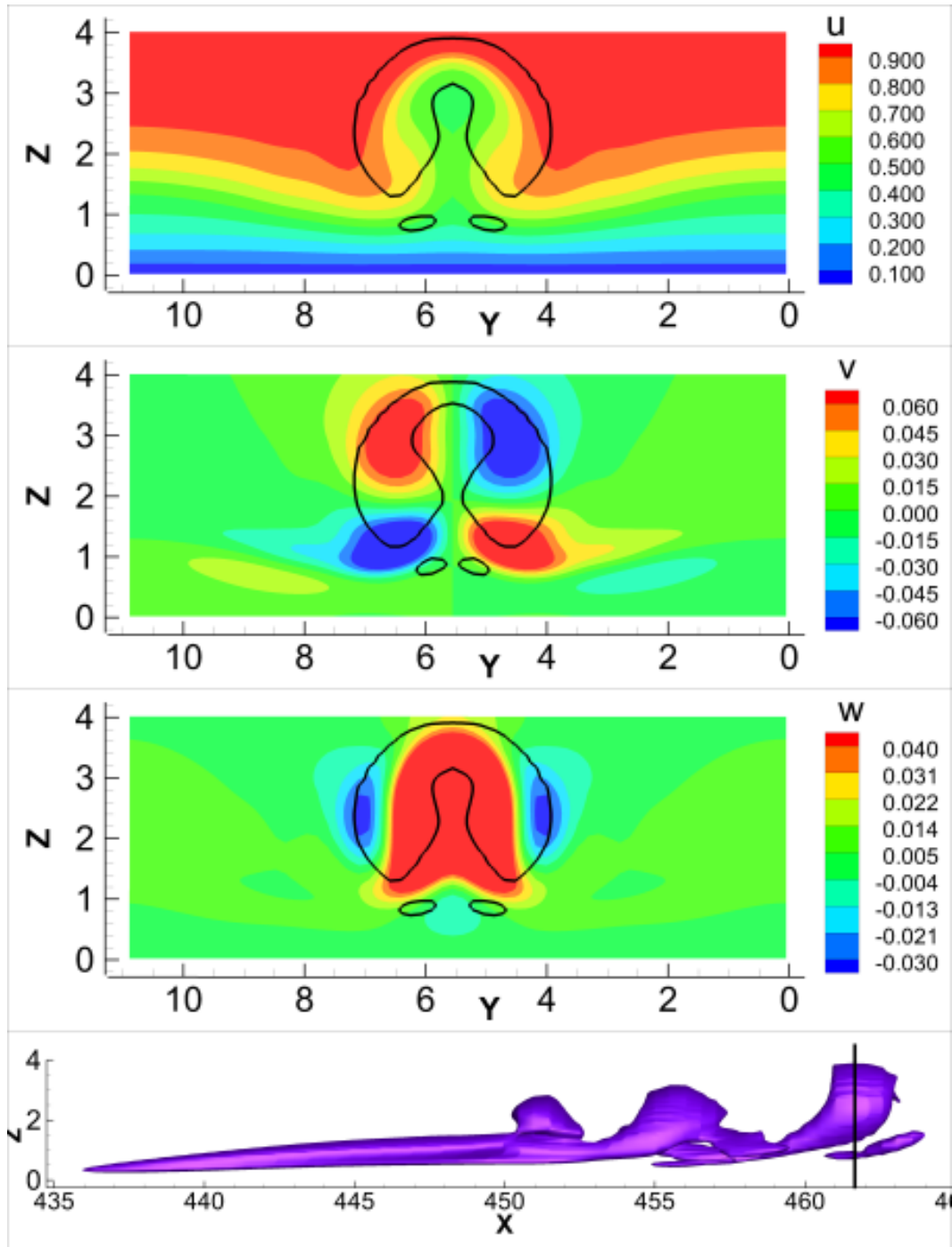
This is also seen from Fig. 20 which shows the location changes of the ring-like vortex in x and z directions. From the process of the first ring-like vortex formation (Fig. 6-12), it can be observed that high strain rate region is formed following the first ring-like hairpin vortex, and the second and the third ring like vortex will generate in the new high strain rate regions with the same mechanism as the first one.



(a)



(b)



(c)

Figure 6-12 The iso-surface of vortices and profiles of the three velocity components in plane across the first ring-like vortex at (a)  $t=6.1T$ ; (b)  $t=6.25T$ ; (c)  $t=6.50$ . The black close curves are the cut section of iso-surface of ring-like vortex plotted by  $\Omega=0.52$ .

As for the normal position of vortices, the spanwise vortices stay in the same height while the

$\Lambda$ -vortex rolls up in a small angle. When the hairpin vortex is form, it rolls up in a around 45 degree angle. Fig. 6-13 and 6-14 shows the roll up of  $\Lambda$ - and hairpin vortices.

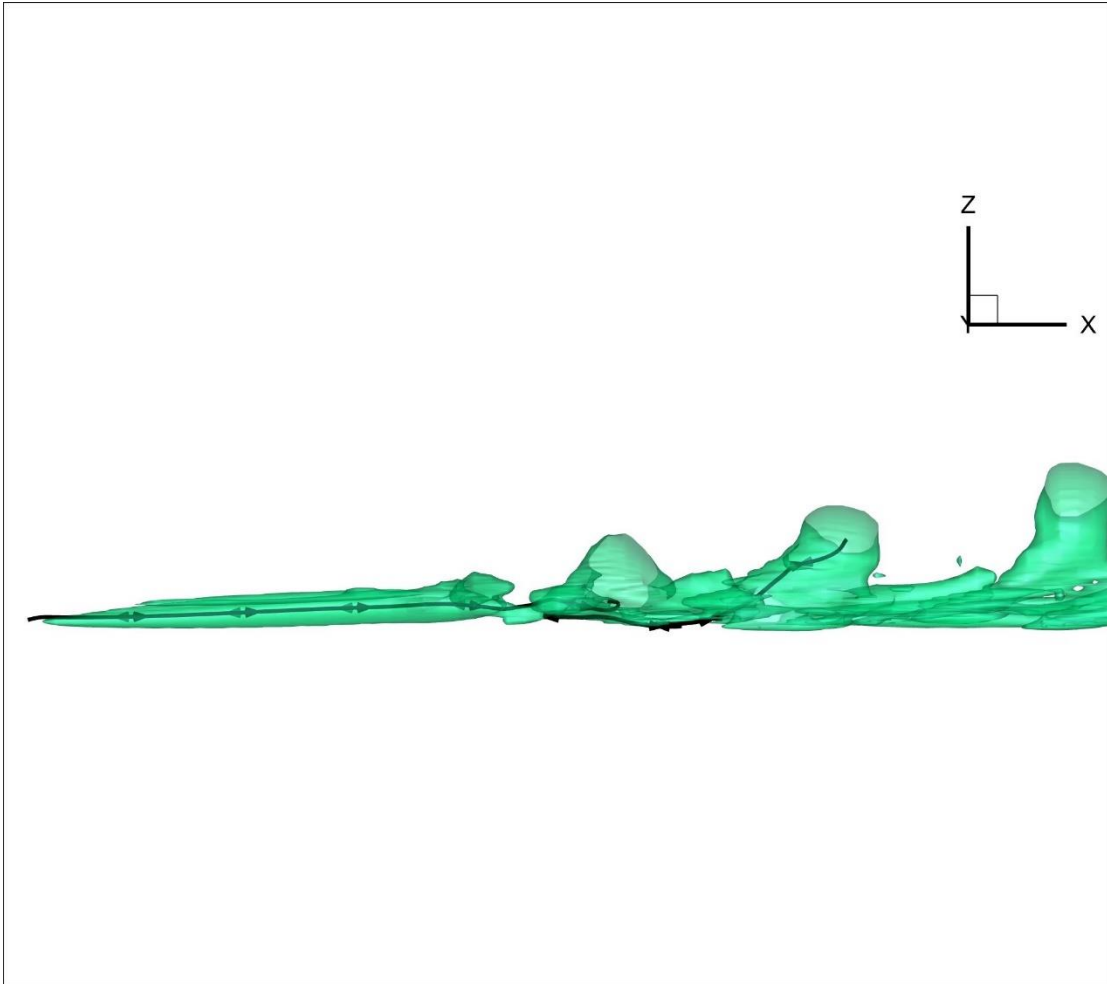


Figure 6-13 roll up of  $\Lambda$ -vortex and hairpin vortex

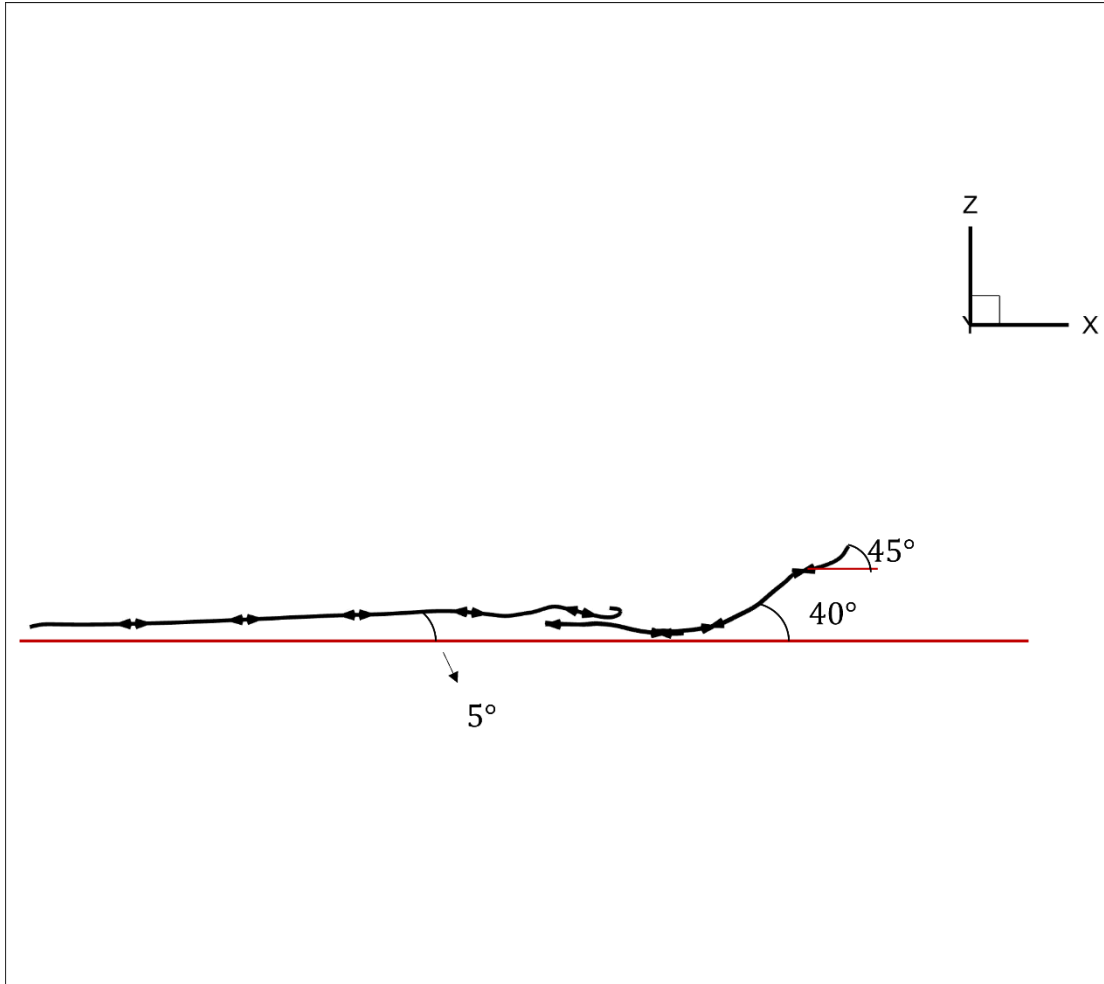


Figure 6-14 roll up angle of  $\Lambda$ -vortex and hairpin vortex

Fig.6-15 shows the streamwise growth of disturbance velocity components. It can be seen that the initial normal disturbance velocity have a amplitude about 1–2% of the free-stream velocity with initial streamwise disturbance slightly greater than it and initial spanwise disturbance lightly less than it. In the initial stage, from  $x=300$  to  $x=360$ , the streamwise and normal disturbances increase slowly while the spanwise disturbance drops greatly to the level of  $10^{-4}$ . Then, streamwise and normal disturbances still

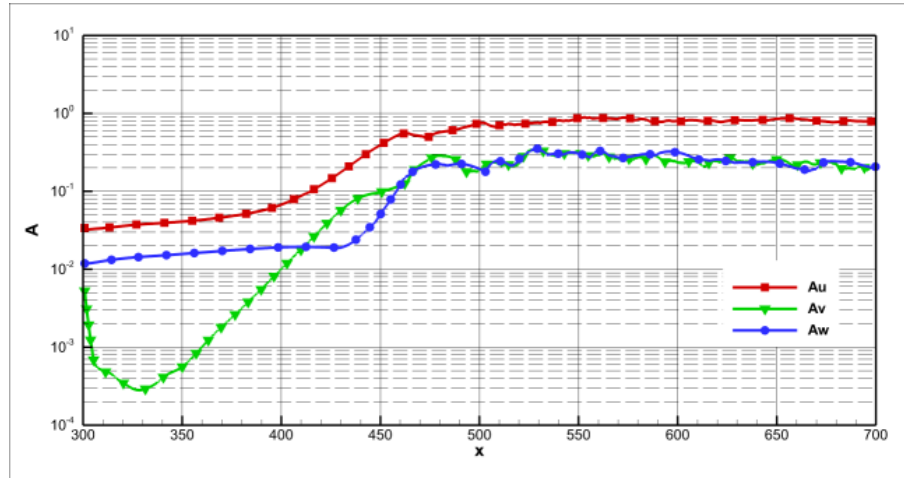


Figure 6-15 The growth of disturbance velocity along streamwise direction

increase slowly but the spanwise disturbance increases rapidly from  $10^{-4}$  to  $10^{-2}$ . When the spanwise disturbance reaches a certain amplitude of the order of 1%, all the perturbation velocity components will grow dramatically and reach an amplitude of around 30% of free stream velocity. The significant growth is completed in a limited streamwise distance of about 75. After this dramatic increase stage, the amplitudes of the disturbance velocity components reach a statistically steady.

After five periods of development in a linear or weak nonlinear mode, the disturbance velocity components, especially in normal and spanwise direction, have a significant growth and the spanwise velocity will reach the same order of magnitude with normal velocity. To better illustrate the development of the perturbation velocity in normal and span-wise direction along the stream, the evolution of the maximum and minimum velocity components along x direction at  $t=5.0T$  is plotted in Fig. 6-16 and 6-17. For the magnitude of the initial perturbation in normal direction, there is not a great growth in the first five periods and the normal disturbance velocity component increases in a linear manner. However, though the absolute value of spanwise velocity is still very

small after an evolution in five periods, there is an exponential growth in its magnitude, from  $10^{-4}$  to  $10^{-2}$ .

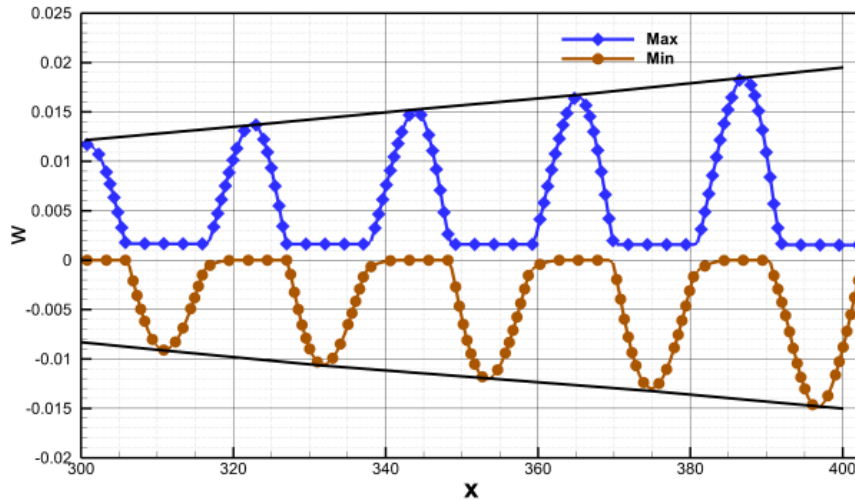


Figure 6-16 The development of the maximum and minimum velocity in spanwise direction along streamwise

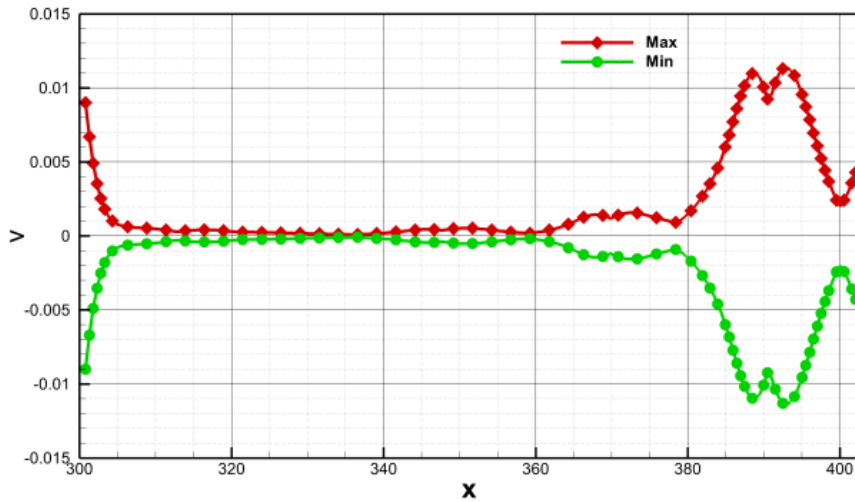


Figure 6-17 The development of the maximum and minimum velocity in normal direction along streamwise

The interesting issues of the observations is why the spanwise perturbation decays rapidly in the initial stage and all perturbances grow quickly when the spanwise perturbation reaches the level of 1%. These questions will be explained in the following sections.

## 6.2 Spanwise vortex formation

The formation of the spanwise vortices can be explained by solving the O-S equation with Blasius solution as the base flow. Blasius solution is an analytical solution of Navier-Stokes equation which provides the accurate velocity profile. Set  $Re = 1000$  and  $\alpha = 0.29919$ , we can get the unstable mode and its corresponding eigenfunctions. The eigenvalues of the O-S equation are shown in Fig.6-18 and

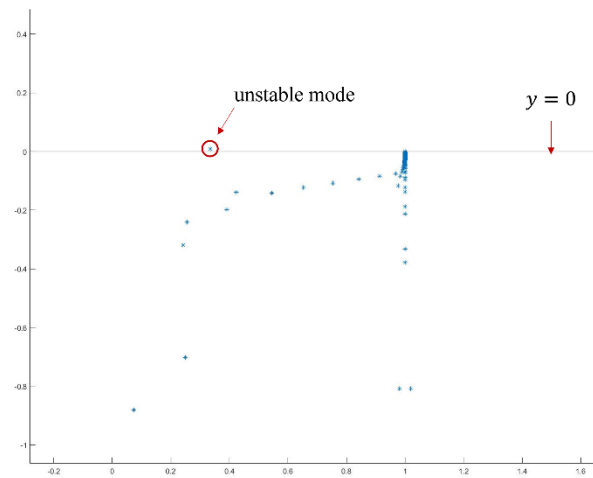


Figure 6-18 Eigenvalues of 2D modes

there is an unstable mode  $\omega = 0.3349 + 0.0094i$  with the eigenfunctions

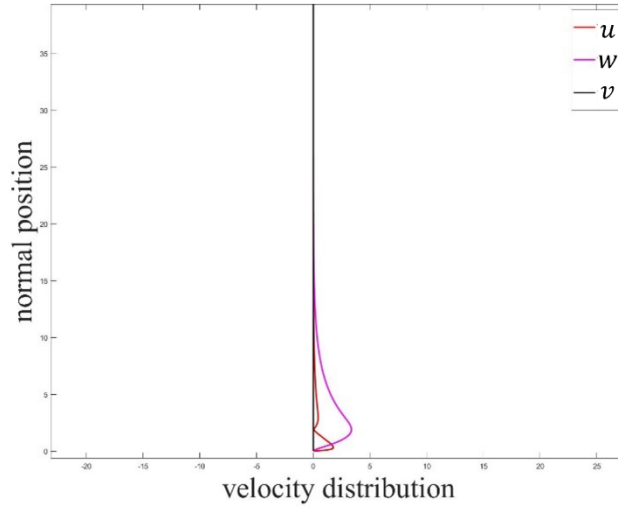


Figure 6-19 Eigenfunction of the unstable 2D modes( $v=0$ )

The perturbations in unstable modes will be amplified with time and other stable modes will decay. In practice, the perturbations exist because there is noise in the environment, or the surface is rough. In our DNS, the initial perturbation is imposed artificially.

Linear stability theory can explain the growth of velocity perturbations, but velocity perturbations do not necessarily lead to vortex. So, we use Liutex to link the velocity perturbations to vortex. According to the linear stability theory, the velocity distribution is

$$u = u_0 + \hat{u}e^{i(\alpha x - \omega t)} \quad (6.1)$$

$$w = w_0 + \hat{w}e^{i(\alpha x - \omega t)} \quad (6.2)$$

$$v = 0 \quad (6.3)$$

The velocity gradient tensor is

$$\text{grad}\vec{v} = \begin{bmatrix} (i\alpha)\hat{u}e^{i(\alpha x - \omega t)} & 0 & \frac{\partial u_0}{\partial z} + \frac{\partial \hat{u}}{\partial z}e^{i(\alpha x - \omega t)} \\ 0 & 0 & 0 \\ (i\alpha)\hat{w}e^{i(\alpha x - \omega t)} & 0 & \frac{\partial w_0}{\partial z} + \frac{\partial \hat{w}}{\partial z}e^{i(\alpha x - \omega t)} \end{bmatrix} \quad (6.4)$$

Obviously, the Liutex direction which is the real eigenvector of  $\text{grad}\vec{v}$  can only be  $[0 \ 1 \ 0]^T$  or

$[0 \ -1 \ 0]^T$  which is dependent on the vorticity direction. The vorticity direction is

$$\omega_y = \frac{\partial u_0}{\partial z} + \frac{\partial \hat{u}}{\partial z} e^{i(\alpha x - \omega t)} - (i\alpha) \hat{w} e^{i(\alpha x - \omega t)} \quad (6.5)$$

At the beginning, the disturbance terms are small, so the sign of  $\omega_y$  direction is dominated by the term  $\frac{\partial u_0}{\partial z}$  which is positive for Blasius profile. Thus, the rotation axis direction is aligning positive y axis direction which coincides with the DNS result as shown in Fig.6-20.

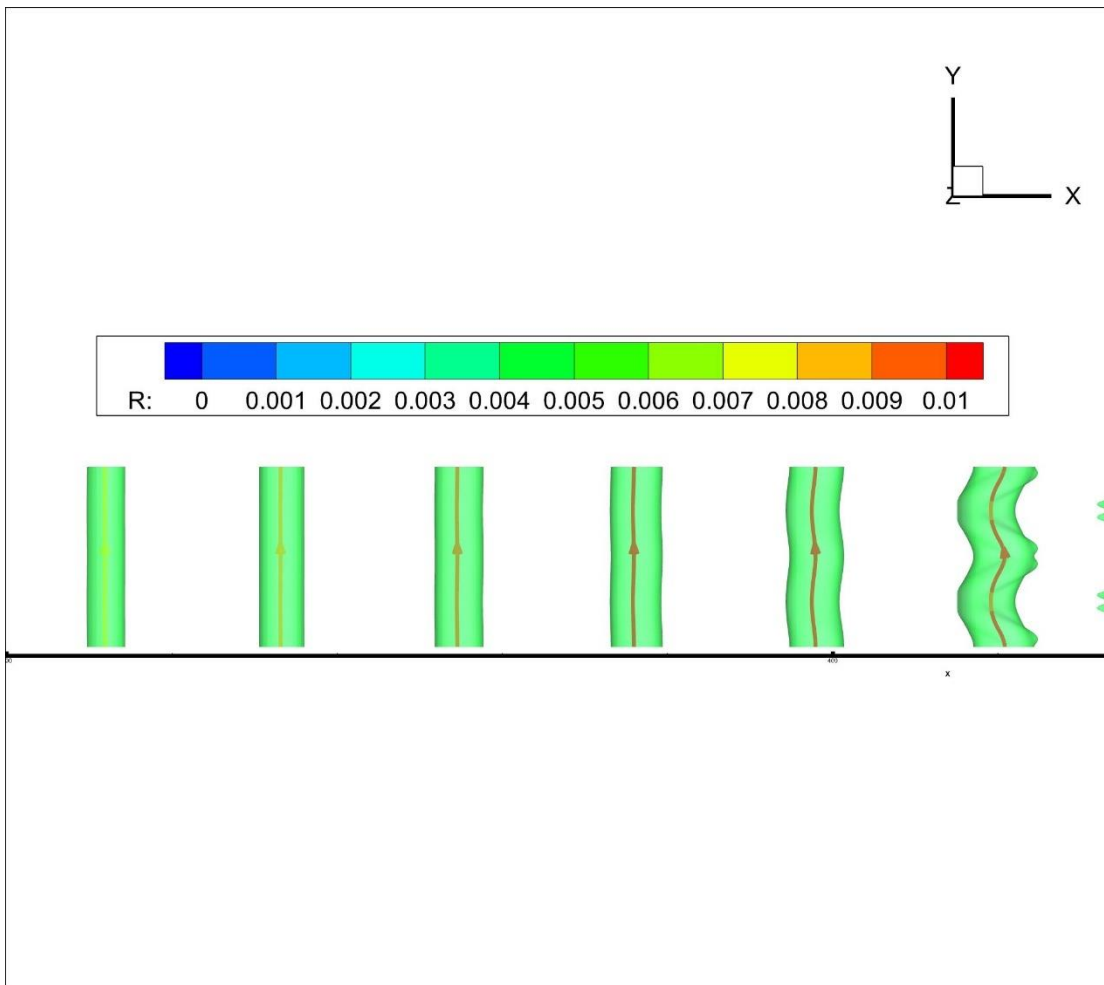


Figure 6-20 Spanwise vortex direction

In the spanwise vortex formation period, the spanwise perturbation experiences a rapid decay until  $x=330$  and then begins increasing. That is because the 3D modes shown imposed at the inlet is stable and it has to decay. Fig 6-21 shows the modes when  $\alpha = 0.2405$  and  $\beta = 0.5712$ . It can be seen all modes are stable.

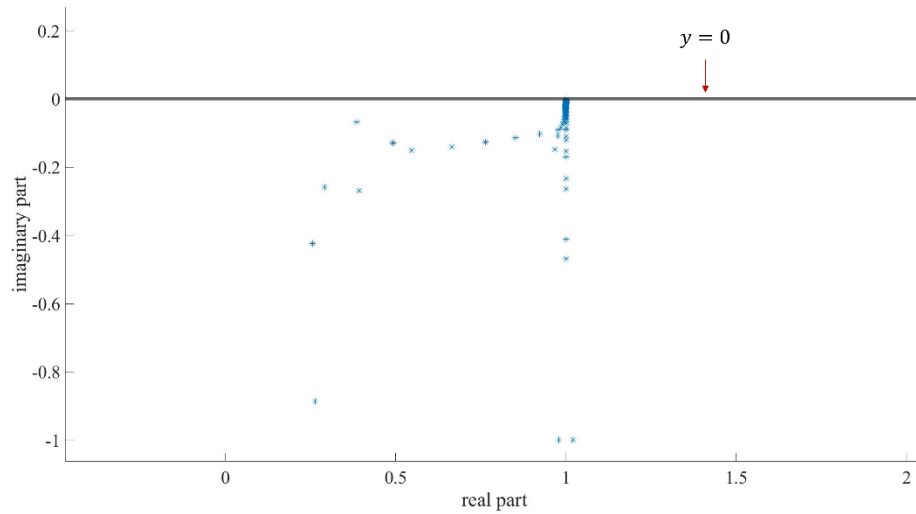


Figure 6-21 Eigenvalues of 3D modes at inlet

Since the linear stability theory is an approximation, its accuracy decreases with  $x$  increasing. We need use the local velocity profile as the base flow to keep the accuracy. When  $x$  reaches 400, the original imposed stable 3D mode becomes unstable because of the change of base velocity profile. Use the local velocity profile at  $x=400$ , test the same 3D mode. We can find the unstable 3D perturbation mode and its corresponding eigenfunctions.

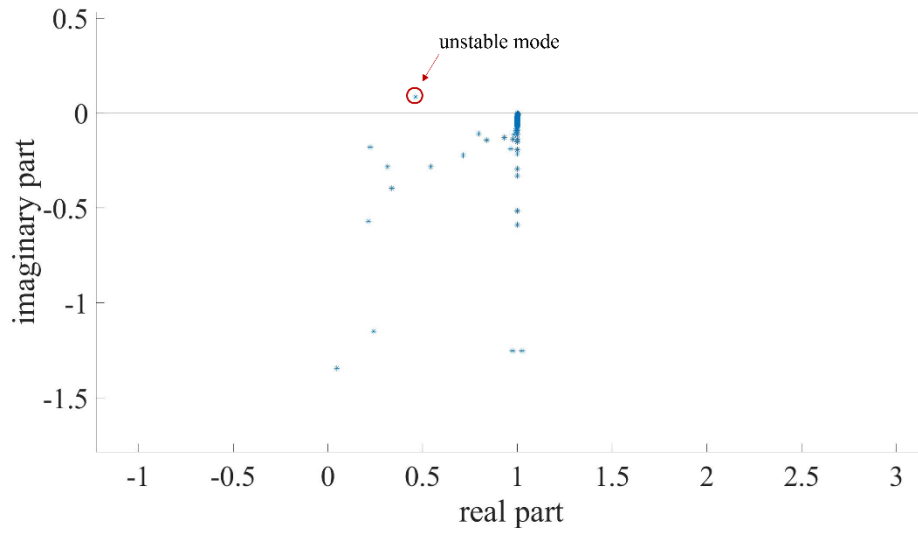


Figure 6-22 Eigenvalues of 3D modes at x=400

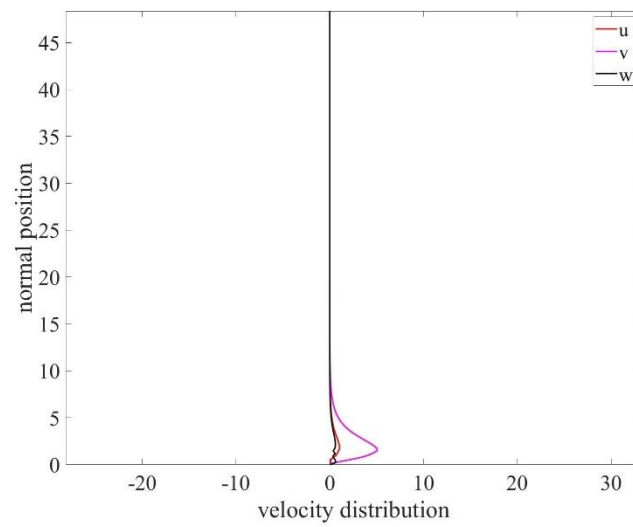


Figure 6-23 Eigenfunctions of 3D modes at x=400

### 6.3 $\Lambda$ -vortex formation

The core reason of the formation of  $\Lambda$ -vortex is 3D modes perturbation becomes dominant.

The velocity distribution can be expressed as

$$u = u_0 + \hat{u}_{2d} e^{i(\alpha_{2d}x - \omega_{2d}t)} + \hat{u}_{3d} e^{i(\alpha_{3d}x + \beta_{3d}y - \omega_{3d}t)} \quad (6.6)$$

$$w = w_0 + \hat{w}_{2d} e^{i(\alpha_{2d}x - \omega_{2d}t)} + \hat{w}_{3d} e^{i(\alpha_{3d}x + \beta_{3d}y - \omega_{3d}t)} \quad (6.7)$$

$$v = v_0 + \hat{v}_{3d} e^{i(\alpha_{3d}x + \beta_{3d}y - \omega_{3d}t)} \quad (6.8)$$

When 2D disturbance is dominated, the disturbance expression only has  $\alpha$  terms which indicates the distribution is uniformly in the spanwise and the vortex is straight as discussed in the previous section. With the increase of the 3D perturbation modes,  $\beta$  plays a more important role in the vortex shape and then the difference in spanwise direction occurs. Suppose at some  $(x,y)$ , the velocity gradient tensor generates rotation, then at the same phase of the cosine function, the velocity gradient tensor is similar. Being the same phase indicates

$$\alpha_{3d}x + \beta_{3d}y = c \quad (6.9)$$

where  $c$  is the phase that generates vortex.

Eq. (6.9) implies,

$$\tan\theta = -\frac{\beta_{3d}}{\alpha_{3d}} = -\frac{0.5712}{0.2405} \approx -2.375 \quad (6.10)$$

So  $\theta$  is around  $67^\circ$ . This prediction coincides with the DNS result.

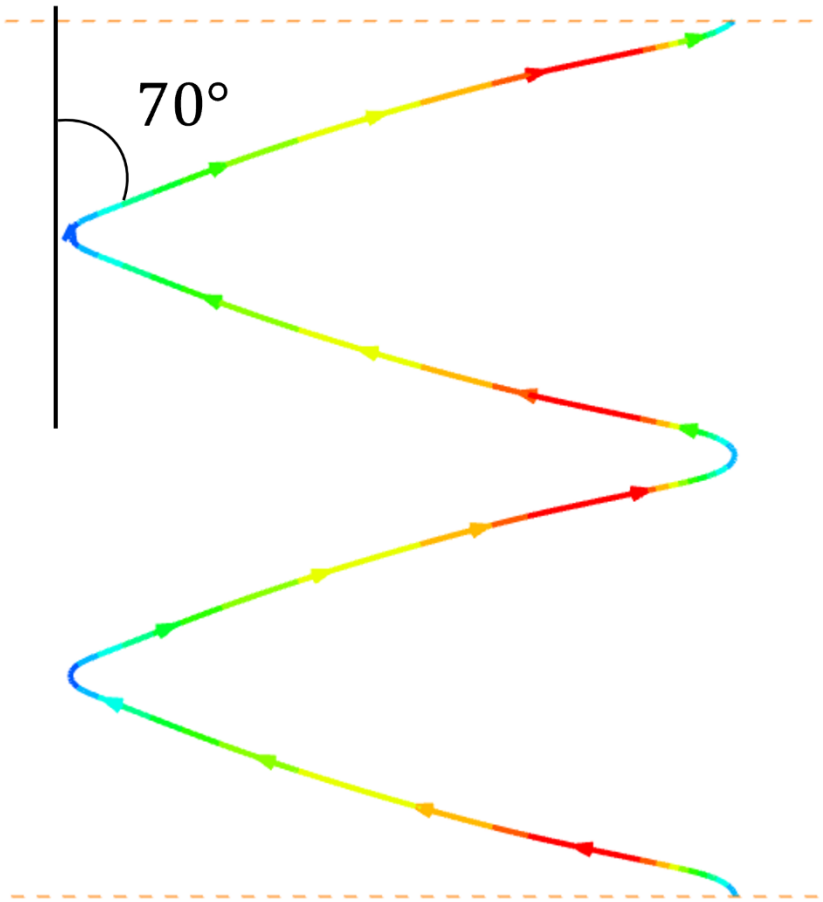


Figure 6-24 Angle between  $\Lambda$ -vortex and spanwise direction without iso-surface

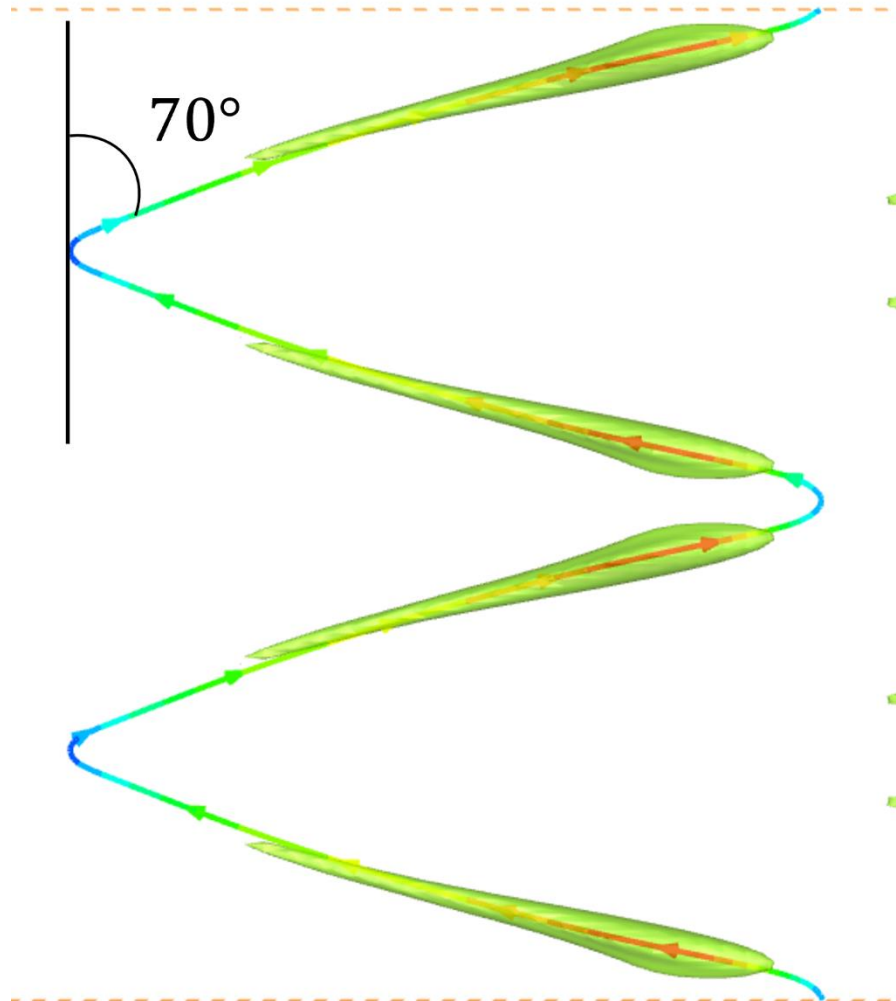


Figure 6-25 Angle between  $\Lambda$ -vortex and spanwise direction with iso-surface

Another evidence that  $\Lambda$ -vortex formation is caused by 3D mode is the  $\Lambda$ -vortex first appears after the 3D mode is excited. As mentioned in section 6.2, 3D mode is excited at  $x=400$  and  $\Lambda$ -vortex is formed right after it.

#### 6.4 Hairpin Vortex formation

After the formation of  $\Lambda$ -vortex, the distance between two  $\Lambda$ -vortex becomes smaller and smaller since the two  $\Lambda$ -vortex are oblique. When the two  $\Lambda$ -vortex are close enough, it generates

a strong shear region as shown in because the rotation motion of the two  $\Lambda$ -vortices eject slow speed fluid from the bottom to the top and sweep the fast speed fluid from the top to the bottom. Use the principal decomposition introduced in section 3.6, we can get the shear distribution which is shown in Fig.6-26 to 6-28. And this shear region is unstable. Use the velocity profile at the shear region, we can get an unstable mode as shown in Fig. 6-29 and its corresponding eigenfunctions shown in Fig. 6-30.

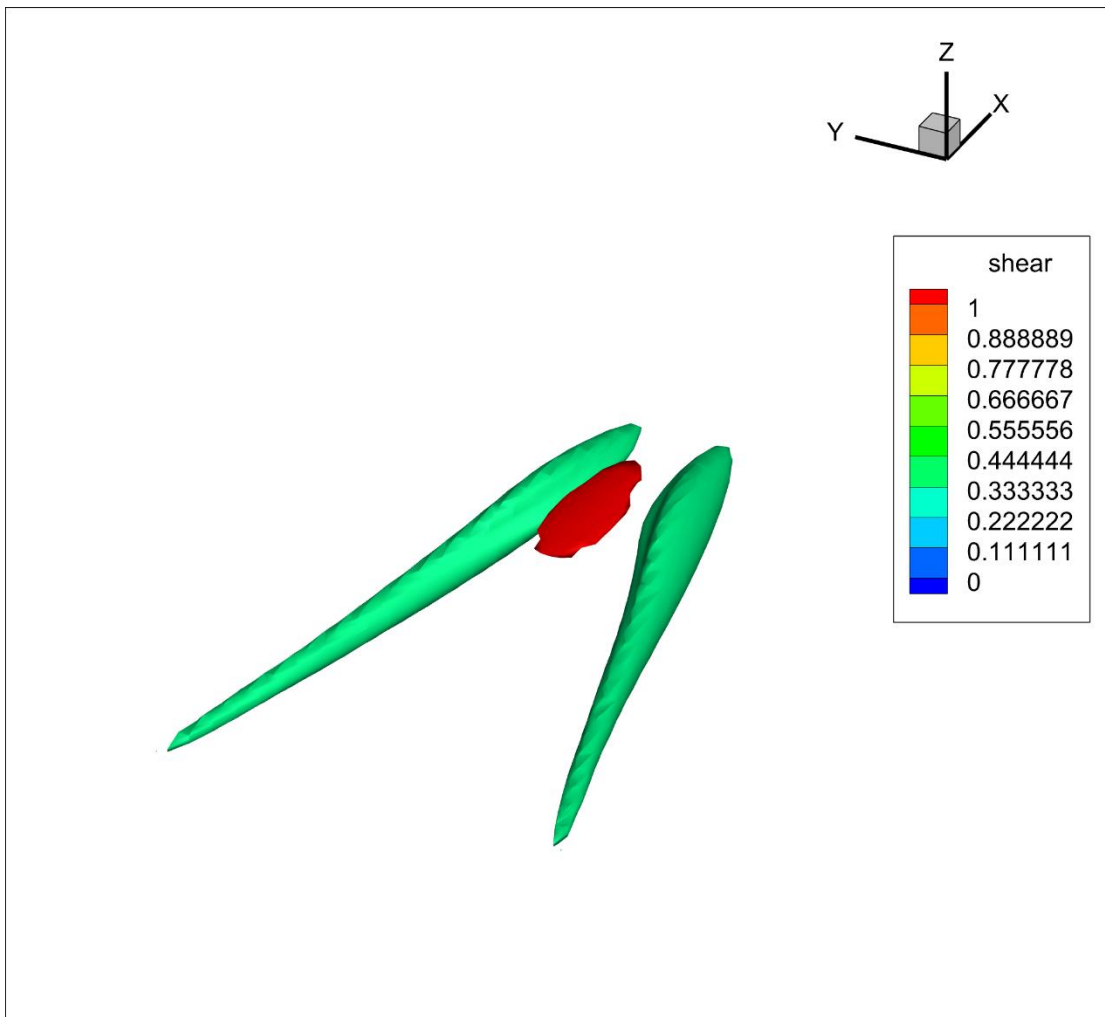


Figure 6-26 shear region between two  $\Lambda$ -vortices

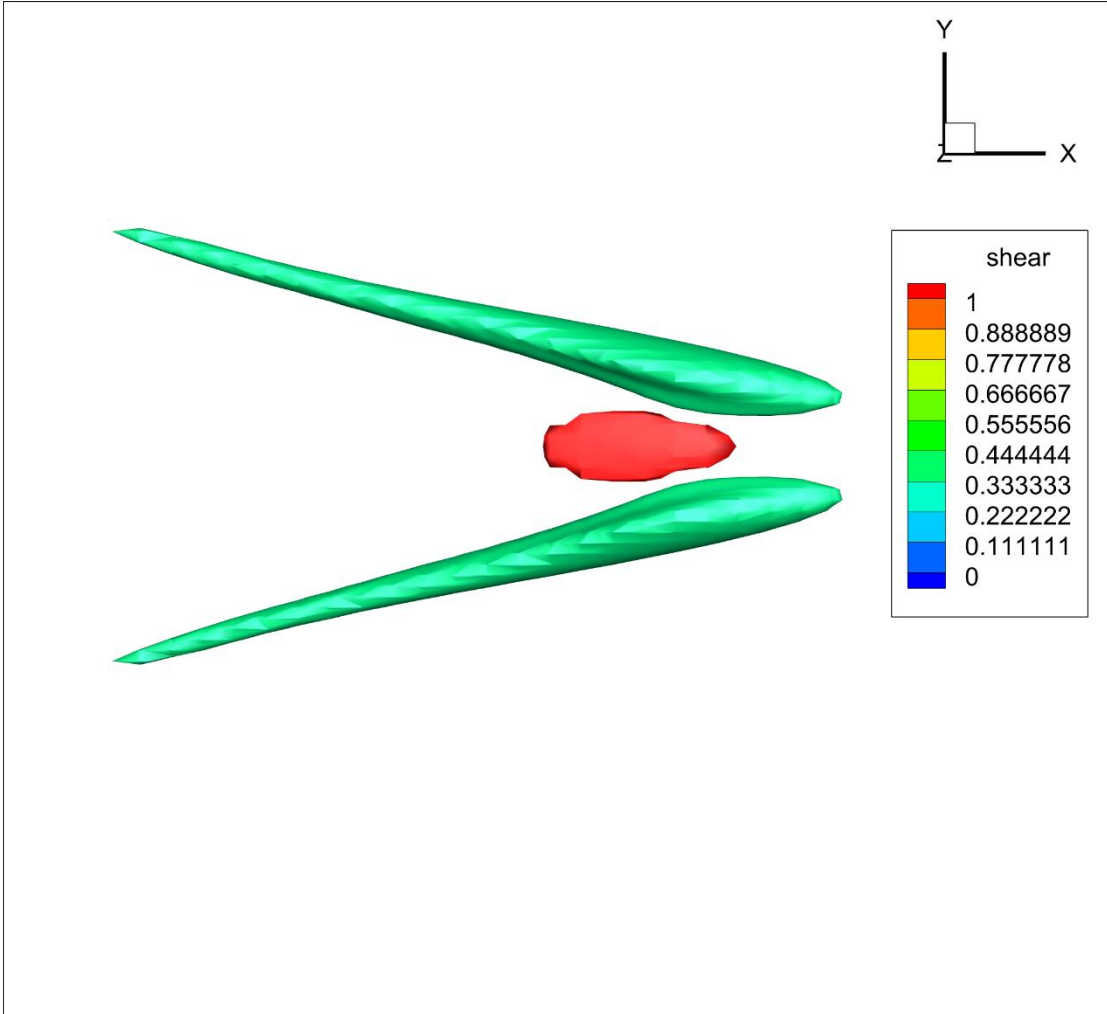


Figure 6-27 Shear region between two  $\Lambda$ -vortices (top view)

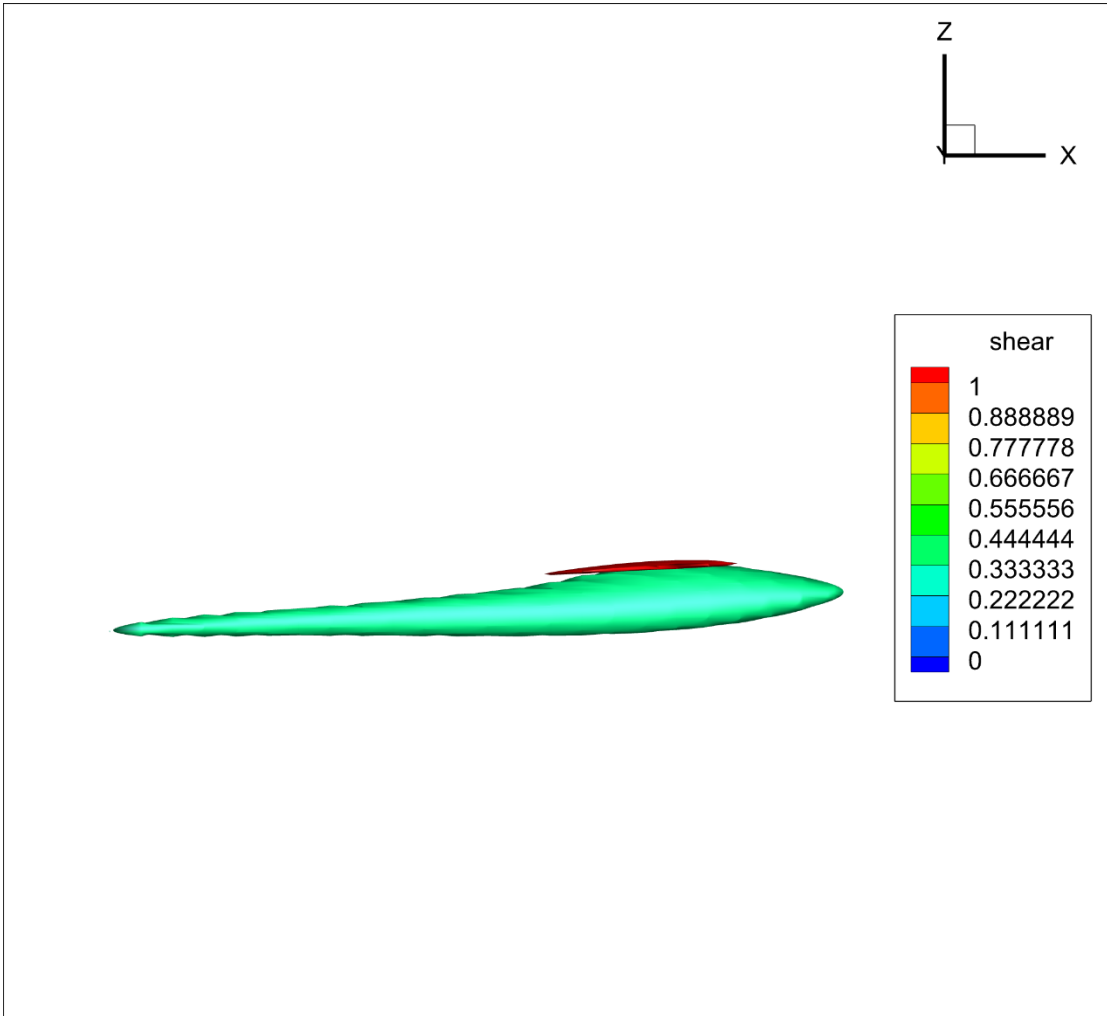


Figure 6-28 Shear region between two  $\Lambda$ -vortices (side view)

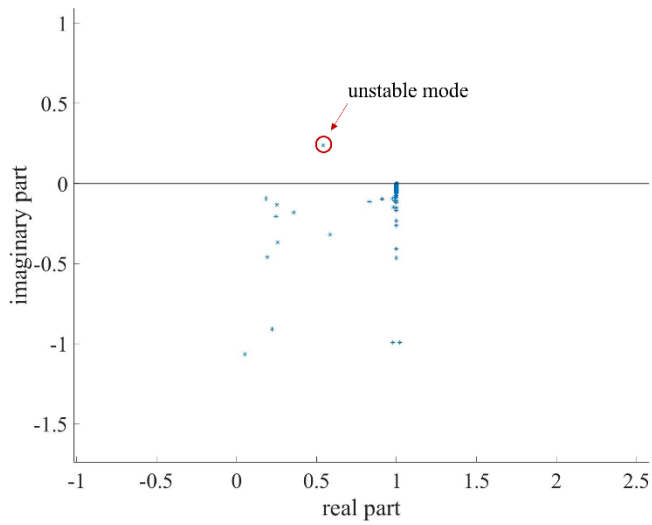


Figure 6-29 Modes at the shear region

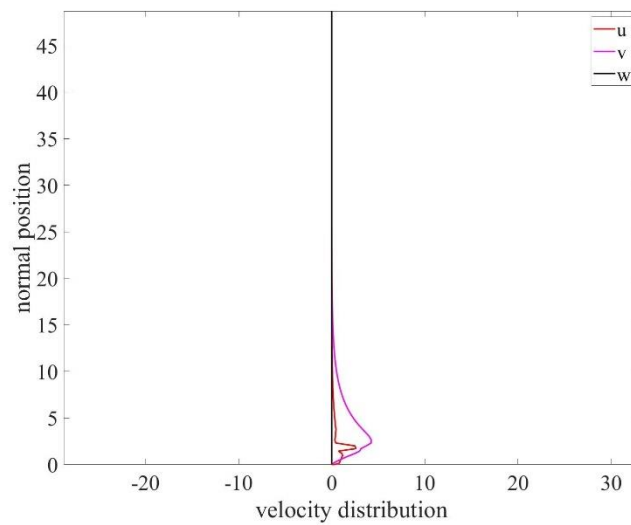


Figure 6-30 Eigenfunctions of the unstable mode at shear region

The hairpin vortices roll up because  $R_z$ , which is the z direction component of Liutex vector. In Fig. 6-31,  $R_z$  distribution in the selected slice is shown.  $R_z$  is zero at the spanwise vortex becomes large at the hairpin vortex locations. This explains the reason why hairpin vortex rolls up while spanwise vortex not.

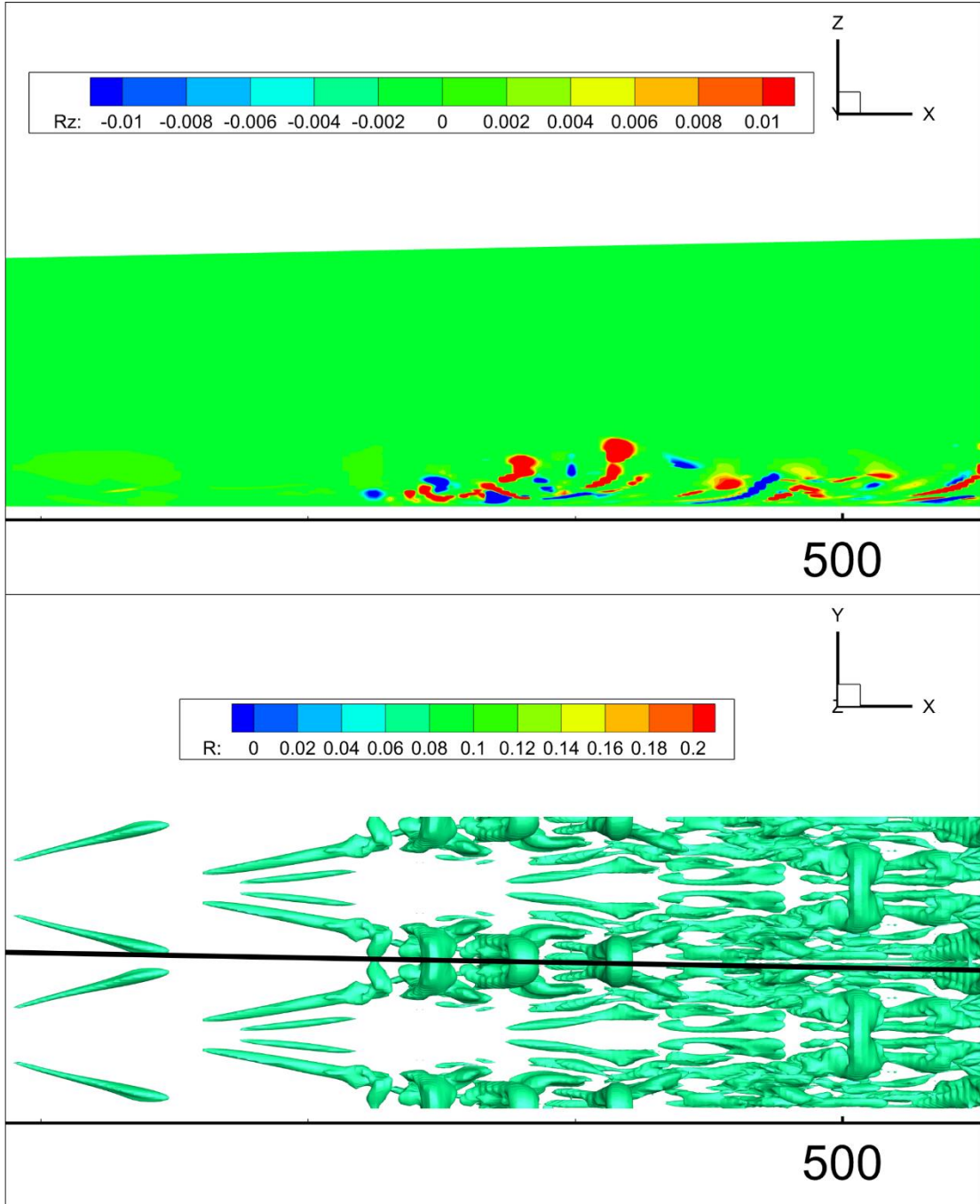


Figure 6-31  $R_z$  distribution at the slice

## 6.5 Chapter summary

In this chapter, the mechanism of hairpin vortex formation is explained. The spanwise vortex comes from the unstable 2D mode of O-S equation with Blasius solution as the base flow. The  $\Lambda$ -vortex calculated from the velocity gradient tensor exhibits the spanwise vortices are straight and predicts the rotation direction clearly. The spanwise perturbation gradually increases as the spanwise vortex becomes curved which introduces  $\beta$  in the disturbance. When  $x$  reaches 400, the unstable 3D mode is excited and gradually becomes dominant in the perturbation. After that,  $\Lambda$ -vortex is formed and the angle between  $\Lambda$ -vortex and spanwise direction can be evaluated by the  $\alpha$  and  $\beta$  in the 3D modes. Hairpin vortex is formed because the  $\Lambda$ -vortices generate a strong shear region which is unstable.  $\Lambda$ -vortices and hairpin vortices roll up because  $R_z$  is greater than 0. The roll up angle of hairpin vortices are larger than that of  $\Lambda$ -vortices since  $R_z$  of hairpin vortices are larger than that of  $\Lambda$ -vortices.

## Chapter 7

### Summary

The third generation vortex identification method, Liutex, overcomes the drawbacks of the previous first generation and second generation methods. It can correctly reveal the direction and strength of the local rotation. With this powerful tool, we revisit the mechanism of the hairpin vortex formation. The spanwise vortices are formed by the unstable 2D mode of O-S equation, which is the governing equation of the perturbations. Liutex correctly predict the direction and shape of the spanwise vortex. The 3D mode enforced at the inlet is original stable, however, with the development of the flow, the base flow profile is change which results in this 3D mode becomes unstable. Thus, the spanwise disturbance grows and gradually reaches the same level as the disturbance in the other two directions. Then  $\Lambda$ -vortex is formed and the angle between  $\Lambda$ -vortex and the spanwise direction can be estimated by the  $\alpha$  and  $\beta$  in the 3D modes. With the development of  $\Lambda$ -vortices, the distance between two  $\Lambda$ -vortices becomes smaller and it introduces a strong shear region because of the “sweep” and “eject” motions. This shear region is unstable and will become the hairpin vortex. The  $R_z$  of spanwise vortex is zero, so spanwise vortex does not change in the normal direction. The  $R_z$  of  $\Lambda$ -vortex and hairpin vortex are greater than 0, therefore these vortices roll up.

Apart from the mechanism of hairpin vortex by Liutex, some of my other work during my Ph.D. student period is also included. To find a decomposition of velocity gradient tensor that can represent rotation, shear and stretching/compression part correctly, principal coordinate and

principal decomposition are developed. Based on this decomposition, the correlation between Liutex and some popular vortex identification methods are analyzed. The result shows the first and second generation methods are more or less contaminated by shear or stretching/compression. To avoid the influence of frame selection, the objective Liutex is proposed. Objective Liutex can obtain Liutex structure in the inertial coordinate system from the data collected in a non-inertial frame.

## Appendix

### Algorithm to find principal coordinate[49]

Step1: Rotate around the z axis.

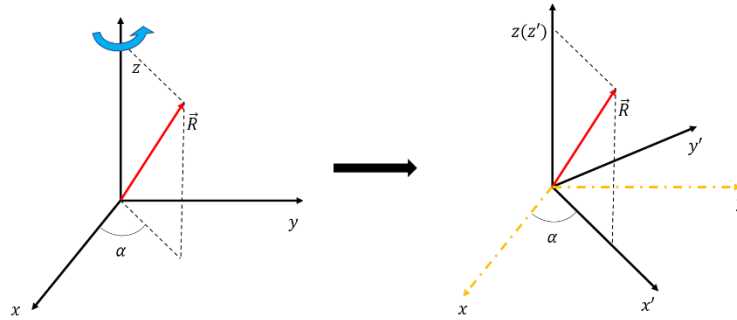


Figure 8-1 Rotation around the z-axis

Suppose  $\vec{R} = (R_x, R_y, R_z)$ . Angle  $\alpha$  can be calculated by

$$\alpha = \arccos\left(\frac{(R_x, R_y) \cdot (1, 0)}{\sqrt{R_x^2 + R_y^2}}\right) \quad (1)$$

where  $(R_x, R_y)$  is the projection of  $\vec{R}$  in the xy-plane and  $(1, 0)$  is the direction of x-axis (Fig 7-

1).

The rotation matrix around the z-axis  $Q_x$  is

$$Q_x = \begin{bmatrix} \cos\alpha & \sin\alpha & 0 \\ -\sin\alpha & \cos\alpha & 0 \\ 0 & 0 & 1 \end{bmatrix} \quad (2)$$

Step 2: Rotate around the  $y'$  axis.

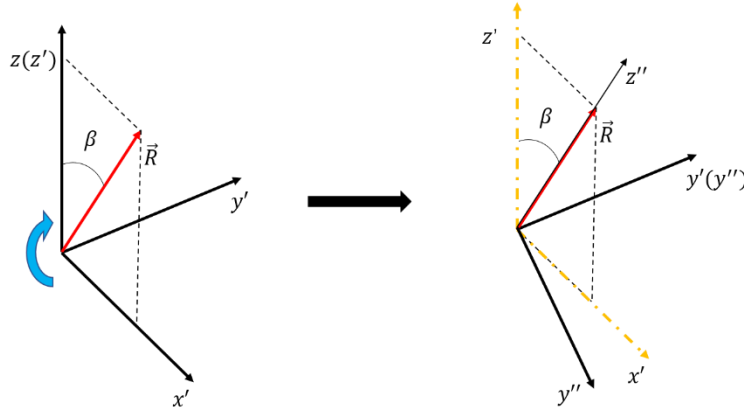


Figure 8-2 Rotation around the  $y'$ -axis

Angle  $\beta$  can be calculated by

$$\beta = \arccos\left(\frac{\vec{R} \cdot (0,0,1)}{\sqrt{R_x^2 + R_y^2 + R_z^2}}\right) \quad (3)$$

where  $(0,0,1)$  is the direction of  $z$ -axis. It is noted that the coordinates of  $\vec{R}$  and  $z$ -axis are both expressed in the original  $xyz$  coordinate system, since step 1 does not change  $\beta$  (Fig 7-2).

The rotation matrix around the  $y'$ -axis  $Q_{y'}$  is

$$Q_{y'} = \begin{bmatrix} \cos\alpha & 0 & -\sin\alpha \\ 0 & 1 & 0 \\ \sin\alpha & 0 & \cos\alpha \end{bmatrix} \quad (4)$$

In general, the rotation matrix  $Q$  is

$$Q = Q_{y'} Q_x \quad (5)$$

By doing  $Q$  rotation, the  $z''$ -axis is along the same direction of Liutex  $\vec{R}$ . The velocity gradient tensor in the  $x''y''z''$  coordinate is

$$\nabla \vec{v}'' = Q(\nabla \vec{v})Q^T \quad (6)$$

Step 3: Rotate around the  $z''$ -axis.

After making the  $z''$ -axis along the same direction of Liutex  $\vec{R}$ , the coordinate will be rotated

around the  $z'$ -axis to make the velocity gradient tensor satisfy the part 2 and 3 of the principal coordinate definition.

The velocity gradient tensor  $\nabla \vec{v}''$  is in the form of

$$\nabla \vec{v}'' = \begin{bmatrix} (\nabla \vec{v}'')_{11} & (\nabla \vec{v}'')_{12} & 0 \\ (\nabla \vec{v}'')_{21} & (\nabla \vec{v}'')_{22} & 0 \\ (\nabla \vec{v}'')_{31} & (\nabla \vec{v}'')_{32} & \lambda_r \end{bmatrix} \quad (7)$$

Suppose it is required to rotate angle  $\theta$ . The rotation matrix is

$$P = \begin{bmatrix} \cos\theta & \sin\theta & 0 \\ -\sin\theta & \cos\theta & 0 \\ 0 & 0 & 1 \end{bmatrix} \quad (8)$$

The velocity gradient tensor after rotation  $\nabla \vec{V}$  (Gao *et al.* 2019a) is

$$\nabla \vec{V} = P \nabla \vec{v}'' P^T = \begin{bmatrix} \frac{\partial U}{\partial X} & \frac{\partial U}{\partial Y} & 0 \\ \frac{\partial V}{\partial X} & \frac{\partial V}{\partial Y} & 0 \\ \frac{\partial W}{\partial X} & \frac{\partial W}{\partial Y} & \lambda_r \end{bmatrix} \quad (9)$$

where

$$\frac{\partial U}{\partial Y} = a \sin(2\theta + \varphi) - b \quad (10)$$

$$\frac{\partial V}{\partial X} = a \sin(2\theta + \varphi) + b \quad (11)$$

$$a = \frac{1}{2} \sqrt{\left( (\nabla \vec{v}'')_{22} - (\nabla \vec{v}'')_{11} \right)^2 + \left( (\nabla \vec{v}'')_{21} + (\nabla \vec{v}'')_{12} \right)^2} \quad (12)$$

$$b = \frac{1}{2} \left( (\nabla \vec{v}'')_{21} - (\nabla \vec{v}'')_{12} \right) \quad (13)$$

$$\varphi = \begin{cases} a \cos\left(\frac{\frac{1}{2}((\nabla \vec{v}'')_{22} - (\nabla \vec{v}'')_{11})}{a}\right), & (\nabla \vec{v}'')_{21} + (\nabla \vec{v}'')_{12} \geq 0 \\ a \sin\left(\frac{\frac{1}{2}((\nabla \vec{v}'')_{21} + (\nabla \vec{v}'')_{12})}{a}\right), & (\nabla \vec{v}'')_{21} + (\nabla \vec{v}'')_{12} < 0, (\nabla \vec{v}'')_{22} - (\nabla \vec{v}'')_{11} \geq 0 \\ a \sin\left(\frac{-\frac{1}{2}((\nabla \vec{v}'')_{21} + (\nabla \vec{v}'')_{12})}{a}\right) + \pi, & (\nabla \vec{v}'')_{21} + (\nabla \vec{v}'')_{12} < 0, (\nabla \vec{v}'')_{22} - (\nabla \vec{v}'')_{11} < 0 \end{cases} \quad (14)$$

Recall that the fundamental Liutex magnitude expression (Liu *et al.* 2018) is  $2(b-a)$ , so when

$2\theta + \varphi = \frac{\pi}{2}$ , the velocity gradient tensor satisfies definition of principal coordinate. Therefore,

$$\theta = \frac{1}{2}\left(\frac{\pi}{2} - \varphi\right) \quad (15)$$

Then the value of each entry is known.

$$P = \begin{bmatrix} \cos\theta & \sin\theta & 0 \\ -\sin\theta & \cos\theta & 0 \\ 0 & 0 & 1 \end{bmatrix} \quad (16)$$

After that, the velocity gradient tensor in the principal coordinate is found.

$$\nabla\vec{V} = P\nabla\vec{v}'P^T = PQ(\nabla\vec{v})Q^T P^T \quad (17)$$

Reference:

- [1] H. v. Helmholtz(1858). "Über Integrale der hydrodynamischen Gleichungen, welche den Wirbelbewegungen entsprechen," **55**, 22-55
- [2] Y. Gao, and C. Liu(2018). "Rortex and comparison with eigenvalue-based vortex identification criteria," *Physics of Fluids* **30**.10.1063/1.5040112
- [3] Y. Yu, P. Shrestha, O. Alvarez, C. Nottage, and C. Liu(2020). "Correlation analysis among vorticity, Q method and Liutex," *Journal of Hydrodynamics* **32**, 1207-1211.10.1007/s42241-020-0069-2
- [4] C. Liu, Y.-s. Gao, X.-r. Dong, Y.-q. Wang, J.-m. Liu, Y.-n. Zhang, X.-s. Cai, and N. Gui(2019). "Third generation of vortex identification methods: Omega and Liutex/Rortex based systems," *Journal of Hydrodynamics* **31**, 205-223.10.1007/s42241-019-0022-4
- [5] C. Liu, Y. Gao, S. Tian, and X. Dong(2018). "Rortex—A new vortex vector definition and vorticity tensor and vector decompositions," *Physics of Fluids* **30**.10.1063/1.5023001
- [6] J.-P. Françoise, G. L. Naber, and S. T. Tsou(2006), *Encyclopedia of mathematical physics*. Elsevier Amsterdam
- [7] J. Z. Wu, H. Y. Ma, and M. D. Zhou(2006), *Vorticity and vortex dynamics*. Springer
- [8] J.-Z. Wu(2018). "Vortex definition and "vortex criteria", " *Science China Physics, Mechanics & Astronomy* **61**.10.1007/s11433-017-9120-8
- [9] S. Robinson, S. J. Kline, and P. Spalart(1989),A review of quasi-coherent structures in a numerically simulated turbulent boundary layer, in the *Quasi-Coherent Structures in the Turbulent*

Boundary Layer, part 2. Verification and New Inform. from a Numerically Simulated Flat-Plate Layer at Memorial Intern. Seminar on Near-Wall Turbulence, NASA-TM-102191

[10] Y. Wang, Y. Yang, G. Yang, and C. Liu(2017). "DNS Study on Vortex and Vorticity in Late Boundary Layer Transition," *Communications in Computational Physics* **22**, 441-459.10.4208/cicp.OA-2016-0183

[11] J. C. Hunt, A. A. Wray, and P. Moin(1988). "Eddies, streams, and convergence zones in turbulent flows," *Studying Turbulence Using Numerical Simulation Databases, 2. Proceedings of the 1988 Summer Program*

[12] M. S. Chong, A. E. Perry, and B. J. Cantwell(1990). "A general classification of three - dimensional flow fields," *Physics of Fluids A: Fluid Dynamics* **2**, 765-777.10.1063/1.857730

[13] J. Jeong, and F. Hussain(1995). "On the identification of a vortex," *Journal of fluid mechanics* **285**, 69-94

[14] J. Zhou, R. J. Adrian, S. Balachandar, and T. M. Kendall(1999). "Mechanisms for generating coherent packets of hairpin vortices in channel flow," *Journal of Fluid Mechanics* **387**, 353-396.10.1017/s002211209900467x

[15] Y.-q. Wang, Y.-s. Gao, H. Xu, X.-r. Dong, J.-m. Liu, W.-q. Xu, M.-l. Chen, and C. Liu(2020). "Liutex theoretical system and six core elements of vortex identification," *Journal of Hydrodynamics* **32**, 197-211.10.1007/s42241-020-0018-0

[16] C. Liu, and Y. Yu(2022). "Mathematical foundation of Liutex theory," *Journal of Hydrodynamics* **34**, 981-993

- [17] Y.-q. Wang, Y.-s. Gao, J.-m. Liu, and C. Liu(2019). "Explicit formula for the Liutex vector and physical meaning of vorticity based on the Liutex-Shear decomposition," *Journal of Hydrodynamics* **31**, 464-474.10.1007/s42241-019-0032-2
- [18] Y.-s. Gao, J.-m. Liu, Y.-f. Yu, and C. Liu(2019). "A Liutex based definition and identification of vortex core center lines," *Journal of Hydrodynamics* **31**, 445-454.10.1007/s42241-019-0048-7
- [19] H. Li, Y. Liu, D. Wang, and H. Xu(2023). "Liutex (vortex) core and tube identification and automatic generation algorithms," *Computers & Fluids* **250**.10.1016/j.compfluid.2022.105731
- [20] H. Xu, X.-s. Cai, and C. Liu(2019). "Liutex (vortex) core definition and automatic identification for turbulence vortex structures," *Journal of Hydrodynamics* **31**, 857-863.10.1007/s42241-019-0066-5
- [21] J. Liu, and C. Liu(2019). "Modified normalized Rortex/vortex identification method," *Physics of Fluids* **31**, 061704.10.1063/1.5109437
- [22] C. Liu, Y. Wang, Y. Yang, and Z. Duan(2016). "New omega vortex identification method," *Science China Physics, Mechanics & Astronomy* **59**.10.1007/s11433-016-0022-6
- [23] Y.-a. Guo, X.-r. Dong, X.-s. Cai, and W. Zhou(2020). "Experimental study on dynamic mechanism of vortex evolution in a turbulent boundary layer of low Reynolds number," *Journal of Hydrodynamics* **32**, 807-819.10.1007/s42241-020-0056-7
- [24] J. C. Cuissa, and O. Steiner(2022). "Innovative and automated method for vortex identification-I. Description of the SWIRL algorithm," *Astronomy & Astrophysics* **668**, A118
- [25] J. R. Canivete Cuissa, and O. Steiner(2020). "Vortices evolution in the solar atmosphere,"

[26] V. Borisov, T. Konstantinovskaya, and A. Lutsky(2023). "Investigation of Vortex Structures in the Supersonic Flow around a Tandem of Wings," *Mathematical Models and Computer Simulations* **15**, 59-72

[27] O. Reynolds(1883). "III. An experimental investigation of the circumstances which determine whether the motion of water shall be direct or sinuous, and of the law of resistance in parallel channels," *Proceedings of the royal society of London* **35**, 84-99

[28] L. Rayleigh(1880). "On the stability, or instability, of certain fluid motions," *Proc. London Math. Soc.* **9**, 57-70

[29] G. I. Taylor(1915). "I. Eddy motion in the atmosphere," *Philosophical Transactions of the Royal Society of London. Series A, Containing Papers of a Mathematical or Physical Character* **215**, 1-26

[30] L. Prandtl(1921). "Bemerkungen über die Entstehung der Turbulenz," *ZAMM - Journal of Applied Mathematics and Mechanics/Zeitschrift für Angewandte Mathematik und Mechanik* **1**, 431-436

[31] W. M. F. Orr(1907),The stability or instability of the steady motions of a perfect liquid and of a viscous liquid. Part II: A viscous liquid, in the *Proceedings of the Royal Irish Academy. Section A: Mathematical and Physical Sciences*,

[32] A. Sommerfeld(1909), *Ein beitrag zur hydrodynamischen erklaerung der turbulenten fluessigkeitsbewegungen.*

- [33] W. Heisenberg(1985), *Über stabilität und turbulenz von flüssigkeitsströmen*. Springer
- [34] H. Schlichting(1933). "Zur Entstehung der Turbulenz bei der Plattenströmung," Nachrichten von der Gesellschaft der Wissenschaften zu Göttingen, Mathematisch-Physikalische Klasse **1933**, 181-208
- [35] C.-C. Lin(1955), *The theory of hydrodynamic stability*.
- [36] M. R. Malik(1990). "Numerical methods for hypersonic boundary layer stability," Journal of computational physics **86**, 376-413
- [37] S. A. Orszag(1971). "Accurate solution of the Orr–Sommerfeld stability equation," Journal of Fluid Mechanics **50**, 689-703
- [38] L. Chen, X. Liu, M. Oliveira, and C. Liu(2010),Dns for late stage structure of flow transition on a flat-plate boundary layer, in the 48th AIAA Aerospace Sciences Meeting Including the New Horizons Forum and Aerospace Exposition,
- [39] S. K. Lele(1992). "Compact finite difference schemes with spectral-like resolution," Journal of computational physics **103**, 16-42
- [40] P. Lu, Z. Wang, L. Chen, and C. Liu(2012). "Numerical study on U-shaped vortex formation in late boundary layer transition," Computers & fluids **55**, 36-47
- [41] L. Jiang, C.-L. Chang, M. Choudhari, and C. Liu(2003),Cross-validation of DNS and PSE results for instability-wave propagation in compressible boundary layers past curvilinear surfaces, in the 16th AIAA Computational Fluid Dynamics Conference,
- [42] C. Liu, and L. Chen(2011). "Parallel DNS for vortex structure of late stages of flow transition,"

Computers & Fluids **45**, 129-137

[43] H. Lamb(1932), *Hydrodynamics*. The University press

[44] S. K. Robinson(1991). "COHERENT MOTIONS IN THE TURBULENT BOUNDARY-LAYER,"  
Annual Review of Fluid Mechanics **23**, 601-639.10.1146/annurev.fluid.23.1.601

[45] B. Epps(2017),Review of vortex identification methods, in the 55th AIAA aerospace sciences  
meeting,

[46] K. Tziotziou, E. Scullion, S. Shelyag, O. Steiner, E. Khomenko, G. Tsiropoula, J. Canivete  
Cuissa, S. Wedemeyer, I. Kontogiannis, and N. Yadav(2023). "Vortex motions in the solar  
atmosphere: Definitions, theory, observations, and modelling," Space Science Reviews **219**, 1

[47] Y. Yu, P. Shrestha, C. Nottage, and C. Liu(2020). "Principal coordinates and principal velocity  
gradient tensor decomposition," Journal of Hydrodynamics **32**, 441-453.10.1007/s42241-020-  
0035-z

[48] Y. W. Y. G. C. Liu(2018). "Letter: Galilean invariance of Rortex," Physics of Fluids  
**30**.10.1063/1.5058939

[49] C. Liu, Y. Yu, and Y.-s. Gao(2022). "Liutex based new fluid kinematics," Journal of  
Hydrodynamics **34**, 355-371

## BIOGRAPHICAL INFORMATION

Yifei Yu received a Bachelor of Engineering in Engineering Mechanics from Nanjing University of Aeronautics and Astronautics in China. He was awarded Second-class Scholarship from Nanjing University of Aeronautics and Astronautics in 2015 and 2016. He was awarded the Merit Student from Nanjing University of Aeronautics and Astronautics in 2016. He received Mathematics Academic Excellence Fund from University of Texas at Arlington in 2020 and 2021. He won Maverick Research Fellowship from University of Texas at Arlington in 2022. His research interests include vortex identification, kinematics and dynamics.